HOKKAIDO UNIVERSITY

Doctoral Dissertation

Fabrication of Polystyrene Colloidal Crystal Films

by Electrophoretic Deposition

and Structural Color Control

Tran Thi Hoai Giang

September, 2020

Materials Chemistry and Engineering Course

Graduate School of Chemical Sciences and Engineering

Hokkaido University

Abstract

Chapter 1

A colloidal crystal is an ordered array of colloid particles. The colloidal crystal film is promising for the different types of photonic materials, such as optical waveguides and sensors, due to its wide range of coloring derived from Bragg diffraction in the visible wavelength region. Colloidal crystal films have been synthesized by the various techniques. However, the low formation rate of the colloidal crystal films has still been one of the key issues in future industrialization for mass production.

Recently, electrophoretic deposition (EPD) is becoming one of the promising candidates to realize the rapid colloidal crystal film fabrication. The EPD process is a widely used coating process for many industrial applications. This process is characterized by the migration of colloidal particles in a liquid under an electric field, i.e., electrophoresis, and the subsequent deposition onto an electrode. In 2000, the colloidal crystal films made of polystyrene (PS) particles with 200 - 300 nm diameters were fabricated for 30 minutes by the EPD technique. Since then, the research of colloidal crystal films was directed to faster fabrication and size enlargement. Nevertheless, they have still remained in the range between 30 minutes and 2 hours, and several cm^2 size, respectively. In this thesis, optimal conditions to fabricate the colloidal crystal films by the EPD technique were explored for the sake of fast and large size fabrication. For this purpose, growth mechanism of the colloidal crystal film was investigated in detail. The sensing applications of the colloidal crystal films were also examined.

Chapter 2

The optimal condition for the EPD colloidal crystal film formation was investigated in detail. The aqueous PS colloidal suspension was not appropriate due to the generation of gas bubbles during the electrolysis and formed only amorphous films. Dialysis and the application of a pulse voltage could avoid the gas bubble generation, however, particle self-assembly was still amorphous. As a suspension for the EPD process, the effectiveness of mixing ethanol (EtOH) and water was confirmed by testing several alcohols as solvents, and explained from the different viewpoints including hydrogen bond, van der Waals dispersion force, and mobility/freedom of PS particles. The higher the EtOH concentration, the better the colloidal crystal film formation. In the investigated range,

the most preferable condition for the EPD colloidal crystal film formation was from the 92.5 vol% EtOH suspension. The substrate withdrawing rate from the suspension also significantly affected the EPD colloidal crystal film fabrication. Too slow and too fast withdrawing rates were not good. The most preferable rate was 3.0 mm/sec. The large area colloidal crystal film formation by the EPD technique was also demonstrated. Comparable quality of EPD colloidal crystal films fabricated on small area indium tin oxide (ITO)-coated glass (ITO/glass) and large area (over 50 cm^2) ITO-coated polyethylene terephthalate (PET) sheet (ITO/PET) substrates was confirmed by the SEM observations and the reflectance spectra. These results demonstrate the advantage of the EPD technique for large scale production of colloidal crystal, considering the fast fabrication rate compared to the other conventional techniques. The growth rate of the colloidal crystal is extremely rapid (within one minute for 900 mm^2 area) compared with those of previous papers, such as oil covering and capillary deposition methods (several to hundreds of hours). This process has the potential for high-speed deposition of the colloidal crystalline thin films.

Chapter 3

A growth mechanism of the colloidal crystal films from the concentrated EtOH aqueous suspension was investigated. Closely packed colloidal crystal film was formed within 55 seconds. By the analysis of the reflection spectra and the optical microscope images, the growth mechanism from the colloidal suspension to the colloidal crystal film was found to consist of 4 stages. The 1st stage is a liquid film of the concentrated colloidal suspension on a substrate. By the progress of evaporation, the phase transition from disorder to order to form the non-closely packed colloidal crystal by self-assembly takes place. At the moment of the phase transition, the Bragg's diffraction peak is detected and the structural color appears. In the 2nd stage, the diffraction peak shifts toward the shorter wavelength direction (blue shift), due to the reduction of the interparticle distance of the non-close packed colloidal crystal. In the end, the closely packed colloidal crystal film is formed. In the 3rd stage, the liquid film covering on the colloidal crystal film evaporated and iridescence color due to thin-film interference is tentatively observed. In the 4th stage, the colloidal crystal film changes from wet to dry, by the evaporation of the interparticle EtOH aqueous solvent. The structural color changes from green to blue and the diffraction peak wavelength goes down with one more stage. This color change is dominated by the

change of the refractive index of the interparticle medium from the liquid to the air.

Chapter 4

The interparticle space of the colloidal crystal film was filled by the PDMS (poly-dimethylsiloxane) elastomer to realize the soft photonic crystals. After filling the interparticle space with PDMS elastomer, the color changed from light blue to green due to the increase of the interparticle distance and the refractive index increase of the interparticle space. By the 4 times PDMS elastomer filling, the color changed to red with the further increase of the interparticle distance. By the tensile test of this film, the deformed area has shown green color with the shrinking of the interplanar distance although non-deformed area has not shown any color change. This result has shown the potential use of the colloidal crystal films with PDMS filling for the strain detection sensors.

Chapter 5

Swelling phenomena was investigated in detail by the different kinds of silicone oil and other organic compounds as solvents. By dripping these solvents onto the colloidal crystal film with PDMS filling, the structural color change was observed as a red shift (the diffraction peak shifts toward the longer wavelength). These red-shifted peaks again blue-shifted to the original green color by drying up the volatile solvent. Since this phenomenon was reversible and repeatable, the possibility of the obtained colloidal crystal film with PDMS elastomer filling as volatile liquid sensor was shown. The swelling ratio for all solvents investigated was determined using the estimated interplanar distance. Generally, the swelling ratio of the solvents was inversely dependent on the solubility parameter. The highest swelling ratio, 1.6114, was obtained by the heptane, of which solubility parameter, 7.4 $\text{cal}^{1/2}\text{cm}^{-3/2}$, was very close to that of PDMS, 7.3 $\text{cal}^{1/2}\text{cm}^{-3/2}$.

Chapter 6

The general conclusions of my research and future prospects are given.

Contents

5   Effect of volatile solvents on the swelling ratio of the colloidal crystal films   83

6   General Conclusions   96

List of research achievements   100

Acknowledgements   101

I would like to dedicate this dissertation to my son,

Taiki.

Chapter 1

Introduction

1.1 Structural color and colloidal crystals

When a light shines on a material which has a fine structure with the same and/or the smaller size than the wavelength of a light, a part of the light is diffracted. This coloring phenomenon based on the spectroscopy is called as a structural color [1]. This phenomenon can be seen nearby [2]. Compact disk, soap bubble and beetles themselves don't have a color, while they show a color by the interference of a light through their fine structures. The color of soap bubbles and oil films is originated from the thin film interference (Fig.1.1). At the thin film with thickness similar to the optical light, the light with the wavelength corresponding to the thickness of the film is seen as a colored light, since the reflected lights at the upper surface and the lower surface of the film interfere. Multi-layered thin films realize variety of colors by the combination of different thickness and the number of thin films. The color rich in metallic luster seen on jewel beetles is coming from the multi-layered thin film structure (Fig.1.2). The unevenness on the aluminum of the CD/DVD optical storage media also interfere optical lights like a diffraction grating. This leads to the iridescent color of the recoding side of CD/DVD. Morpho butterfly wings are called living jewels and show brilliant blue color (Fig.1.3). This blue color is a structural color due to the lattice-like structure engraved on the scale surface. Jewelry opals show a variety of colors by the optical interference through the silicate fine particles regularly arranged (Fig.1.4).
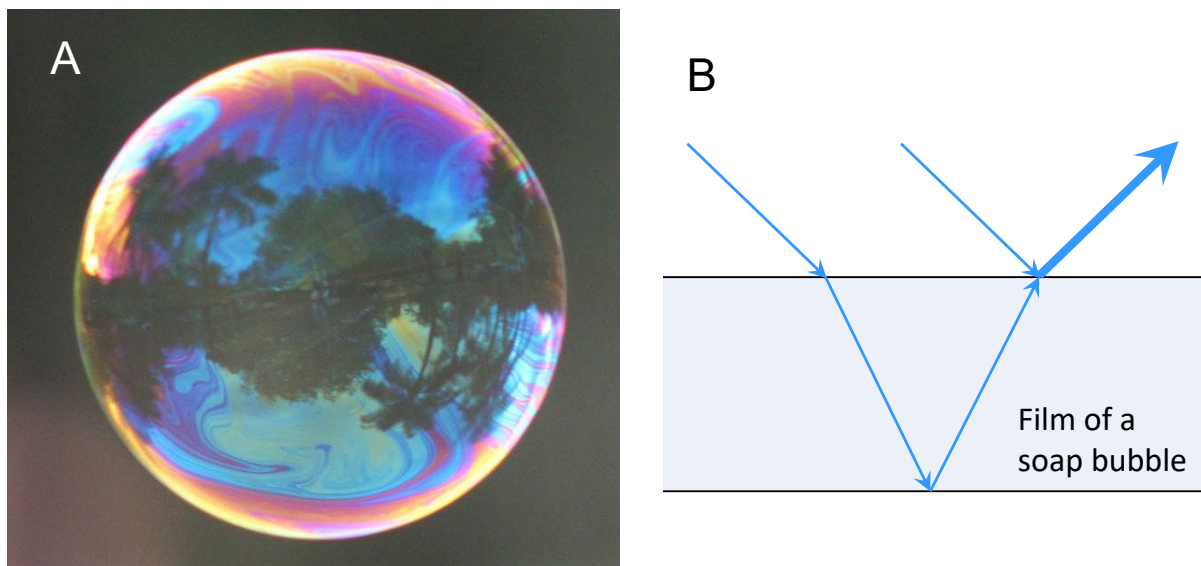
Figure 1.1 Colors appear on a soap bubble (A) and a schematic of a light interference at a soap bubble film (B).
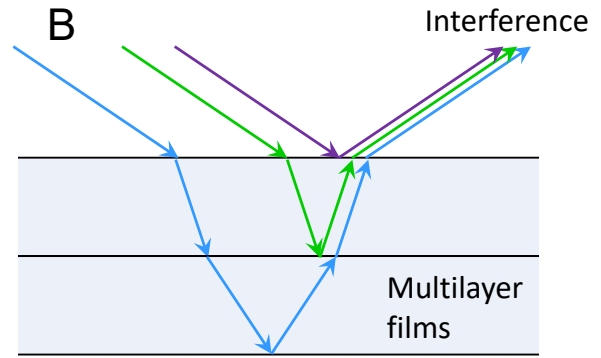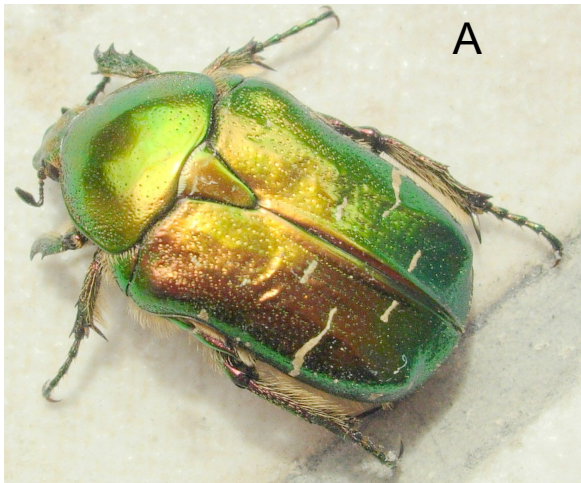
Figure 1.2 The color rich in metallic luster on a jewel beetle (A) and a schematic of a multilayer interference (B).
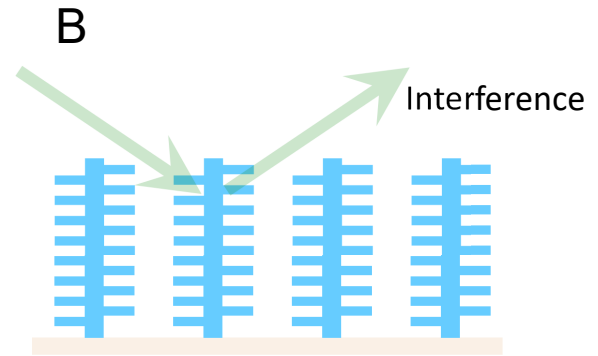
Figure 1.3 Brilliant blue color of morpho butterfly wings (A) [3] and a schematic of a light interference at morpho butterfly wing scales (B).
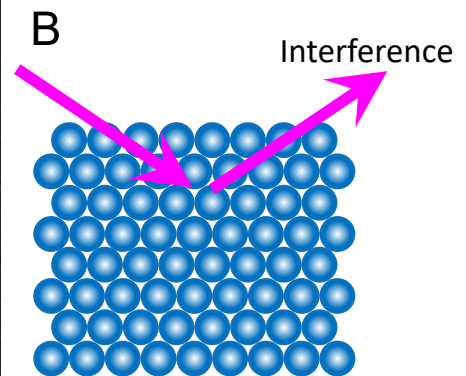
Figure 1.4 A variety of colors on Opal (A) [4] and a schematic of a light interference at an opal structure (B).

This structural color is characterized by the color variation depending the angle to see. Different from color materials, since the structural color does not decolorize by ultraviolet rays and free from poisonous heavy metals, the industrial application of it for the texture and automobile coloring has been investigated.

A fine particle with a diameter about 1 to 500 nm is called as a colloidal particle. When colloidal particles with uniform particle size arrange periodically, it is called as a colloidal crystal by the similarity of the standard crystals. In most of the cases, colloidal crystals have about the same structural periodicity as the optical wavelength of a visible light. Therefore, they diffract such wavelength selectively (Bragg's reflection), and shine beautifully.

Materials which have periodically distributed refractive index are in general called photonic crystals [5]. Normally, that periodicity is nearly the same as the wavelength of the visible light. They diffract the optical light with nearly the same wavelength as their periodicity by the Bragg's reflection, and exhibit the characteristic optical properties which are different from the uniform optical materials. That is why, these materials are specially called as photonic crystals to distinguish their unique optical functions and properties. A typical schematic example of photonic crystals is shown in Fig.1.5. One-dimensional (1D) photonic crystal shown in Fig.1.5-A is represented by the multi-layered thin film. This 1D periodical structure was intensively investigated and applied as the reflection structure of DFB (distributed feedback) laser. Two-dimensional (2D) photonic crystal represented by Fig.1.5-B is composed of the regularly arrangement of infinitely long structures in a grid pattern. Three-dimensional (3D) photonic crystal has the regularly arranged structure similar to a crystal structure as shown in Fig.1.5-C. In nature, similar structures have been reported for all from 1 to 3 dimensional types. In addition, the photonic crystal has a photonic band gap (PBG) that blocks a specific wavelength of light.

The concept of PBG is introduced by E. Yablonovitch [6] and S. John [7]. PBG can be explained in the same way as the origin of the band gap for electrons in solid crystals. In a standard solid crystal, the electron which has certain energy cannot either propagate in the crystal or even exist by the Bragg reflection at any direction because of the existence of the periodical potential created by the atomic nucleus. This is so-called band-gap. Similar to this, the optical light which has certain wavelength cannot either propagate in the crystal or even exist by the Bragg reflection at any direction because of the existence

of the periodical refractive index distribution created in the photonic crystal. When the 3D refractive index distribution is formed as shown in Fig.1.6, the frequency range which cannot propagate in any direction appears as shown in the band diagram of Fig.1.7 (the horizontal axis is corresponding to the different optical propagation direction, the vertical axis is the frequency). This is the photonic band gap, PBG [8]. Usage of the PBG may realize the light confinement. Therefore, the application for the future quantum computer is also expected.
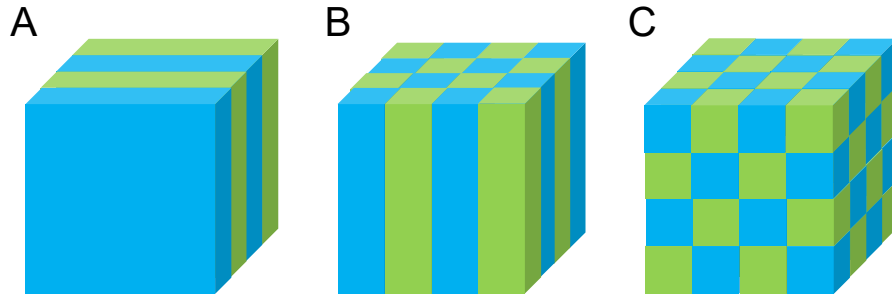
Figure 1.5 Schematic of photonic crystals, 1 dimensional (A), 2 dimensional (B) and 3 dimensional (C).
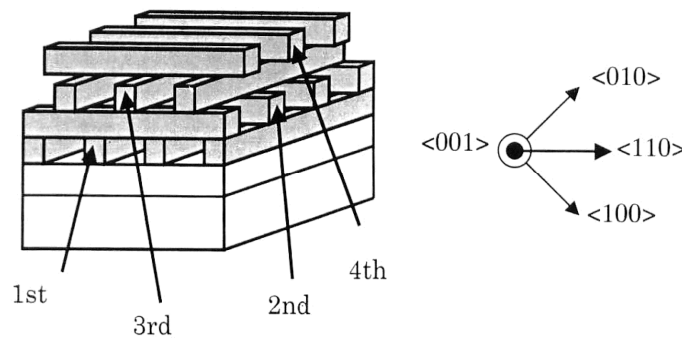
Figure 1.6 Example of the 3D photonic crystal [8]. Photonic band gap appears by forming the 3D refractive index distribution.

Colloidal crystals are one type of photonic crystals. Both colloidal crystals and photonic crystals have the name of 'crystal', however, colloidal crystals are named from the view points of structural unit while photonic crystals are named focusing on the functions. Photonic crystals in general have a variety of types without the limitation to the particle arrangement. In this sense, sometimes, colloidal crystals are called colloidal photonic crystals.

Representative of natural photonic crystal is Opal. Opal's characteristic iridescent color is called in general play-of-color. Opal is a soft rock composed of hydrous silica.
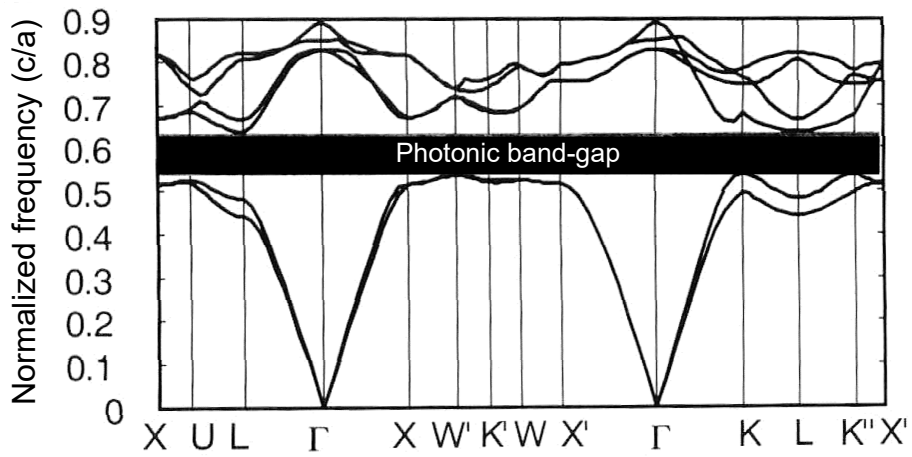
Figure 1.7 Band structure of the 3D photonic crystal in Fig.1.6 [8]. Horizontal axis is the propagation direction of the optical light, vertical axis is the frequency (wavelength) of the optical light.

Sanders reported that fine particles formed closed-packed crystal structure (face centered cubic structure) in Opal (Fig.1.8) [9]. Therefore, a colloidal crystal of which fine particles have close-packing are called an Opal crystal.
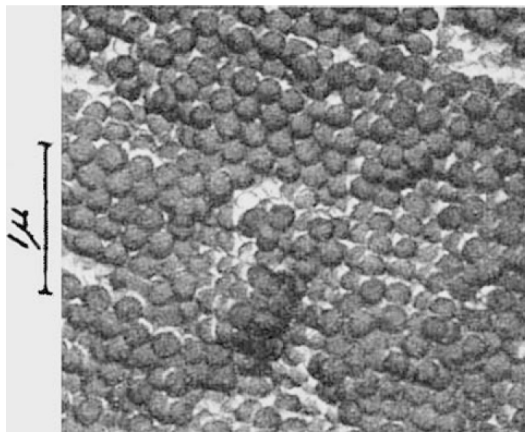
Figure 1.8 Micrographs of heavily etched fracture surface of a colored Opal [9].
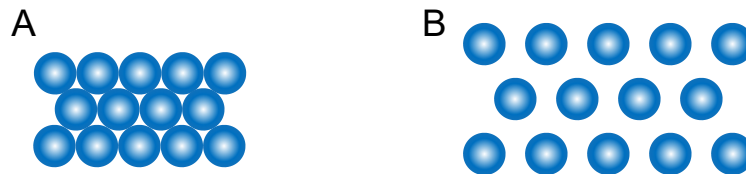
Figure 1.9 Schematic of a colloidal crystal, A: close-packed crystal structure, B: non-close-packed colloidal crystal.

Colloidal crystals are mostly categorized into a closely-packed colloidal crystal

(Fig.1.9-A) and a non-closely-packed colloidal crystal (Fig.1.9-B) [10]. In the case of Fig.1.9-A, each particle contacts each other and forms periodical arrangement (system of hard spheres). In the case of Fig.1.9-B, all particles have the same electrostatic charge, and each particle keeps the certain constant distance by the electrostatic repulsion (system of charged particles). A colloidal crystal of polystyrene (PS) particles is one of the representative in this system. When PS particles are dispersed in water, the surface of particles is negatively charged due to the dissociation of the surface dissociative groups such as sulfate groups.

The colloidal crystal film, i.e. an ordered array of colloid particles, is promising for the different types of 2D/3D-photonic materials and structural color substances, such as optical waveguides and sensors, due to its wide range of coloring derived from Bragg's diffraction in the visible wavelength region. In the past decades, several potential applications have been reported such as photonic ink systems, photonic rubber sheet and photonic crystal lasers, bio/chemical sensors and bio-inspired materials including pH and ion concentration detection [11–23].

1.2 Techniques to fabricate the colloidal crystals

Colloidal crystal films have been synthesized by the various techniques, such as the solvent evaporation method [24, 25], the template-directed crystallization method [26], the natural sedimentation method [27], the spin coating method [28, 29], the Langmuir-Blodgett method [30], and the sealed cell method [31], floating packing [32], electric-field assisted convective assembly [33] and air-pulse-drive assembly [34]. Technical improvement toward a better film fabrication process represented by vertical deposition methods [35, 36] and the cell packing method [37] has also been continued. Fudouzi et al. reported the oil covering method to form a high quality, self-assembled closest packing flat colloidal crystal film over a large area [38].

Among thees techniques, here, there kinds of representative techniques are overviewed.

A typical method is the vertical deposition method. This method was proposed by Colvin et al. [35] and is also called the Colvin method. As shown in the schematic diagram of Fig.1.10, when a substrate such as a glass slide is vertically immersed in a suspension in which colloidal spherical particles are dispersed and allowed to stand, a meniscus is formed at the contact portion with the substrate. When the solvent evaporates from

the tip of the meniscus, convection is generated to compensate for the evaporation, and the particles are carried to the tip of the meniscus, and are regularly arranged by the capillary force acting between the particles [39]. In addition, the evaporation rate of the solvent can be controlled by the temperature of the solvent and the kind of the solvent. Colvin et al. have succeeded in depositing single crystals of colloidal spherical particles on a wide variety of substrates, and could easily fabricate films in thicknesses from single to 100 layers by controlling the volume fraction and size of the particles [35]. Zhao et al. [40] succeeded in producing crack-free colloidal crystals by adding a silica precursor to the suspension. When no silica precursor was added, cracks were formed between the particles originated from volume shrinkage due to solvent evaporation. However, it was reported that when a silica precursor was added, the silica precursor penetrated into the gaps between the spherical silica particles, and the effect of volumetric shrinkage during solvent evaporation could be counteracted.
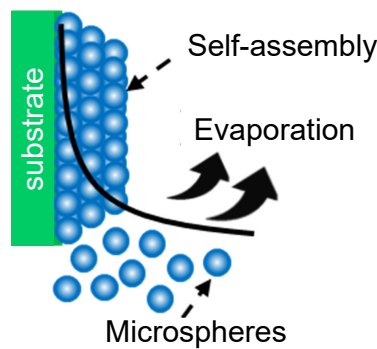
Figure 1.10 Schematic of the vertical deposition method.

Another method is the dip coating method. This method was proposed by Sato et al. [36]. In this method, a colloidal crystal is formed using the capillary phenomenon as in the vertical deposition method. In the vertical deposition method, the film thickness was controlled by the solvent evaporation rate. However, if the number of particles changes during the solvent evaporation, the film thickness may be affected. To solve this problem, the film thickness was controlled by lifting the substrate from the suspension at a constant speed, rather than relying on solvent evaporation, as shown in the schematic diagram of Fig.1.11. Sato et al. [36] reported that high-quality and uniform colloidal crystals could be prepared by controlling the particle concentration or the withdrawing rate.

The other method is the oil coating method. The oil coating method was proposed by Fudouzi et al. [38]. As shown in the schematic diagram of Fig.1.12, this method
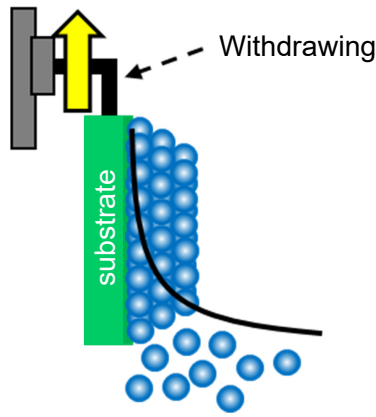
Figure 1.11 Schematic of the dip coating method.

utilizes the phenomenon that the suspension concentrates and crystallizes on a horizontal substrate under a silicone oil coating. The oil coating method has the advantages that the solvent evaporation rate of the suspension can be controlled, and the formation of cracks due to volume shrinkage can be prevented by infiltration of silicone oil into the voids of the particles during the solvent evaporation. Fudouzi et al. succeeded in producing colloidal crystals with a particle size of 200 μm or more on a substrate of 75 cm^2 without special equipment [38]. They also reported its application as a sensor that changes color in response to environmental changes using the unique optical property of the colloidal crystal of which structural color changes due to microscopic deformation [41, 42]. For example, research has been reported on smart materials [43] that can easily detect liquids, and strain visualization sheets [44] that allow visual inspection of deformation of structural materials, using the property that the structural color changes due to the swelling phenomenon.
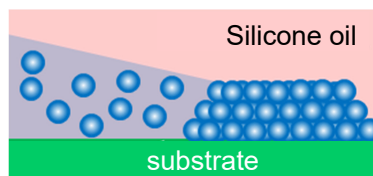
Figure 1.12 Schematic of the oil coating method.

The above method has the merit that colloidal crystals can be easily prepared without the need for special equipment, since colloidal crystals are formed by self-assembly of the colloidal particles. However, these methods need a very long time for the film fabrication. Therefore, to realize the industrial low cost and mass production, a faster film fabrication

17

technique has been desired.

1.3 The electrophoretic deposition method

Recently, electrophoretic deposition (EPD) is becoming one of the promising candidates to realize the rapid colloidal crystal film fabrication.

The EPD process itself is a widely used coating process for many industrial applications. This process is characterized by the migration of colloidal particles in a liquid under an electric field, i.e., electrophoresis, and the subsequent deposition onto an electrode. The rubber coating by means of electrodeposition has been known since 1925 based on the fact that the colloid particles in latex are generally negatively charged [45]. This negatively charged nature leads to the subsequent research of the EPD of polystyrene (PS) spheres to form colloidal crystals, together with the inquiry of forming photonic crystals.

As an alternative method to fabricate the colloidal crystal films, the electrophoretic deposition (EPD) method [46] was focused in this work. The EPD method is positioned as one of the colloid processes. Solidification molding is performed by applying an electric field to the suspension of the raw material powder and causing the particles to electrophoresis in the direction of the positive or negative electrode whose surface charge differs from that of the electrode. Although the mechanism of particle deposition in the EPD process is not completely elucidated, in general, particles migrate under the application of an electric field, and when they reach the substrate surface, the repulsive potential between the particles decreases, resulting the agglomeration of the particles by van der Waals attraction. Figure 1.13 shows the migration and deposition of particles and ions in the suspension to which an electric field is applied. Particles following the electric double layer migrate in the solvent, and when they reach the substrate, they gradually lose their electric double layer and aggregate and deposit.

Whereas other colloidal crystal deposition methods are uniaxial growth, the EPD method is expected to significantly reduce the deposition time because particles are deposited in the perpendicular direction to the substrate. In addition, it is expected that the cost can be reduced because the base material can be easily scaled up and uniform coating can be performed on a large area in a short time [45, 47–53].

In 1999, Lopez et al. [49] produced colloidal crystals made of SiO_2 particles with
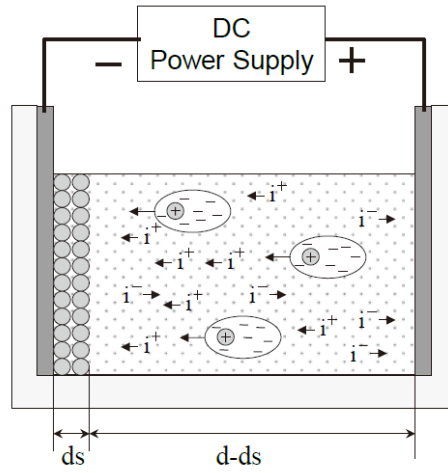
Figure 1.13 Schematic of electrophoresis and deposition of the particles and ions in the suspension [46].

a particle size in the range of 300 to 550 nm by the EPD method using a horizontal substrate, demonstrating the importance of applying the concept of EPD to colloidal sedimentation. In 2000, under the conditions of a deposition time of 30 min and an applied electric field strength of 4 V/cm, Rogach et al. produced a colloidal crystal made of PS nanoparticles with 200 - 300 nm diameters on a 3×0.5 cm^2 indium tin oxide (ITO) coated glass (ITO/glass) electrode with higher crystallinity than other methods, and dramatically improved the production time [47]. Since then, the research of colloidal crystal films was directed to faster fabrication, size enlargement, and quality control.

In 2006, Gonzalez et al. [50] mentioned the importance to consider the detailed arrangement of apparatus in EPD methods. They have succeeded in fabricating colloidal crystals with larger domain size and fewer defects by EPD method, considering the liquid flow from the view points of fluid dynamics, e.g. proposed by Von Karman et al. [54]. In 2008, Pu-Wei Wu [48] et al. arranged a substrate vertically, and under the conditions of deposition time 120 min, applied electric field strength of 20 V/cm, and pH 10, a colloidal crystal with an average domain size of 400 μm^2 was successfully obtained. The results show that the colloidal crystals were much larger than the particle area (<90 μm^2 [47, 55–64]) of the colloidal crystals obtained by other methods, so that highly crystalline colloidal crystals could be produced.

One of the investigations for size enlargement can be seen using SiO$_2$ (which has a narrower processing window than PS) colloidal crystals in 2008 by Huang et al. [48]. They demonstrated SiO$_2$ colloidal crystal film formation on a 1×1 cm^2 n-type Si wafer for

19

120 minutes. Recently, Katagiri et al. reported a SiO_2 colloidal crystal film on 1×4 cm^2 ITO/glass for 25 minutes [65]. These reports demonstrated a faster film fabrication rate than the conventional techniques that takes days [35, 36], however, the fabrication rate of the EPD technique has still remained in the range between 30 minutes and 2 hours. Either ethanol (EtOH) or a mixture of water and EtOH was chosen as the solvent for the EPD suspension [47, 48, 65]. This was effective to reduce the bubble formation caused by the electrolysis of water, and to realize a closest packing structure. However, the detailed effect of EtOH as well as that of other alcohols is still not yet clear regarding the EPD colloidal crystal film formation process.

In addition, the preparation of colloidal crystal films by the EPD process has been advanced, and the most recent topic is the production of amorphous colloid array by the EPD process [65, 66]. It has been pointed out that the feature of this aggregate is that it can replace ink and pigment with colloidal particles because it shows angle-independent structural color.

1.4   Interaction energy between two particles

At the surface of the particle in a liquid medium, the electric double layer is formed by the electric charge of the particle surface and opposite electric charge of the counter ions which exist around the particle surface in the suspension. The electric charge of the colloidal particle surface can be formed by the following two cases. One is the adsorption of either positive ions or negative ions at the particle surface. The other is the ionization of the constituent substances of the colloid particle itself. The electric double layer is considered to be composed of the fixed layer and the diffusion layer as shown in Fig.1.14. When the surface electric charge density of the particle, i.e. the electric charge per unit area, is σ_0, the opposite electric charge density of the counter ions is $-\sigma_0$. The part of $-\sigma_0$, i.e. $-\sigma_\delta$, exists in the fixed layer called Stern layer, and the rest of $-\sigma$ exists in the diffusion layer which forms ionic atmosphere at outside. This is called Gouy-Chapman diffusion double layer. Counter ions distribute in a wide area and do not exist at the constant distance from the particle surface. The average distance where counter ions exist from the particle surface is expressed by $1/\kappa$, and this is called the thickness of the electric double layer. This κ is a parameter of the Debye-Huckel equation [67], and can be expressed in Eq.1.1. Conventionally, slipping plane which separates mobile fluid from

fluid that remains attached to the surface, is introduced. This is corresponding to the thickness of the electric double layer. ζ potential is considered to be the electric potential at the slipping plane.

$$\kappa = \sqrt{\frac{8\pi F^2}{1000\epsilon RT}} \times \sqrt{J} \qquad (1.1)$$

where F, ϵ, R and T are faraday constant, dielectric constant of the solvent, gas constant and absolute temperature, respectively. J is an ionic strength and is expressed as follows with the electrolyte concentration in the solvent, C, and the valence of the ions, Z;

$$J = \sum Z^2 C \qquad (1.2)$$

Therefore, by the enlargement of the ionic strength adding the electrolytes in the colloidal solution, the thickness of the electric double layer $1/\kappa$ decreases. Further, by the increase of the counter ion valence, the shrinking effect of the electric double layer becomes remarkable.

The concentration of the electrolytes in the suspension becomes important if the aggregation of particles on the electrode substrates accords the DLVO (Derjaguin-Landau-Verwey-Overbeek) theory [68]. DLVO theory is formulated by the former Soviet Union group of Derjaguin-Landau et al. and the Netherlands group of Verwey-Overbeek et al. When the stability of the colloid dispersion system is discussed, DLVO theory is frequently used. Major acting forces which affect the particle dispersion and aggregation phenomena in a liquid medium are electrostatic repulsion (V_R), van der Waals attractive force (V_A), gravity (V_G), and buoyancy (V_B). V_G and V_B are not considered by DLVO theory though they are also major forces acting on the particles. Especially in the case of particles dispersed in the suspension, the dominant forces to control the particle dispersion and aggregation are V_R and V_A, and the interaction energy between particles are expressed as follows;

$$V = V_R + V_A \qquad (1.3)$$

Figure 1.15 shows the relation between interaction energy and particle distance, r. The repulsive energy V_R decrease with r exponentially in the relation ($e^{-\kappa r}$), while the absolute value of the attractive energy V_A decreases in inverse proportion to the square of the

A

Electric charge

σ_0 $-\sigma_\delta$ $-\sigma_0$ $-\sigma$

Particle surface

Diffusion layer

Fixed layer: Stern layer

B

Electric potential

φ_0

Stern plane

Slipping plane

Electric double layer

φ_δ

ζ

0

$1/\kappa$

δ

Distance from the particle surface
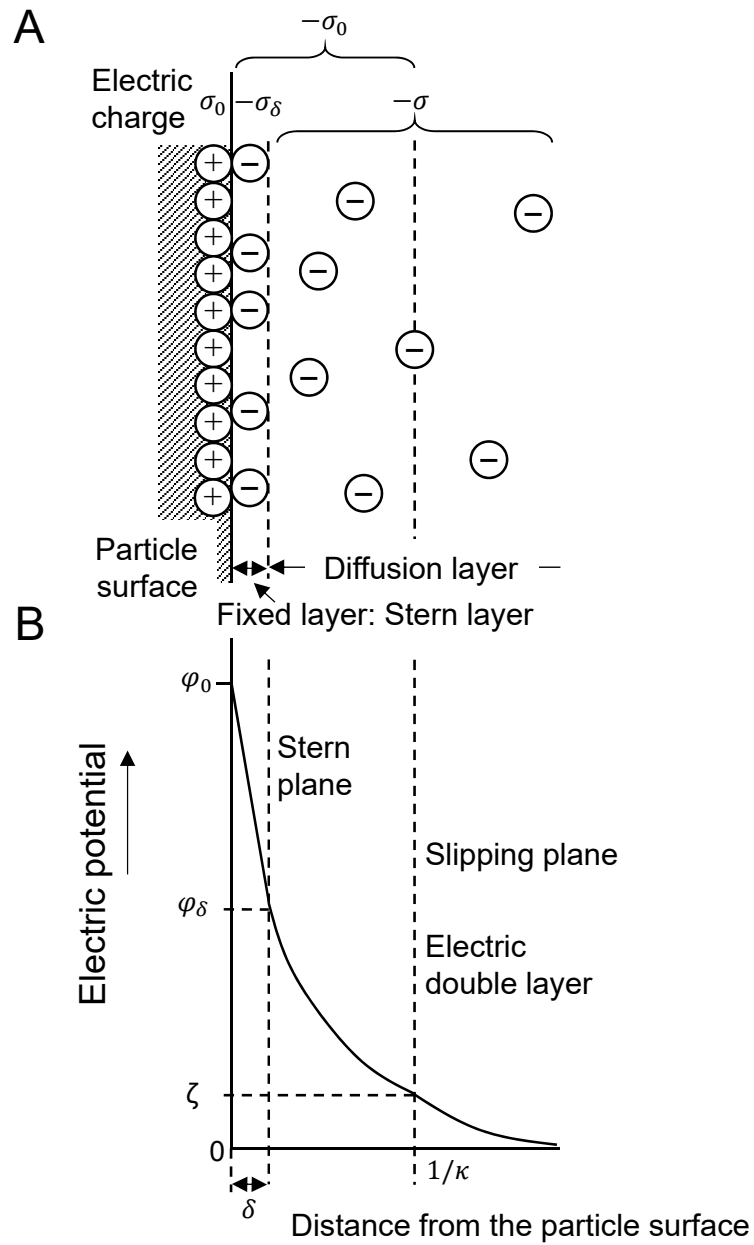
Figure 1.14 Structure of the electric double layer (A) and the electric potential curve (B).

distance r $(\frac{1}{r^2})$ (when r becomes long, it decreases inversely proportional to r^6). The total energy combined by these two energies, shows the general behavior of two particles when they come close each other. When the distance is relatively long, weak attractive energy is dominant. When the distance gets shorter, the repulsive force becomes dominant. When particles get closer further over the maximum point (V_{max}), the attractive energy becomes dominant. Therefore, particles need to get over the maximum point of the interaction energy so that particles get closer and aggregate. If this maximum point of the interaction energy is bigger than the thermal kinetic energy of particles, particles cannot get closer over the maximum point. Even if particles get closer, they rebound from the shortest distance, and cannot aggregate. In this condition, a colloidal suspension is stable without particle aggregation.
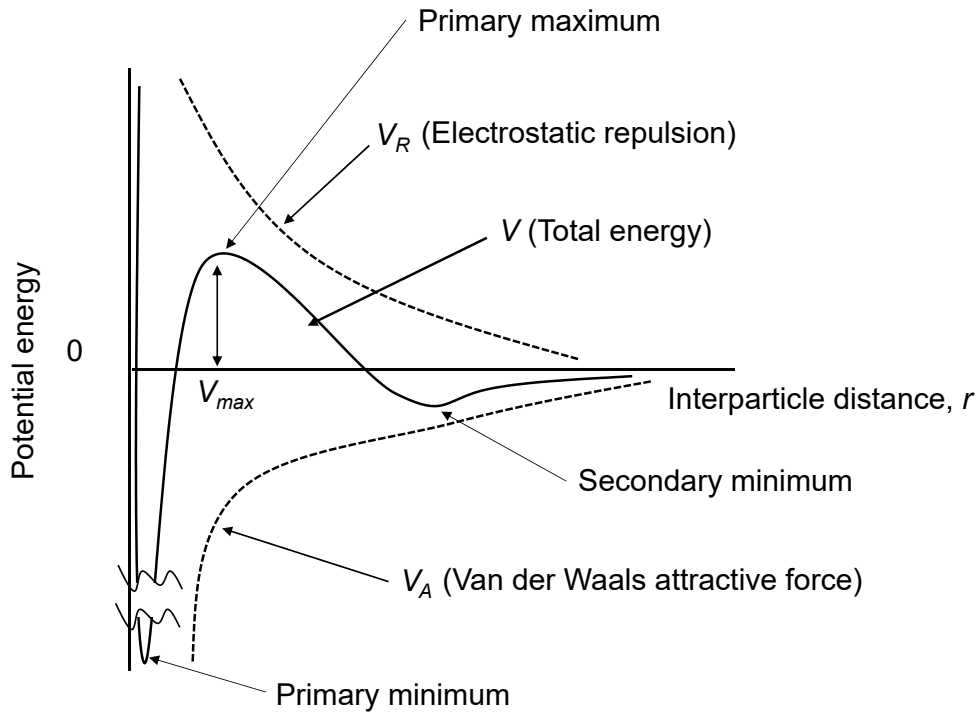
Figure 1.15 Interaction energy potential curve between particles in the suspension.

For the case of the certain colloidal particles, the height of the maximum point of the interaction energy is mostly defined by the potential curve of the electrostatic repulsion. The electrostatic repulsion becomes large when the ζ potential of the particle and/or the thickness of the electric double layer $1/\kappa$ becomes large, and therefore are affected strongly by the concentration of the electrolytes and the valence of the ions. This means that the change of the electrolyte concentration bring the change of the total potential energy curve shape. Figure 1.16 shows the effect of the electrolyte concentration on

23

the interparticle interaction energy. The curve (a) of Fig.1.16 is the case of the low electrolyte concentration. In this case, the height of the maximum point is enough high, and the colloidal suspension is stable without aggregation. However, by increasing the electrolyte concentration, the curve (a) moves to the curve (b) and (c). By the increase of the electrolyte concentration, a part of the particle surface charge is neutralized, and the thickness of the electric double layer becomes thinner. Consequently, the electric repulsion force decreases, and particles begin to aggregate. As shown in Fig.1.16-(b), the height of the maximum point becomes quit low, and particles get close easier because particles can get over the maximum point easier. Under the very high electrolyte concentration of Fig.1.16-(c), the maximum point disappears, resulting the inevitable aggregation of the particles.

Figure 1.16 Effect of the electrolyte concentration on the interparticle interaction energy.

These explanation indicate that the low electrolyte concentration in the colloidal suspension makes the electric double layer thicker, and increase the dispersibility of particles in the suspension, which correspond to the stability of the suspension. This condition could be advantageous for the EPD growth of the colloidal crystal films.
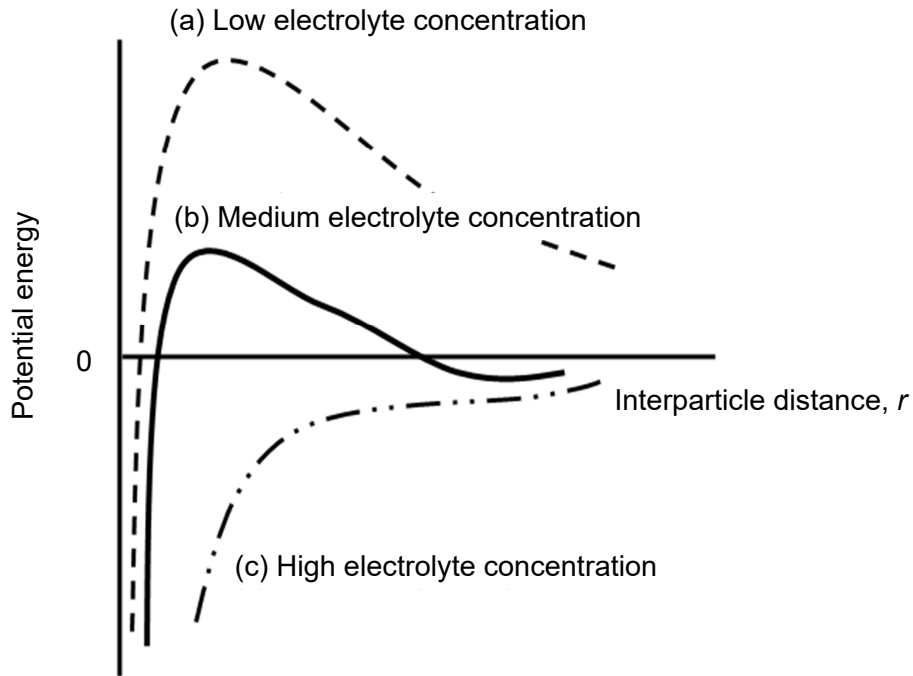
1.5　Purpose of this study and thesis overview

To date, there have been many examples of colloidal crystals produced by the EPD method, but the film area is relatively small (<4.0 cm^2 [27-33, 46, 47]) and no roll-shaped substrate has been used. In order to commercialize colloidal crystal films, it is necessary to break away from batch processing and mass-produce, so it is promising to combine roll-to-roll film formation technology with large-area substrates. Therefore, in this study, ITO-coated polyethylene terephthalate (PET) sheets (5×7.5, 10×15 cm^2) as a large-area roll-shaped substrate was used, and only polystyrene particles with aqueous or the mixture of H$_2$O and alcohol suspensions were used. The conditions for producing a colloidal crystal film at high speed from aqueous suspension mixed with ethanol (EtOH) by the EPD method were investigated. In addition, the subsequent crystallization process during solvent evaporation was discussed because the film immediately after EPD showed interesting behavior during drying in the experiment. Furthermore, silicone elastomer was filled in the gaps between the three-dimensionally accumulated colloidal particles, and a film in which polystyrene particles were fixed was fabricated. The possibility of applying the colloidal crystal film produced by the EPD method to a sensor for detecting volatile liquid and a sheet for visualizing strain was also examined.

　　This thesis is organized in six chapters as follows:

Chapter 2　Detailed investigation of the optimal condition for the EPD colloidal crystal film formation. The effect of the aqueous PS colloidal suspension and the mixture with alcohol on the colloidal crystal film growth is discussed.

Chapter 3　Investigation and discussion on the growth mechanism of the colloidal crystal films from the concentrated aqueous ethanol suspension.

Chapter 4　The effect of the poly-dimethylsiloxane (PDMS) elastomer filling to the interparticle space of the colloidal crystal film to realize the soft photonic crystals. The potential use of the colloidal crystal films with PDMS filling for the strain detection sensors is demonstrated.

Chapter 5　Characterization of swelling phenomena by immersing different kinds of silicone oil and other organic compounds as solvents. The possibility of the obtained

colloidal crystal film with PDMS elastomer filling as volatile liquid sensor is demonstrated.

Chapter 6 The general conclusions of my research and future prospects are given.

References

[1] J. Sun, B. Bhushan, and J. Tong. Structural coloration in nature. *RSC Adv.*, 3:14862–14889, 2013.

[2] S. Kinoshita. Structural colors in the realm of nature. *World Scientific*, 2008.

[3] E. Armstrong and C. O'Dwyer. Artificial opal photonic crystals and inverse opal structures - fundamentals and applications from optics to energy storage. *J. Mater. Chem. C*, 3:6109–6143, 2015.

[4] B. Rondeau, E. Fritsch, F. Mazzero, J. P. Gauthier, B. Cenki-Tok, E. Bekele, and E. Gaillou. Play-of-color opal from wegel tena, wollo province, ethiopia. *GEMS and GEMOLOGY*, 46:90–105, 2010.

[5] Á. Blanco and C. López. Photonic crystals: fundamentals and applications. *Annual Review of Nano Research*, 1:81–152, 2006.

[6] E. Yablonovitch. Inhibited spontaneous emission in solid-state physics and electronics. *Phys. Rev. Lett.*, 58:2059–2062, 1987.

[7] S. John. Strong localization of photons in certain disordered dielectric superlattices. *Phys. Rev. Lett.*, 58:2486–2489, 1987.

[8] S. Noda. Photonic crystals. *Jpn. J. Optics*, 30:56–64, 2001.

[9] J. V. Sanders. Colour of precious opal. *Nature*, 204:1151–1153, 1964.

[10] F. Meseguer and R. Fenollosa. Non-close packed colloidal crystals. *J. Mat. Chem.*, 15:4577–4580, 2005.

[11] A. C. Arsenault, H. Miguez, V. Kitaev, G. A. Ozin, and I. Manners. A polychromic, fast response metallopolymer gel photonic crystal with solvent and redox tunability: A step towards photonic ink (P-Ink). *Adv. Mater.*, 15:503–507, 2003.

[12] H. Fudouzi and Y. N. Xia. Photonic papers and inks: Color writing with colorless materials. *Adv. Mater.*, 15:892–896, 2003.

[13] J. Zhang, Y. Li, X. Zhang, and B. Yang. Colloidal self-assembly meets nanofabrication: from two-dimensional colloidal crystals to nanostructure arrays. *Adv. Mater.*, 22:4249–4269, 2010.

[14] T. Zhang, Y. Ma, and L. Qi. Bioinspired colloidal materials with special optical, mechanical, and cell-mimetic functions. *J. Mater. Chem. B*, 1:251–264, 2013.

[15] H. Cong, B. Yu, J. Tang, Z. Li, and X. Liu. Current status and future developments in preparation and application of colloidal crystals. *Chem. Soc. Rev.*, 42:7774–7800, 2013.

[16] A. Stein, B. E. Wilson, and S. G. Rudisill. Design and functionality of colloidal-crystal-templated materials-chemical applications of inverse opals. *Chem. Soc. Rev.*, 42:2763–2803, 2013.

[17] N. Vogel, M. Retsch, C. A. Fustin, A. D. Campo, and U. Jonas. Advances in colloidal assembly: the design of structure and hierarchy in two and three dimensions. *Chem. Rev.*, 115:6265–6311, 2015.

[18] C. F. Lai and Y. C. Wang. Colloidal photonic crystals containing silver nanoparticles with tunable structural colors. *Crystals*, 6:61–1–10, 2016.

[19] K. Lee and S. A. Asher. Photonic crystal chemical sensors: pH and ionic strength. *J. Am. Chem. Soc*, 122:9534–9537, 2000.

[20] Y. J. Lee and P. V. Braun. Tunable inverse opal hydrogel pH sensors. *Adv. Mat.*, 15:563–566, 2003.

[21] O. L. J. Pursiainen, J. J. Baumberg, K. Ryan, J. Bauer, H. Winkler, B. Viel, and T. Ruhl. Compact strain-sensitive flexible photonic crystals for sensors. *Appl. Phys. Lett.*, 87:101902, 2005.

[22] Y. Iwayama, J. Yamanaka, Y. Takiguchi, M. Takasaka, K. Ito, T. Shinohara, T. Sawada, and M. Yonese. Optically tunable gelled photonic crystal covering almost the entire visible light wavelength region. *Langmuir*, 19:977–980, 2003.

[23] H. Fudouzi and T. Sawada. Photonic rubber sheets with tunable color by elastic deformation. *Langmuir*, 22:1365–1368, 2006.

[24] A. S. Dimitrov and K. Nagayama. Continuous convective assembling of fine particles into two-dimensional arrays on solid surfaces. *Langmuir*, 12:1303–1311, 1996.

[25] S. Rakers, L. Chi, and H. Fuchs. Influence of the evaporation rate on the packing order of polydisperse latex monofilms. *Langmuir*, 13:7121–7124, 1997.

[26] A. van Blaaderen, R. Ruel, and P. Wiltzius. Template-directed colloidal crystallization. *Nature*, 385:321–324, 1997.

[27] R. Mayoral, J. Requena, J. S. Moya, C. López, A. Cintas, H. Miguez, F. Meseguer, L. Vázquez, M. Holgado, and A. Blanco. 3D long-range ordering in ein SiO_2

submicrometer-sphere sintered superstructure. *Adv. Mater.*, 9:257–260, 1997.

[28] P. Jiang and M. J. McFarland. Large-scale fabrication of wafer-size colloidal crystals, macroporous polymers and nanocomposites by spin-coating. *J. Am. Chem. Soc.*, 126:13778–13786, 2004.

[29] A. Mihi, M. Ocana, and H. Miguez. Oriented colloidal-crystal thin films by spin-coating microspheres dispersed in volatile media. *Adv. Mater.*, 18:2244–2249, 2006.

[30] S. Reculusa and S. Ravaine. Synthesis of colloidal crystals of controllable thickness through the Langmuir-Blodgett technique. *Chem. Mater.*, 15:598–605, 2003.

[31] S. H. Park, B. Gates, and Y. Xia. A three-dimensional photonic crystal operating in the visible region. *Adv. Mater.*, 11:462–466, 1999.

[32] Y. Fu, Z. Jin, G. Liu, and Y. Yin. Self-assembly of polystyrene sphere colloidal crystals by in situ solvent evaporation method. *Synth. Met.*, 159:1744–1750, 2009.

[33] J. Kleinert, S. Kim, and O. D. Velev. Electric-field-assisted convective assembly of colloidal crystal coatings. *Langmuir*, 26:10380–10385, 2010.

[34] T. Kanai, T. Sawada, A. Toyotama, and K. Kitamura. Air-pulse-drive fabrication of photonic crystal films of colloids with high spectral quality. *Adv. Funct. Mater.*, 15:25–29, 2005.

[35] P. Jiang, J. F. Bertone, K. S. Hwang, and V. L. Colvin. Single-crystal colloidal multilayers of controlled thickness. *Chem. Mater.*, 11:2132–2140, 1999.

[36] Z. -Z. Gu, A. Fujishima, and O. Sato. Fabrication of high-quality opal films with controllable thickness. *Chem. Mater.*, 14:760–765, 2002.

[37] B. Gates and Y. Xia. Fabrication and characterization of chirped 3D photonic crystals. *Adv. Mater.*, 12:1329–1332, 2000.

[38] H. Fudouzi. Fabricating high-quality opal films with uniform structure over a large area. *J. Coll. Interf. Sci.*, 275:277–283, 2004.

[39] K. Shimizu, S. Watanabe, and M. T. Miyahara. Controlling self-assembled periodic structures of colloidal particles by convective self-assembly. *J. Soc. Powder Technol., Japan*, 54:23–26, 2017.

[40] L. Wang and X. S. Zhao. Fabrication of crack-free colloidal crystals using a modified vertical deposition method. *J. Phys. Chem. C*, 111:8538–8542, 2007.

[41] H. Fudouzi. Optical properties caused by periodical array structure with colloidal particles and their applications. *J. Soc. Powder Technol., Japan*, 43:287–294, 2006.

[42] H. Fudouzi. Colloidal photonic crystal films: Fabrication and tunable structural color and applications. *Nanomaterials and Nanoarchitectures, Springer*, Chapter 1:1–19, 2015.

[43] H. Fudouzi and T. Sawada. Photonic crystal sensing of components of a liquid mixture using an optical fiber spectrometer. *Prod. of SPIE*, 6767:676704, 2007.

[44] H. Fudouzi, T. Sawada, Y. Tanaka, I. Ario, T. Hyakutake, and I. Nishizaki. Smart photonic coating as a new visualization technique of strain deformation of metal plates. *Proc. SPIE*, 8345:83451S, 2012.

[45] S. E. Sheppard and L. W. Eberlin. The electrodeposition of rubber. *Ind. Eng. Chem.*, 17:711–714, 1925.

[46] T. Uchikoshi. Microstructure design of ceramics by controlling the dispersion of fine particles in a liquid, and the application of the design technique to fabricate novel materials. *The Micromeritics*, 57:36–42, 2014.

[47] A. L. Rogach, N. A. Kotov, D. S. Koktysh, J. W. Ostrander, and G. A. Rgaisha. Electrophoretic deposition of latex-based 3D colloidal photonic crystals: A technique for rapid production of high-quality opals. *Chem. Mater.*, 12:2721–2726, 2000.

[48] Y. J. Huang, C. H. Lai, and P. W. Wu. Fabrication of large-area colloidal crystals by electrophoretic deposition in vertical arrangement. *Electrochem. Solid State Lett.*, 11:P20–P22, 2008.

[49] M. Holgado, F. García-Santamaría, A. Blanco, M. Ibisate, A. Cintas, H. Míguez, C. J. Serna, C. Molpeceres, J. Requena, A. Mifsud, F. Meseguer, and C. López. Electrophoretic deposition to control artificial opal growth. *Langmuir*, 15:4701–4704, 1999.

[50] M. Yoldi, W. González-Vi nAs, M. C. Arcos, and R. Sirera. Electrophoretic deposition of colloidal crystals assisted by hydrodynamic flows. *J. Mater. Sci.*, 41:2965–2969, 2006.

[51] J. Hamagami. Fabrication of particle assembly by using electropboretic deposition process. *J. Soc. Powder Technol., Japan*, 45:229–235, 2008.

[52] C. H. Lai, Y. J. Huang, P. W. Wu, and L. Y. Chen. Rapid fabrication of cylindrical colloidal crystals and their inverse opals. *J. Electrochem. Soc.*, 157:P23–P27, 2010.

[53] D. Mokude, A. Takasu, and M. Higuchi. Electrophoretic non-ionic nano-spheres (latexes) for structural coloring. *Polymer*, 117:243–248, 2017.

[54] P. J. Zandbergen and D. Dijkstra. Von karman swirling flows. *Annu. Rev. Fluid*

Mech., 19:465–491, 1987.

[55] L. Liu, P. Dong, R. Liu, Q. Zhou, X. Wang, G. Yi, and B. Cheng. Preparation and self-assembly of uniform TiO_2/SiO_2 composite submicrospheres. *J. Colloid Interface Sci.*, 288:1–5, 2005.

[56] Y. Masuda, T. Itoh, M. Itoh, and K. Koumoto. Self-assembly patterning of colloidal crystals constructed from opal structure or NaCl structure. *Langmuir*, 20:5588–5592, 2004.

[57] Y. H. Ye, F. LeBlanc, A. Haché, and V. V. Truong. Self-assembling three-dimensional colloidal photonic crystal structurewith high crystalline quality. *Appl. Phys. Lett.*, 78:52–54, 2001.

[58] C. A. Fustin, G. Glasser, N. W. Spiess, and U. Jonas. Parameters influencing the templated growth of colloidal crystals on chemically patterned surfaces. *Langmuir*, 20:9114–9123, 2004.

[59] P. Ferrand, M. J. Minty, E. Egen, J. Ahopelto, R. Zentel, S. G. Romanov, and C. M. S. Torres. Micromoulding of three-dimensional photonic crystals on silicon substrates. *Nanotechnology*, 14:323–326, 2003.

[60] C. H. Chan, C. C. Chen, C. K. Huang, W. H. Weng, H. S. Wei, H. Chen, H. T. Lin, H. S. Chang, W. Y. Chen, and W. H. Chang. Self-assembled free-standing colloidal crystals. *Nanotechnology*, 16:1440–1444, 2005.

[61] R. C. Hayward, D. A. Saville, and I. A. Aksay. Electrophoretic assembly of colloidal crystals with optically tunable micropatterns. *Nature*, 404:56–59, 2000.

[62] E. Kumacheva, R. K. Golding, M. Allard, and E. H. Sargent. Colloid crystal growth on mesoscopically patterned surfaces: Effect of confinement. *Adv. Mater.*, 14:221–224, 2002.

[63] M. H. Kim, H. K. Choi, S. H. Im, and O. O. Park. Fabrication of robust, high-quality two-dimensional colloidal crystals from aqueous suspensions containing water-soluble polymer. *Appl. Phys. Lett.*, 88:143127, 2006.

[64] S. Badilescu, A. R. Hajiaboli, N. Seirafianpour, R. B. Sadeghian, M. Kahrizi, and V. V. Truong. Study of the structural evolution within polystyrene and polystyrene-gold composite colloidal crystals by atomic force microscopy and scanning electron microscopy. *Appl. Phys. Lett.*, 90:023113, 2007.

[65] K. Katagiri, Y. Tanaka, K. Uemura, K. Inumaru, T. Seki, and Y. Takeoka. Structural color coating films composed of an amorphous array of colloidal particles via

electrophoretic deposition. *NPG Asia Mater.*, 9:e355, 2017.

[66] K. Katagiri, K. Uemura, R. Uesugi, K. Inumaru, T. Seki, and Y. Takeoka. Structurally colored coating films with tunable iridescence fabricated via cathodic electrophoretic deposition of silica particles. *RSC Adv.*, 8:10776–10784, 2018.

[67] P. Debye and E. Huckel. The theory of electrolytes. I. Lowering of freezing point and related phenomena. *Physikalische Zeitschrift*, 24:185–206, 1923.

[68] M. Elimelech, J. Gregory, and X. Jia. Particle deposition and aggregation, 1st edition, measurement, modelling and simulation. *Elsevier*, 1995.

Chapter 2

Fast fabrication of PS colloidal crystal films by the electrophoretic deposition

2.1 Introduction

In this work, the EPD technique was chosen to fabricate the colloidal crystal films faster than the other techniques. Nevertheless, the fabrication rate of the previously reported EPD technique has still remained in the range between 30 minutes and 2 hours. Either ethanol (EtOH) or a mixture of water and EtOH was chosen as the solvent for the EPD suspension [1–3]. This was effective to reduce the bubble formation caused by the electrolysis of water, and to realize a closest packing structure. However, the detailed effect of EtOH as well as that of other alcohols is still not yet clear regarding the EPD colloidal crystal film formation process.

In this study, removal of ionic contaminants, applications of a pulsed current and the effect of the water+alcohol mixture solvent on the formation of colloidal crystal film by the EPD process were investigated. Subsequently, the detail effect of the EtOH solvent was investigated taking into account the withdrawing rate of the substrate. Proper EPD conditions satisfying both the film quality and fast processing rate less than 10 minutes order were discussed. Based on these conditions, the large area EPD colloidal film formation was also demonstrated.

2.2 Experimental procedure

Figure 2.1A shows the photograph of the EPD apparatus. Either an ITO/glass or an ITO coated PET (polyethylene terephthalate) sheet (ITO/PET) was used as the substrate/anode. In contrast, a stainless-steel plate was used as the counter electrode/cathode. The distance from the ITO/glass or ITO/PET to the stainless-steel plate was 1.0 and 2.5 cm, respectively. After immersing the electrodes in the colloidal suspension, a DC voltage ranging from 3 to 20 V/cm was applied for 5 minutes (Fig.2.1B). Figure 2.1D shows the concept image of the electrophoresis, where PS colloid particles migrate to the anode electrode since the PS colloid is negatively charged in the suspension. After the EPD process, the substrate was removed from the suspension at different withdrawing rates from 0.1 to 10 mm/sec. The substrate was then dried horizontally at room temperature. The thickness of the films was several to several tens of microns depending on the preparation conditions. The effect of the pulse voltage application during the EPD process was also investigated for comparison with the constant voltage

[4, 5]. In the present experiment, the pulse voltage with a duty cycle of 50 %, i.e., the voltage is on half the time and off the other half as shown in Fig.2.1E, was applied. PS colloids were synthesized by the standard emulsion polymerization method [6]. Subsequently, the PS colloids were monodispersed in water. The average diameter of the PS colloids was $\phi 204.2$ nm. This as-formed aqueous PS colloidal suspension (7.54 wt%, Fig.2.1C) was used to investigate the effect of water as the solvent on the EPD. For the investigation of the alcohol solvent effect on the EPD, the aqueous PS colloidal suspension was mixed with different alcohols at several weight ratios. As alcohols, methanol (MeOH) (99.5 %, Kanto Chemical Co., Inc.), ethanol (EtOH) (99.5 %, Kanto Chemical Co., Inc.), 1-propanol (1-PrOH) (99.5 %, Kanto Chemical Co., Inc.), 2-propanol (2-PrOH) (99.7 %, Nacalai Tesque, Inc.), and 1-butanol (1-BuOH) (99 %, Kanto Chemical Co., Inc.) were used. The ITO/glass and ITO/PET were purchased from GEOMATEC Co., Ltd. and Sigma-Aldrich Co. LLC., respectively. The ITO/glass and ITO/PET were cut in the dimensions of 1×4 cm^2 or 2×3 cm^2, and 10×15 cm^2, respectively. The same sizes of a stainless-steel plate (SUS304), i.e., corresponding to those of the ITO/glass and ITO/PET, were obtained from the NILACO Corporation. The microstructure of the colloidal crystal films was observed using a Scanning Electron Microscope, SEM (JSM-6500F, JEOL). The local reflection spectra were measured by a miniature fiber-optic spectrometer (USB2000+, Ocean Optics).

2.3 Fabrication from the aqueous PS colloidal suspension

2.3.1 Effect of the constant voltage application and the dialysis of the suspension

Figure 2.2 shows optical photographs of the EPD grown films from the aqueous PS colloidal suspension at a constant voltage. These samples were fabricated for 5 minutes at different constant voltages, and subsequently removed at the withdrawing rate of 3 mm/sec. Notable was the formation of the non-flat and highly inhomogeneous film surface regardless of the applied voltage from 3 to 15 V/cm. As the applied voltage increased, the film thickness increased. At the applied voltage of 3 V/cm, thin film
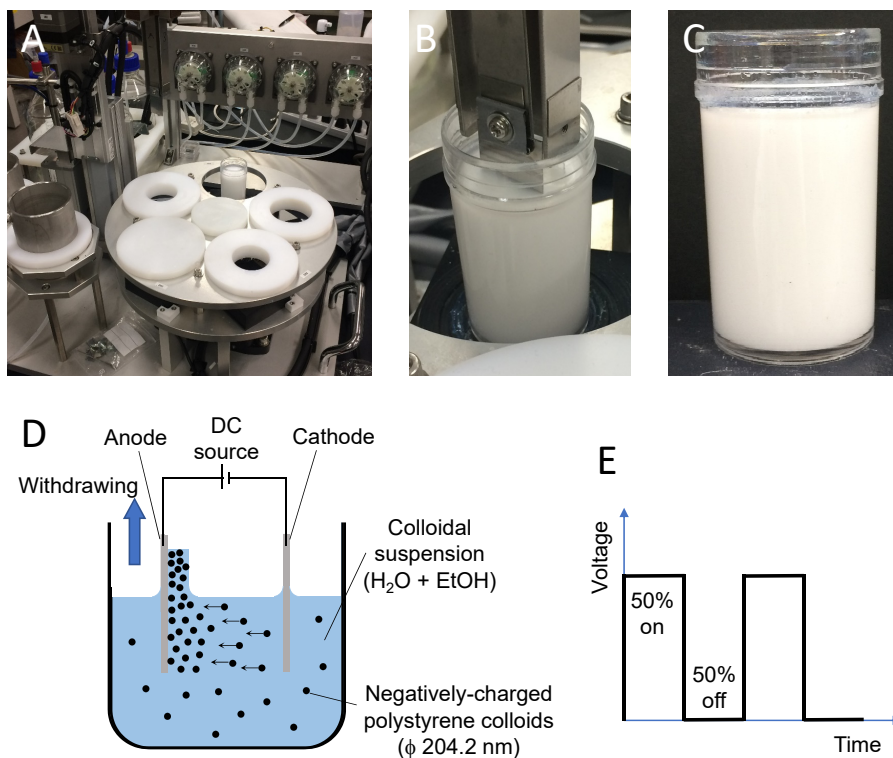
Figure 2.1 Photographs of (A) the EPD apparatus, (B) the EPD set-up, and (C) the PS colloidal suspension. (D) Schematic diagram of the EPD process, Anode: ITO/glass or ITO/PET, and Cathode: Stainless steel sheet. (E) Schematic of pulse voltage program.

formation was observed. Above the applied voltage of 10 V/cm, the produced film had many cracks on the surface. None of these samples showed an angle dependent structural color. The angle independent color changed from light blue to white depending on the applied constant voltage, i.e., the samples at 5 V/cm and 10 V/cm were light blue and white, respectively. This angle independent color change was clearly observed in the reflection spectra shown in Fig.2.3. By the increase in the applied constant voltage, the peak position shifted from the blue region to red region, and the width of the reflection peak increased. This spectra change is strongly related to the change in the film color depending on the applied voltage. The surface SEM images of the films fabricated using applied voltage of 5V/cm, shown in Fig.2.2 exhibit the aggregation of colloidal amorphous array of the PS particles. A somewhat flat image is shown at the higher magnification, while a completely inhomogeneous state is observed at the lower magnification. The inhomogeneous and non-flat film formation could be attributed to gas bubble generation by the electrolysis of the water-based suspension during the EPD process.

Applied voltage [V/cm]

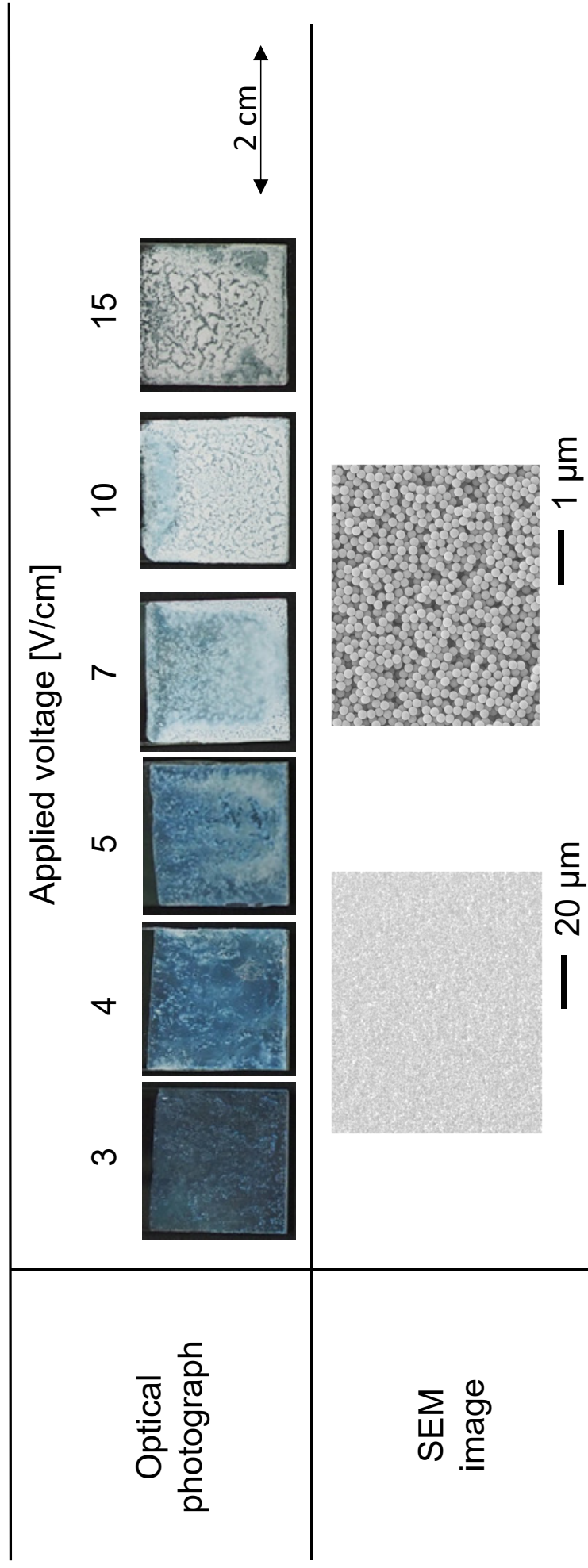|	3	4	5	7	10	15
Optical photograph						
SEM image						

20 µm

1 µm

2 cm

Figure 2.2 Optical photographs and surface SEM images of EPD films from the aqueous PS colloidal suspension under the different constant applied voltages. SEM images were taken from the sample fabricated at 5 V/cm applied voltage.
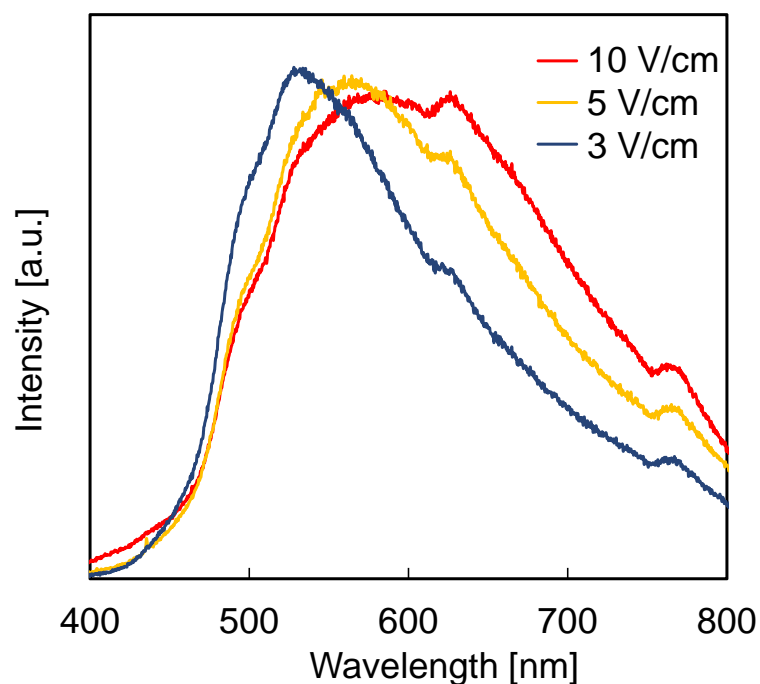
Figure 2.3 Reflection spectra of constant voltage EPD films from the aqueous PS colloidal suspension in Fig.2.2.

In order to avoid the electrolysis of the water-based suspension, dialysis of the suspension was considered. Dialysis was done by immersing the semipermeable cellulose membrane tube, which contained the aqueous PS colloidal suspension, into purified water. Since the semipermeable membrane gap was about 1 nm, electrolytes smaller than 1 nm were discharged outside of the semipermeable membrane, while PS particles with about a 200-nm diameter were not discharged. In this way, the concentration of electrolytes in the suspension decreased with time. A one-time dialysis was done for 1 day. Subsequently, another dialysis was done by exchanging the purified water. In order to lower the concentration of the electrolysis as low as possible, this process was repeated many times. After the dialysis, the EPD process was done at a constant voltage for 5 minutes with the substrate withdrawing rate of 3 mm/sec after the EPD. However, gas bubble generation due to the electrolysis of water was always observed. As shown in Fig.2.4, the removal of electrolytes in the suspension was evidenced by the decrease in the electrical conductivity and the increase in pH, and became more effective by repeating the dialysis. In this way, i.e., by increasing the number of dialyses, the films became flat and dense. However, peeling off of the film increased by repeating the dialysis, even though a higher constant voltage was applied. Furthermore, any of obtained films showed a white color without

any angle dependent structural color. These results show that gas bubble inclusion seems to be suppressed, however, the homogeneity of the film was not improved and the particle arrangement was still amorphous.

Applied voltage [V/cm]	7	5	10
Optical photograph ◄——— 1 cm ———►			
Dialysis	non	4 times	7 times
Electrical conductivity [mS/cm]	1.475	0.192	0.032
pH	2.04	2.96	4.08

Figure 2.4 Optical photographs of the EPD films obtained from the aqueous PS colloidal suspension at constant voltage, as well as the change in the electrical conductivity and pH of the suspension after the dialysis.

2.3.2   Effect of the pulse voltage application

Since the dialysis was not effective, applying the pulse voltage instead of a constant voltage was investigated. Charged particles in the suspension continue to migrate by the inertia force even at the applied voltage is 0 V. The EPD process was done under the pulse voltage for 5 minutes at the substrate before withdrawal at the rate of 3 mm/sec after the EPD. Figure 2.5 shows optical photographs of the obtained films. All the films have shown an angle independent white color. The applied pulse voltage required for film formation decreased as the pulse voltage interval increased. With short pulse voltage intervals, i.e., 2 and 3 ms, particle agglomeration on the substrate was reduced, even with applied pulse voltages as high as 80 or 100 V/cm. When the pulse voltage interval was long, i.e., 60 and 100 ms, the film was inhomogeneously formed due to the bubble generation by the electrolysis of water, even though the applied pulsed voltage was low such as 8 and 15 V/cm. On the contrary, when the pulse voltage interval was in the range of 5 and 10

ms, obtained films were relatively uniform without gas bubble generation during the EPD process. Figure 2.5 also shows SEM images of the film obtained using 20 V/cm applied pulse voltage with 10 ms pulse voltage interval for 5 min. These images show a random particle arrangement with an amorphous state. However, particles were arranged denser than that shown in Fig.2.2, since gas bubble generation was prevented.

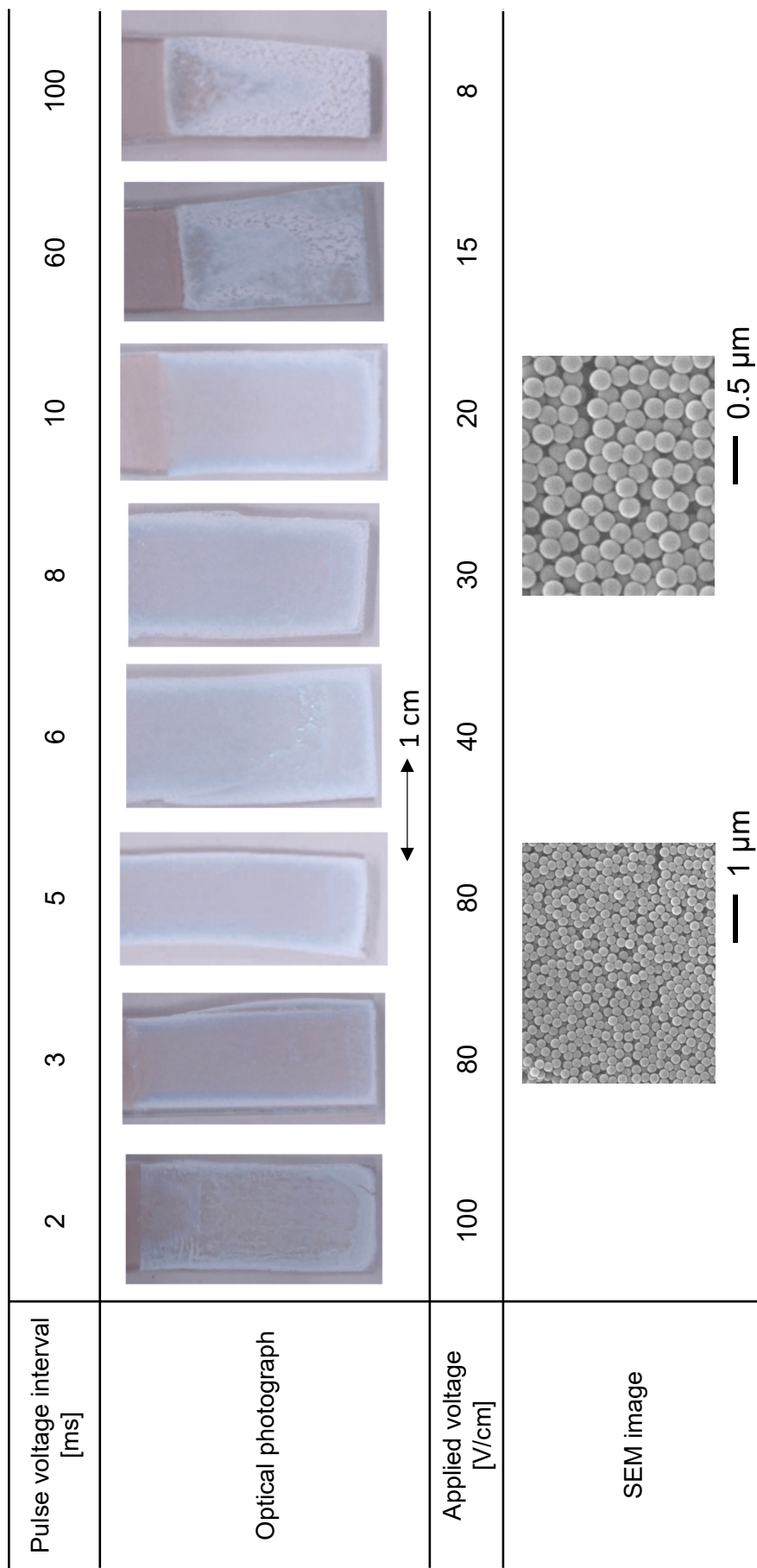| Pulse voltage interval [ms]	2	3	5	6	8	10	60	100
Optical photograph								
Applied voltage [V/cm]	100	80	80	40	30	20	15	8
SEM image								

Figure 2.5 Optical photographs of the EPD film obtained from the aqueous PS colloidal suspension at different pulse voltages, as well as the SEM image of the obtained film after 20 V/cm applied pulse voltage with 10 ms pulse voltage interval for 5 min.

40

2.4 Fabrication from the aqueous alcohol solvents

2.4.1 Effect of different alcohols

These results show that the aqueous PS colloidal suspension is not preferable to form the colloidal crystal film. Based on these results, the effect of aqueous alcohol on the EPD film fabrication was examined. Figure 2.6 shows the effect of different aqueous alcohol solvents on the colloidal crystal film formation by the EPD process. The constant voltage applied duration and subsequent substrate withdrawing rate were 5 minutes and 3 mm/sec, respectively. Alcohols miscible with water, such as MeOH, EtOH, 2-PrOH and 1-PrOH, were mixed with the aqueous PS colloidal suspension at the weight ratio of 2 : 1. The ratio between 1-BuOH and the aqueous PS colloidal suspension was intentionally adjusted to 1 : 1, because 1-BuOH is known to be non-miscible with water. When MeOH was used as the alcohol solvent, highly uniform and flat colloidal films were obtained, regardless of the applied voltage. A mixture with either EtOH or 2-PrOH as an alcohol solvent still realized uniform and flat films at over a 5 V/cm applied voltage. An applied voltage of 3 V/cm was not sufficient to realize a high-quality film. The use of 1-PrOH as the alcohol solvent seemed not very good because the obtained films are no longer flat and uniform. Even many macro defects that look like voids could be visually observed. All the films obtained from MeOH, EtOH, 2-PrOH and 1-PrOH-mixtured suspensions with a constant applied voltage have shown a clear angle dependent structural color of light blue. Gas bubble generation by electrolysis was also not observed during the EPD process. Figure 2.7 shows the comparison of the reflection spectra of colloidal crystals fabricated from an aqueous colloidal PS suspension mixed with EtOH and that of fabricated from the aqueous PS colloidal suspension. The sample obtained using the EtOH-mixed suspension clearly showed the blue color peaked spectrum, while the sample obtained using water suspension showed a broader spectrum. The 1-BuOH based solvent could not form a film itself, and even the PS particles could not adhere well to the substrate. These results show that MeOH, EtOH and 2-PrOH are suitable alcohol solvents. However, as MeOH and 2-PrOH are more toxic than EtOH, EtOH was chosen for the following experiment as the preferred solvent.

Applied voltage [V/cm]

	3	4	5	7	10

1 cm

Mixing weight ratio

Suspension : MeOH = 1 : 2

Suspension : EtOH = 1 : 2

Suspension : 2-PrOH = 1 : 2

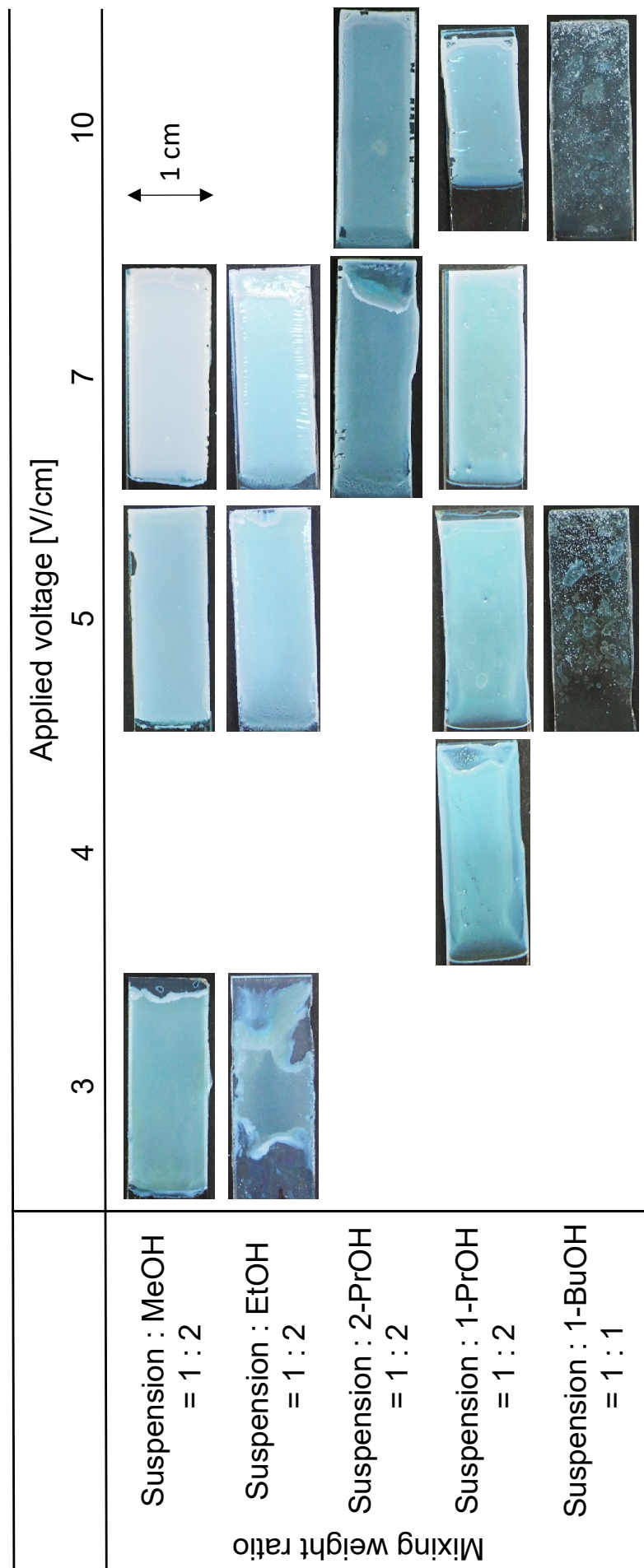Suspension : 1-PrOH = 1 : 2

Suspension : 1-BuOH = 1 : 1

Figure 2.6 Optical photographs of colloidal crystal films prepared by EPD from the aqueous PS colloidal suspensions mixed with different alcohol solvents under different constant applied voltages. Photographs are 90° rotated and shown sideways, i.e., substrates were withdrawn up from left side toward right side..
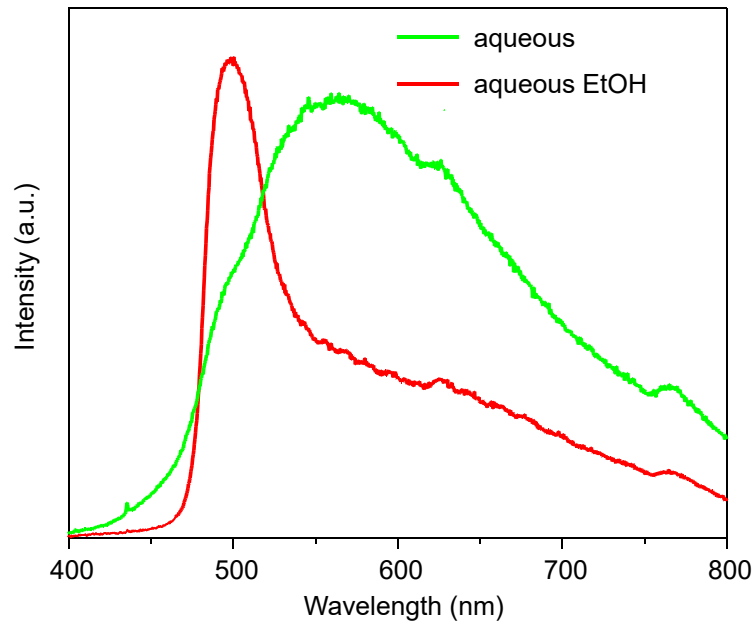
Figure 2.7 Reflection spectrum of EPD colloidal crystal film fabricated from an aqueous PS colloidal suspension mixed with EtOH (weight ratio of aqueous suspension : EtOH = 1:2) under constant voltage application of 5 V/cm. This is compared to that of the EPD film from the aqueous PS colloidal suspension.

Figure 2.8 shows optical photographs of the EPD grown colloidal crystal films at the different EtOH solvent ratios and applied voltages. All of these samples were prepared with a deposition time of 5 minutes and a subsequent withdrawing rate of 3 mm/sec. In general, samples fabricated from the EtOH-containing suspension have shown a light blue structural color with an angle dependency. The homogeneity and flatness of the film was dependent on the applied voltage and EtOH content in the suspension. In the case of the 74.2 Vol% EtOH suspension, only a 5 V/cm applied voltage formed a somewhat flat film surface, although both 4 V/cm and 7 V/cm could not. In the case of the 81.7 Vol% EtOH suspension, over a 5 V/cm applied voltage could form a relatively homogeneous and flat film surface. Independent of the applied voltage was revealed using the 92.5 Vol% EtOH suspension. At any applying voltage from 3 to 20 V/cm, a homogeneous and flat film surface was obtained. This could not be achieved by the suspension with a lower EtOH concentration. Additionally, the thickness of film increased by increasing the applied voltage.
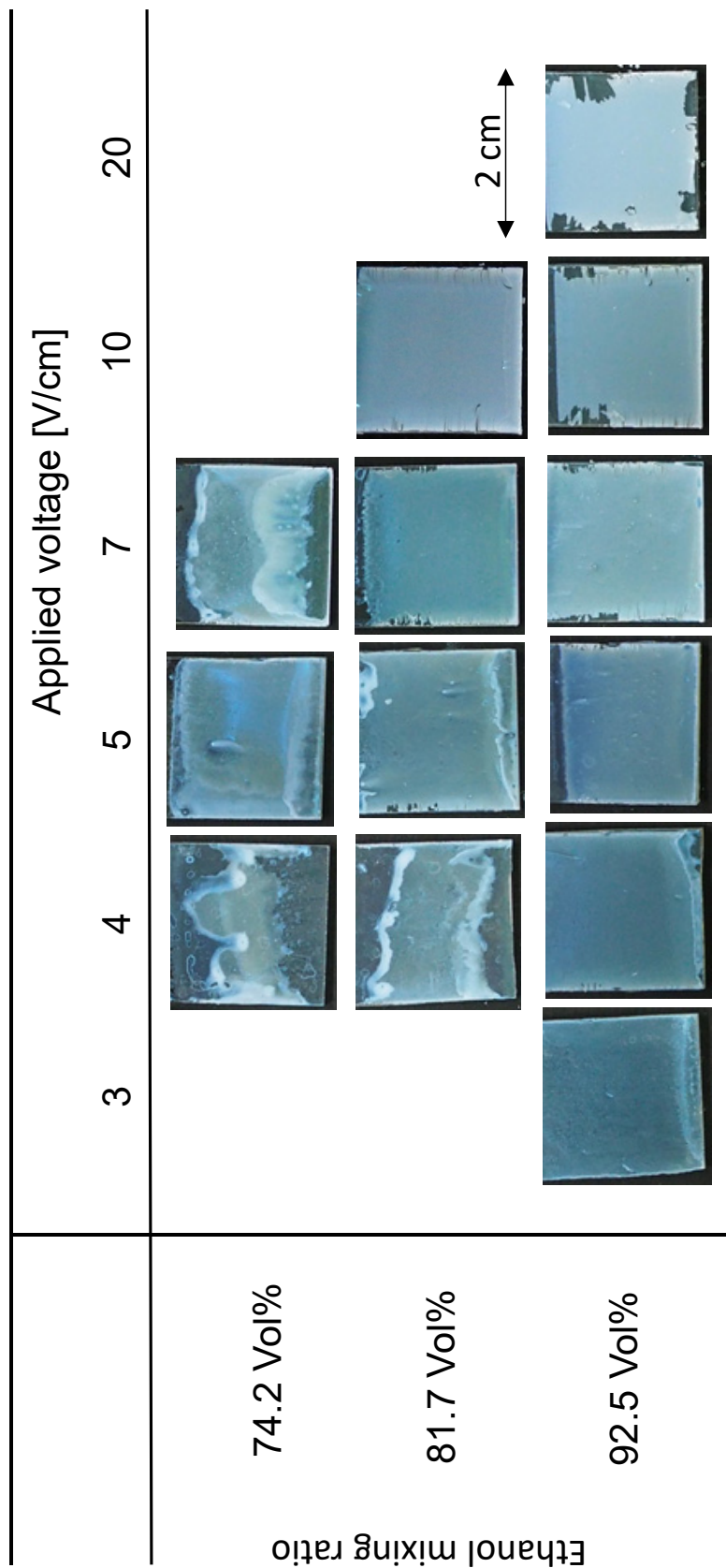
Figure 2.8 Optical photographs of colloidal crystal films prepared by EPD from suspensions with different EtOH solvent ratios and applied voltages. All films were fabricated at 5 V/cm applying voltage for 5 minutes and subsequent substrate withdrawing at 3 mm/sec.

Figure 2.9 shows surface SEM images of films obtained using EPD suspensions with different solvent ratios of EtOH and H_2O with an applied voltage of 5 V/cm for 5 min. In the case of the 74.2 and 81.7 Vol% EtOH suspensions, a periodic structure formation was observed at the higher magnification. However, the distance between the particles was still relatively high, and a number of voids and irregular particle arrangement could also be seen. This could be due to still higher proportion of water. Compared to the film surface from the aqueous PS colloidal suspension, grain formation was observed at a lower magnification. For the 92.5 Vol% EtOH suspension, the achievement of the closest packing in most of the areas, and fairly less structural defects, such as voids and an irregular particle arrangement, were clearly seen at the higher magnification. A larger grain size formation than from the other suspensions was also observed at the lower magnification. These results show that the mixture of EtOH and water in the EPD suspension is preferable, and that the higher EtOH concentration relative to water fabricates a better EPD colloidal crystal film.
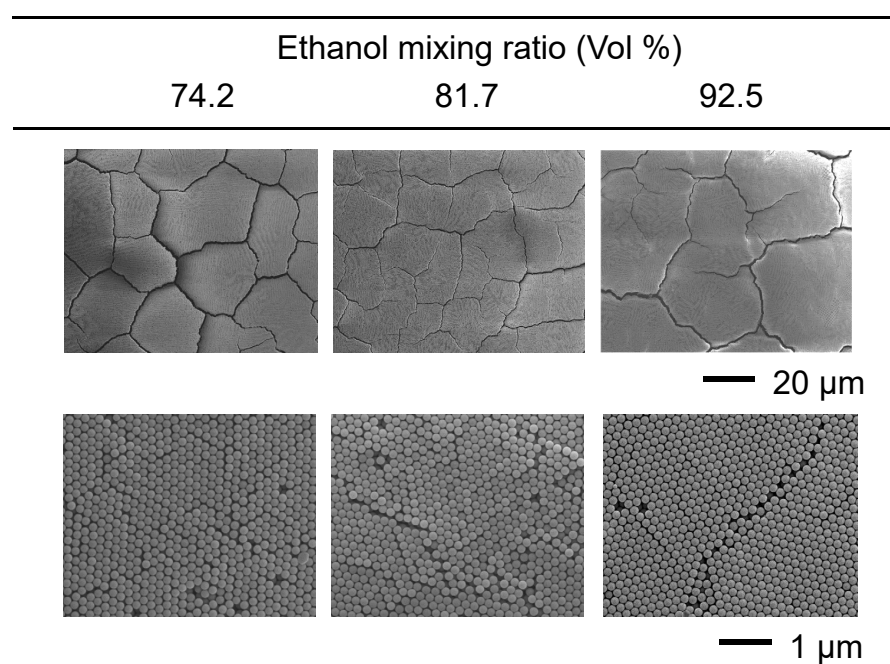
Figure 2.9 Surface SEM images of colloidal crystal films prepared by EPD from suspensions with different solvent ratios of EtOH and H_2O. All films were fabricated at 5 V/cm applying voltage for 5 minutes.

As shown in Fig.2.2-2.9, water is not preferable to form the colloidal crystal structure by EPD. This is due to the bubble generation by the electrolysis during the EPD process, but also the effect of hydrogen bonds. In the case of water, hydrogen bonds will be

dominant. Since the PS particles are slightly negatively charged, the PS particles were surrounded and bonded with hydrogen bonds by water molecules. As the water molecule is small, this effect is high. Consequently, water molecules disturb the self-assembly of the PS particles, i.e., the formation of the colloidal crystal structure is interrupted, and an amorphous state is formed. On the contrary, in the case of aqueous alcohol, the effect of hydrogen bonds is weak and independent of the increase in the carbon chain. Instead, the van der Waals force is dominant and dependent on the increase of the carbon chain. This affects the increase in the alcohol viscosity by the increase in the carbon chain, i.e., the viscosities of MeOH, EtOH, 2-PrOH, 1-PrOH and 1-BuOH are 0.594, 1.144, 1.77, 1.959 and 2.5875 mPa·s, respectively. This means that the mobility, i.e., the freedom, of the PS particles decreases by the increase in the carbon chain. Consequently, PS particles can self-assemble easier to form colloidal crystal films with MeOH and EtOH. In the case of MeOH, even a low voltage, such as 3 V/cm, was sufficient to form the colloidal crystal film, while no film formation was observed in the case of 1-BuOH due to the very low aggregation of PS particles on the electrode. Furthermore, the higher concentration of EtOH is advantageous to form the colloidal crystal film because the effect of water molecules, i.e., the effect of hydrogen bonding, is minimized. In this sense, the fact that the higher EtOH concentration was preferable to form the closely packed state, is understandable. The zeta potential of the PS particles in the different mixture ratios of EtOH and H_2O are shown in Table2.1. The measurement was performed using three differently-prepared suspensions. The zeta potentials in H_2O and EtOH exhibited higher absolute values, around -40 mV, while the H_2O and EtOH mixture showed somewhat similar values of around -10 mV irrespective of the EtOH concentration. In the mixed suspension of H_2O and EtOH, the zeta potential hardly changes even if the amount of EtOH added changes. From this, it is considered that the surface tension of the solvent and the drying rate, not the zeta potential, have a great influence on the quality of the colloidal crystals.

Table 2.1: Zeta potential of the PS particles in different mixture ratios of H_2O and EtOH. The measurement was performed using three differently prepared suspensions.

H_2O:EtOH (weight ratio)	1:0	9:1	7:1	4:1	1:1	0:1
Zeta potential_1 (mV)	-39.4	-10.8	-10.5	-12.0	-12.1	-41.0
Zeta potential_2 (mV)	-40.7	-12.0	-10.3	-11.7	-10.8	-46.3
Zeta potential_3 (mV)	-42.9	-13.6	-11.0	-12.1	-8.27	-45.1

According to the DLVO (Derjaguin-Landau-Verwey-Overbeek) theory [7, 8], interparticle forces for assembling particles can be described as the sum of the van der Waals force and the electrostatic repulsion. Changing the volume fraction of EtOH modifies the surface tension and viscosity of the mixed solvent. These changes, in turn, modify the competition between the stress relaxation due to cracking and the stress increase due to solvent loss [9]. However, these results imply that the bonding force of the liquid solvent is more dominant for the self-assembly of PS particles in the EPD.

2.4.2   Effect of substrate withdrawing rate

Figure 2.10 shows the effect of the substrate withdrawing rate on the EPD colloidal crystal film quality. When a substrate was withdrawn from the suspension at the rates of 0.1 and 0.5 mm/sec, no EPD colloidal crystal film was observed on the substrate. This indicated that this rate range was too slow to allow adhesion for the particles on the substrate, and the particles flowed back into the suspension. In the case of the 1.0 and 3.0 mm/sec withdrawing rates, a relatively uniform EPD colloidal crystal film was fabricated. When the rate was 5.0 mm/sec, the formed film became inhomogeneous. At the rate of 10 mm/sec, peeling off of the EPD colloidal crystal film was again observed. This indicated that particles could not continue to adhere on the substrate due to too fast a rate, and even the remaining particles could not form the proper structure. Figure 2.11 shows a comparison of the reflectance spectra from the samples in Fig.2.10. Samples with the withdrawn rate from 1.0 to 5.0 mm/sec show a structure color with a clear reflectance peak. Especially, the sample with the withdrawn rate at 3.0 mm/sec shows the highest reflectance, which corresponds to the highest quality film. These results show that the optimum withdrawing rate is 3.0 mm/sec. Additionally, this result shows that the colloidal crystallization is not taking place during the EPD process. EPD is defined by the electrophoresis phenomenon and subsequent deposition. However, if the deposition really takes place during the EPD process, peeling off phenomena by the different substrate withdrawing rate cannot be well explained. Rather than that, a 2-step process, i.e., aggregation of the particles on the substrate during the EPD process and subsequent particle deposition/formation of the colloidal crystal structure during the drying process, can well explain the phenomena. As for the formation of the colloidal crystals, it seems that the applied electric field effectively accumulates the

colloidal particles on the substrate surface. As a result, the suspension on the substrate was concentrated to an extremely high concentration. Immediately after the electric field is turned off, the accumulated particles in the wet state have not lost the electric double layer, and aggregation and immobilization are not yet completed. Therefore, when the withdrawal rate of the substrate is too fast or too slow, the accumulated particles slip down or are pulled back into the slurry. After the EPD process, the accumulated particles on the substrate are rearranged in the subsequent drying process and solidified by taking the closed-packing structure. In other words, it is considered that the EPD process plays a role in accumulating particles just before the transition from the random array to the periodic array.
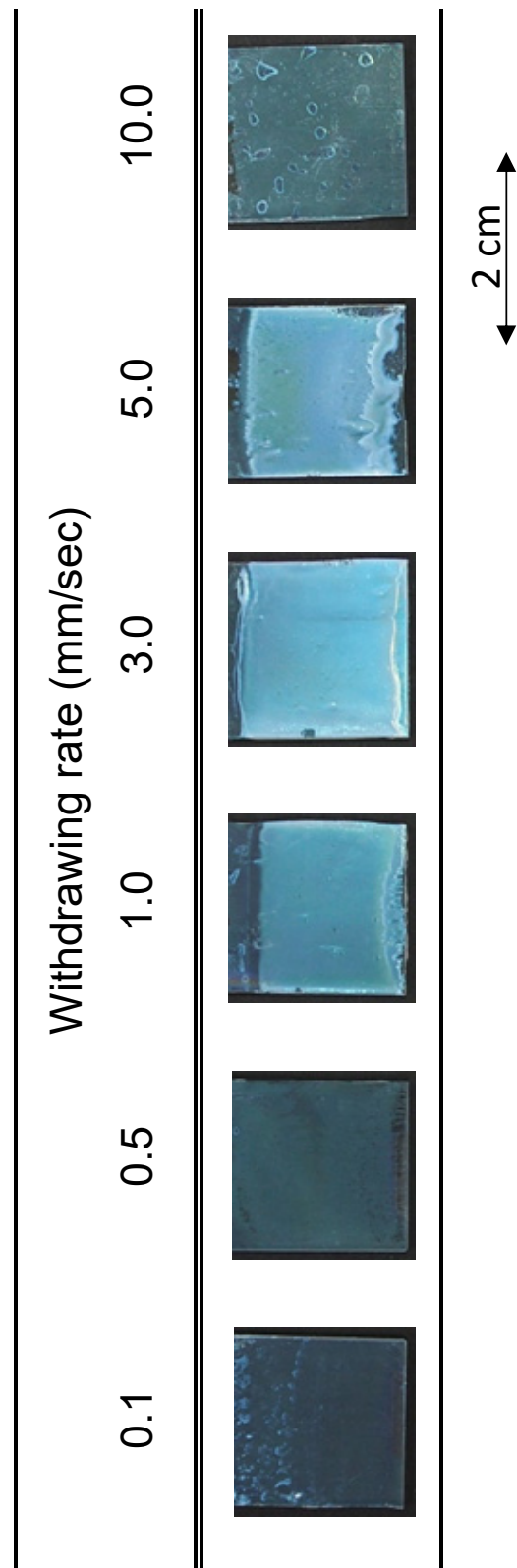
Figure 2.10 Optical photographs of colloidal crystal films fabricated by different withdrawing rates (0.1-10.0 mm/sec) from aqueous ethanol solution of 92.5 Vol%. EPD process conditions were 5 V/cm DC voltage for 5 minutes.
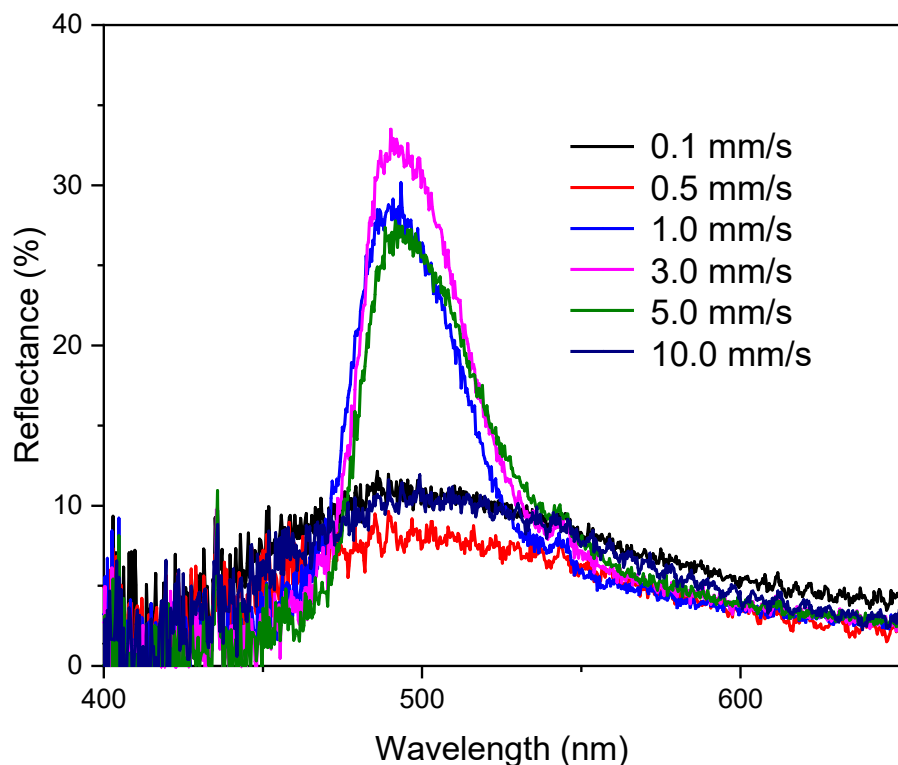
49

Figure 2.11 Reflectance spectra comparison of colloidal crystal films fabricated by different withdrawing rates (0.1-10.0 mm/sec) from ethanol solution of 92.5 Vol%. EPD process condition were at a constant DC of 5 V/cm for 5 minutes.

2.5 Fabrication of the large area colloidal crystal film

Figure 2.12A shows the effect of the surface area of the electrode substrates by the EPD process. The EPD colloidal crystal film was formed on the ITO/PET as a flexible large area substrate compared to the ITO/glass as a small area substrate. In the aqueous ethanol solution of 81.7 Vol%, which is not the best but still an acceptable concentration from the above results, 10 V/cm and 5 V/cm were applied using the ITO/PET and ITO/glass, respectively, for 5 min. The withdrawing rate of the substrates after EPD was 3 mm/sec for both cases. Both films, i.e., large area film as well as small area film, have shown flat and homogeneous EPD colloidal crystal film formation and a light blue structural color with an angle dependence. Figure 2.12B shows the cross-sectional SEM image of the large area film. The EPD colloidal crystal film had over 40 layers with a closest packing structure, which are sufficient for the colloidal crystal to show the structural color. In Fig.2.13, the reflection spectra measured at 4 different points on the

EPD colloidal crystal film on the ITO/PET (Fig.2.12A) are shown. A similar intensity and spectral shape peaking at around 500 nm, which correspond to those of the reflection spectrum obtained from the colloidal crystal film fabricated by the vertical deposition technique [10], were observed from every point. This indicated that the reflection from the large area EPD film on the ITO/PET is based on Bragg's reflection, and that this film achieved the closest packing structure of relatively high quality.
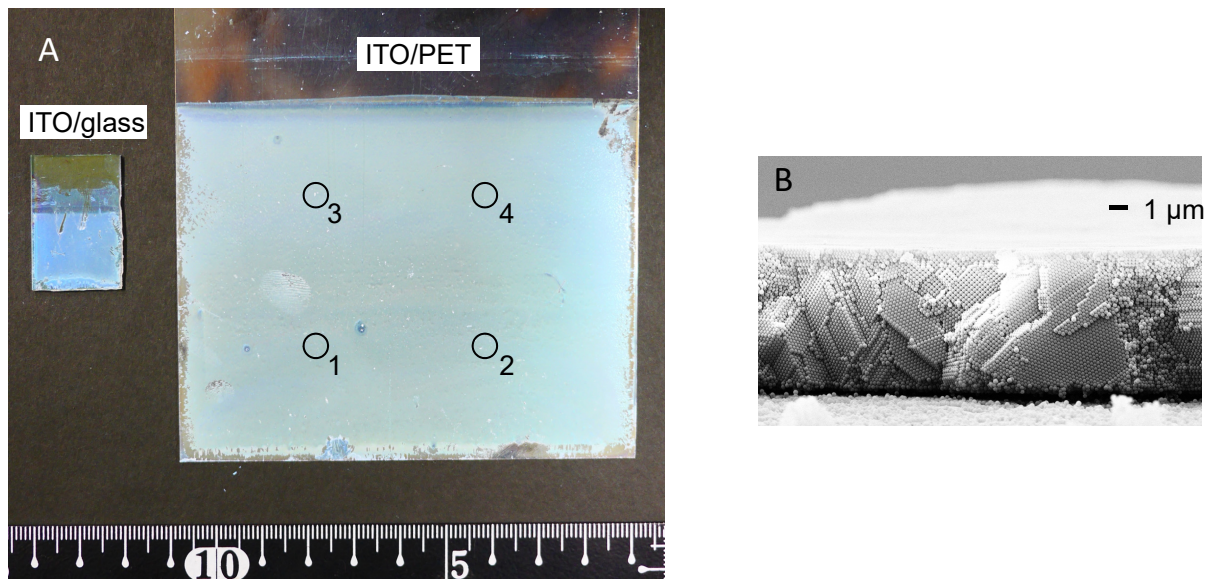

Figure 2.12 Optical photograph of EPD colloidal crystal film formed on ITO/PET compared with that on ITO/glass. Constant voltage of 10 and 5 V/cm was applied for ITO/PET and ITO/glass, respectively, for 5 minutes (A). Substrate withdrawing rate after EPD was 3 mm/sec for both cases. Black circles on ITO/PET are points where reflectance spectra were measured. Cross-sectional SEM image of EPD colloidal crystal film on the ITO/PET (B).

2.6   Summary

The optimum condition for the EPD colloidal crystal film formation was investigated in detail. The aqueous PS colloidal suspension was not appropriate due to the generation of gas bubbles during the electrolysis and formed only colloidal amorphous array. Dialysis and the application of a pulse voltage could avoid the gas bubble generation, however, particle self-assembly was still amorphous. As a suspension for the EPD process, the effectiveness of mixing EtOH and water was confirmed by testing several alcohols as solvents, and explained from the different viewpoints including hydrogen bond, van der Waals dispersion force, and mobility/freedom of PS particles. The higher the EtOH
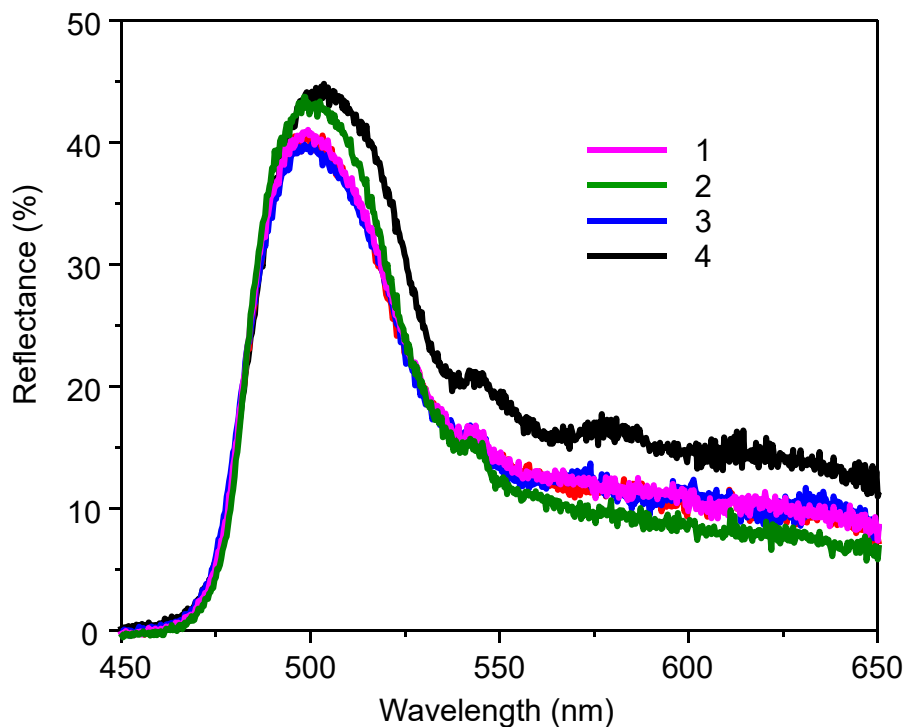
Figure 2.13 Reflectance spectra of EPD colloidal crystal film on ITO/PET measured at the points indicated in Fig.2.12A as black circles.

concentration, the better the colloidal crystal film formation. In the investigated range, the most preferable condition for the EPD colloidal crystal film formation was from the 92.5 Vol% aqueous EtOH suspension. The substrate withdrawing rate from the suspension also significantly affected the EPD colloidal crystal film fabrication. Too slow and too fast withdrawing rates were not good. The most preferable rate was 3.0 mm/sec. The large area colloidal crystal film formation by the EPD technique was also demonstrated. Comparable quality of EPD colloidal crystal films fabricated on small area ITO/glass and large area ITO/PET substrates was confirmed by the SEM observations and the reflectance spectra. These results demonstrate the advantage of the EPD technique for large scale production of colloidal crystal, taking into account the fast fabrication rate compared to the other conventional techniques. Additionally, a 2-step EPD colloidal crystal film formation mechanism was also implied.

References

[1] A. L. Rogach, N. A. Kotov, D. S. Koktysh, J. W. Ostrander, and G. A. Rgaisha. Electrophoretic deposition of latex-based 3D colloidal photonic crystals: A technique

for rapid production of high-quality opals. *Chem. Mater.*, 12:2721–2726, 2000.

[2] Y. J. Huang, C. H. Lai, and P. W. Wu. Fabrication of large-area colloidal crystals by electrophoretic deposition in vertical arrangement. *Electrochem. Solid State Lett.*, 11:P20–P22, 2008.

[3] K. Katagiri, Y. Tanaka, K. Uemura, K. Inumaru, T. Seki, and Y. Takeoka. Structural color coating films composed of an amorphous array of colloidal particles via electrophoretic deposition. *NPG Asia Mater.*, 9:e355, 2017.

[4] L. Besra, T. Uchikoshi, T. S. Suzuki, and Y. Sakka. Bubble-free aqueous electrophoretic deposition (EPD) by pulse-potential application. *J. Am. Ceram. Soc.*, 91:3154–3159, 2008.

[5] L. Besra, T. Uchikoshi, T. S. Suzuki, and Y. Sakka. Application of constant current pulse to suppress bubble incorporation and control deposit morphology during aqueous electrophoretic deposition (EPD). *J. European Ceram. Soc.*, 29:1837–1845, 2009.

[6] S. Furumi, H. Fudouzi, and T. Sawada. Dynamic photoswitching of micropatterned lasing in colloidal crystals by the photochromic reaction. *J. Mater. Chem.*, 22:21519–21528, 2012.

[7] B. V. Derjaguin and L. Landau. Theory of the stability of strongly charged lyophobic sols and of the adhesion of strongly charged particles in solution of electrolytes. *Acta Physicochim. URSS*, 14:633–62, 1941.

[8] E. J. W. Verwey and J. T. G. Overbeek. Theory of the stability of lyophobic colloids. *Elsevier Publishing Company*, 1948.

[9] H. L. Li and F. Marlow. Solvent effects in colloid crystal deposition. *Chem. Mater.*, 18:1803–1810, 2006.

[10] H. Fudouzi and Y. N. Xia. Photonic papers and inks: Color writing with colorless materials. *Adv. Mater.*, 15:892–896, 2003.

Chapter 3

Growth mechanism of the colloidal crystal films from the concentrated aqueous ethanol suspension

3.1 Introduction

Rogach *et al.* reported the colloidal crystal film formation within 30 minutes by the EPD process [1]. Since then, this process was considered to be advantageous for the rapid formation of the colloidal crystal structure. Several groups reported the colloidal crystal film formation by the EPD process [2–4].

In Chapter 2, the detailed EPD process to realize the rapid colloidal crystal film fabrication was investigated. The mixture of water and ethanol (EtOH) with high EtOH concentration was found as a proper suspension. On the way to optimize the EPD colloidal crystal film formation process, multiple step mechanism was implied. Although EPD process is characterized by the migration of colloidal particles in a liquid under an electric field and the subsequent deposition, we have recently found that the colloidal crystal film formation did not take place by the EPD process itself. It seems that the colloidal crystal film formation took place during the following drying up process.

In another sense, a colloidal crystal film formation mechanism has not been understood well in the previous EPD process. At the drying step in our EPD experiment, we have observed the color change from milky white to green within a few minutes. Similar phenomena were reported in previous papers on the colloidal crystal film formation. The color change was observed at the crystallization process and the peak shift of Bragg's diffraction was investigated [5–11]. In this study, the detailed mechanism to form a colloidal crystal structure from the concentrated aqueous EtOH suspension in the drying process will be elucidated.

3.2 Experimental procedure

Polystyrene (PS) colloids were synthesized by the standard emulsion polymerization method. PS colloids were monodispersed in the water at 7.54 wt%. The average diameter of the PS colloid was 204.2 nm measured by a scanning electron microscope image. For the EPD experiment, the aqueous PS colloidal suspension was mixed with ethanol (99.5 %, Kanto Chemical Co., Inc.) at 1:4 weight ratio based on our previous work [12, 13]. As a result, the mixed solvent was 81.7 Vol% aqueous EtOH. An indium tin oxide (ITO) coated glass as the anode electrode was obtained from GEOMATEC Co., Ltd. A stainless-steel (SUS304) plate as the cathode electrode was obtained from The NILACO Corporation.

Colloidal crystal films were formed on ITO glass substrates by electrophoresis deposition. Figure 3.1 shows the schematic of the electrophoresis and drying process. Figure 3.1-A is a set-up layout for electrophoresis in PS colloidal suspension. An ITO/glass plate cut in the dimensions of 20 mm × 30 mm was used as an anodic substrate. A stainless-steel plate with the same size was used as a counter electrode/cathode. The distance from ITO/glass to a stainless-steel plate was 1.0 cm. After immersing the electrodes in the colloidal suspension, DC voltage of 5 V/cm was applied for 5 minutes. As shown in the insert illustration of Fig.3.1-A, where PS colloid particles migrate to the anodic substrate since PS colloids are negatively charged in the suspension. After the EPD process, the substrate was pulled out from the suspension as shown in Fig.3.1-B. The surface of the anode substrate was covered with concentrated PS colloidal suspension liquid film. The liquid film shows a white milky color and no structural color, *i.e.*, colloidal PS particles are randomly arranged in the suspension. The optimum withdrawing speed was set at a rate of 3 mm/sec [13]. The change of the suspension during drying evolution was observed by CCD camera with an optical microscope at room temperature. In addition, the colloidal crystallization was measured by reflectance spectroscopy with a fiber probe as shown in Fig.3.1-B.
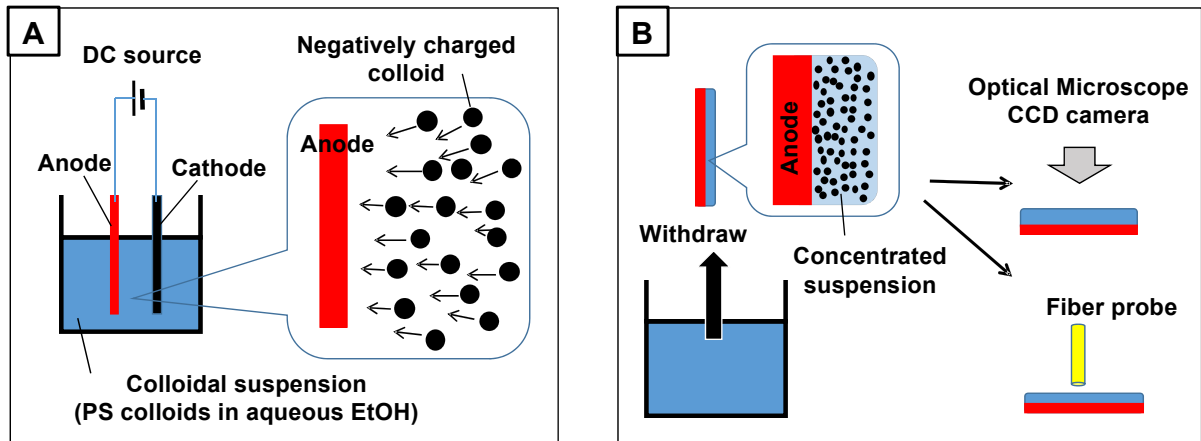
Figure 3.1 Experimental procedure of electrophoresis and drying process. A: Negatively charged PS colloids migrated to anode substrate. B: Drying process after withdrawing from colloidal suspension and observation and measurement for the formation of colloidal crystal film.

The drying processes were observed with a digital 4K video camera (PANASONIC, HC-VX985M). Changes in the microstructure during the drying process were observed with an optical microscope (NIKON, OptiPhoto II) mounted with CMOS camera

(TrueChrome HD, TUCSEN). Microstructure of colloidal crystal films was observed by the Scanning Electron Microscope, SEM (JSM-6500F, JEOL). Local reflection spectra were measured by a miniature fiber-optic spectrometer (USB2000+, OCEAN OPTICS) with a reflection fiber probe (R200-7-UV-VIS). The incident light was aligned perpendicular to the surface of the specimens. The SpectraSuite was used as an operating software for spectrometer. The spectra changes were monitored by high-speed acquisition mode (Capture period: 0.5 sec).

3.3 Color change of the colloidal crystal film depending on the elapsed time

In recent our previous papers, we have developed a rapid EPD process to form the colloidal crystal film with aqueous EtOH colloidal suspension [12, 13]. However, the detailed mechanism of the process is still not clear yet. And, we have observed the color change during the drying stage. Thus, in this chapter, we have focused on the drying stage after pulling out the ITO/glass substrate from the PS colloidal suspension. Figure 3.2 shows the SEM images of the colloidal crystal film on ITO/glass substrate after the EPD and drying processes. Figure 3.2-A shows the top surface of the colloidal crystal film on the substrate. A closely packed PS colloidal hexagonal array was observed for almost whole area, while a very small part of the area was a cubic array. Figure 3.2-B shows the cross-sectional image of the colloidal crystal film edge which has blue-green coloring. From the SEM images and previous our study, PS colloidal particles are closely packed and forming a face-centered cubic (fcc) lattice with (111) planes aligned to the substrate. This film has shown the structural color peaked at 498.6 nm due to Bragg's diffraction of the colloidal crystal film. In general, the wavelength of the diffraction peak, λ, of the light diffraction from the colloidal crystal film, *i.e.*, structural color, is expressed by the modified Bragg's diffraction considering the Snell's refraction law as follows [5];

$$\lambda = 2dn_{eff} = 2d\sqrt{V_p n_p^2 + V_m n_m^2} \tag{3.1}$$

where d, n_{eff} , n_p, n_m, V_p and V_m are the lattice spacing of arrayed colloids, the effective refractive index of the colloidal crystal, refractive indices of PS particles and surrounding medium (either air or mixture of ethanol and water), volume fractions of the PS particles
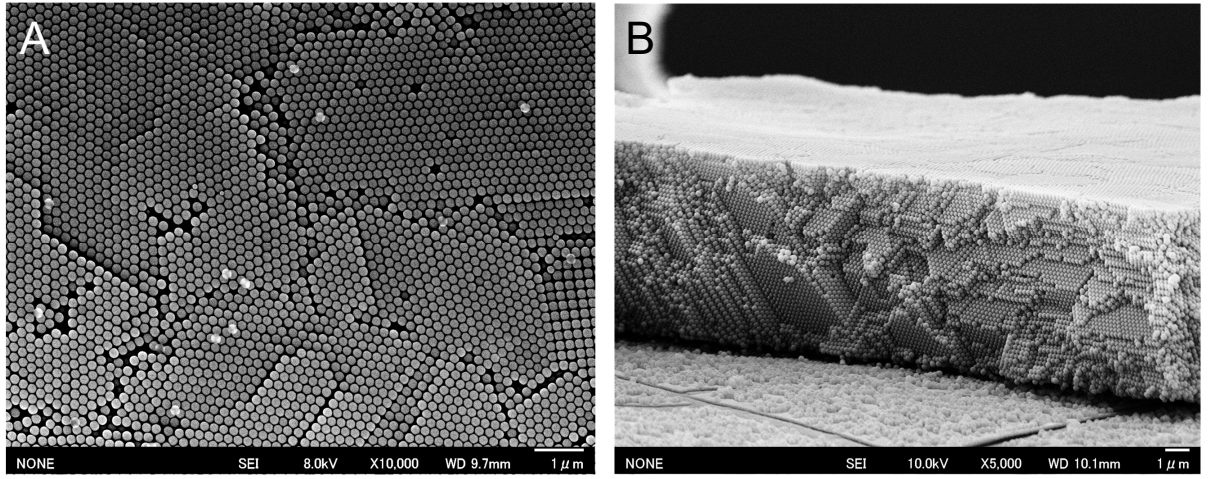
Figure 3.2 SEM images of the colloidal crystal film, A) top surface and B) cross-section.

and the surrounding medium, respectively. In the case of the fcc lattice, the eq.3.1 becomes as follows since V_p and V_m are 0.74 and 0.26, respectively;

$$\lambda_{cal} = 2d_{111}\sqrt{0.74n_p^2 + 0.26n_m^2} \tag{3.2}$$

where $n_p = 1.59$ (PS particle), $n_m = 1$ (air), and $d_{111} = \sqrt{\frac{2}{3}}D = 166.7$ nm (D is the diameter of the PS particle). From the eq.3.2, the calculated peak diffraction wavelength, λ_{cal}, becomes 486.8 nm. This is almost the same as the measured one, λ_{mes} (498.6 nm).

Figure 3.3 shows the color change of the colloidal crystal film depending on the elapsed time after pulling out the substrate from the colloidal suspension. In the beginning, all surfaces of the wet colloidal suspension film showed the milky white color. Then it turned to the uniform reddish color. Drying up the solvent proceeded along with the substrate withdrawn direction, *i.e.*, top to bottom direction of the substrate. This is because the drying process is already accompanied by pulling out the film from the suspension, and the upper suspension liquid film becomes thinner than the lower one on the substrate. By the progress of the drying, the iridescent structural color development was observed, i.e., red, orange, yellow, green and light blue. Finally, the whole surface of the film was dried up and showed blue-green color. The drying up process was completed within 55 seconds. As described later, the color change in the drying stage was due to the variation of Bragg's diffraction conditions, especially the lattice spacing of the arrayed colloids and the effective refractive index of colloidal crystal film from wet to dry condition.
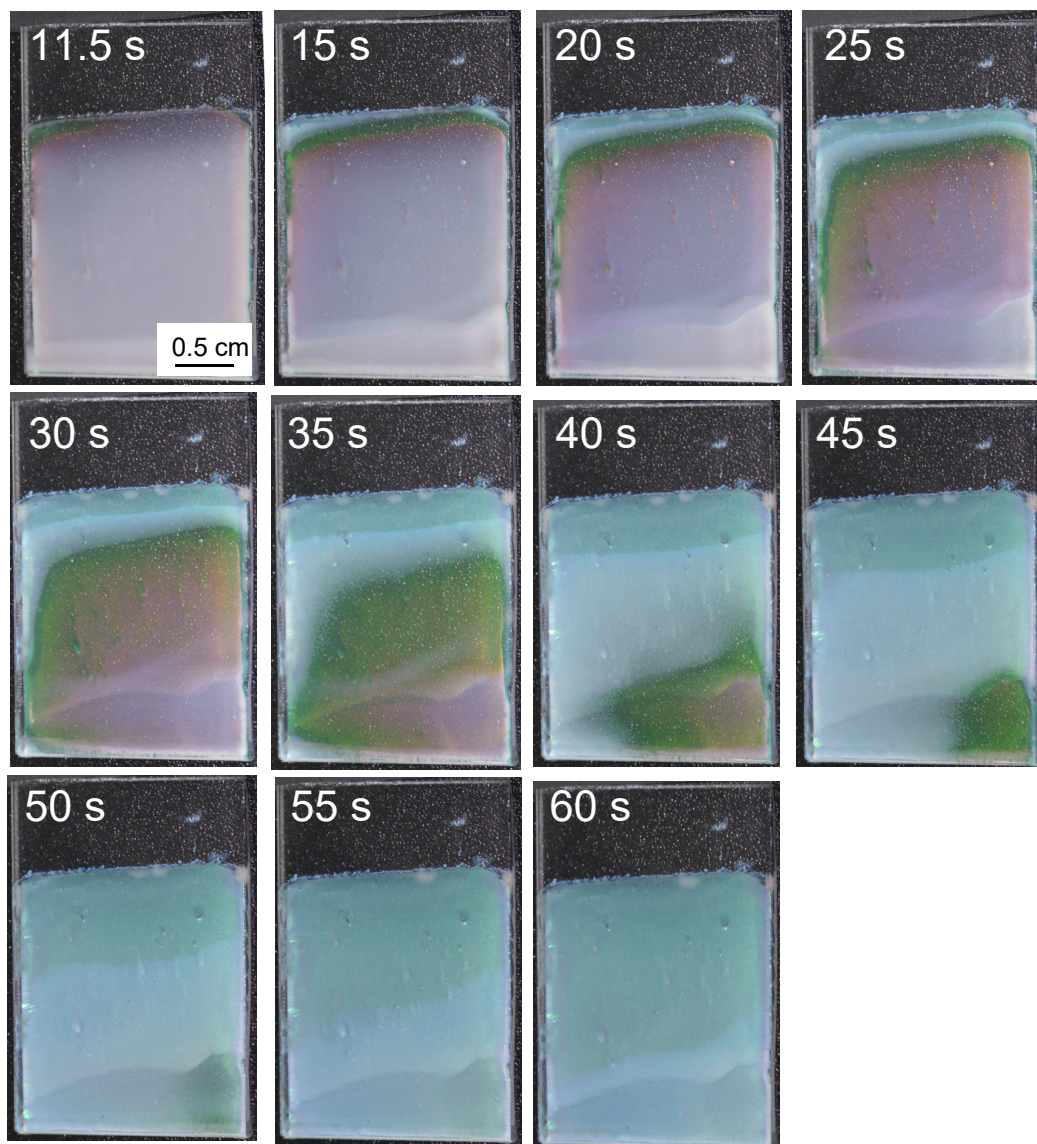
Figure 3.3 Color change from a wet liquid film to the dry colloidal crystal film after pulling out the substrate from the suspension. CCD snap shot images at each elapsed time.

3.4 Reflection peak wavelength shift depending on the elapsed time

The color change in the drying stage was investigated by the local spectroscopy. After the complete withdrawal of the substrate from the suspension, it took about 10 sec until the substrate was fixed at the proper position to measure the reflection spectra. Figure 3.4 shows the representative reflection spectra measured at the film. Until 11.0 seconds (A) after the substrate was removed from the suspension, the liquid film showed milky white color and no reflection peak was observed. At 15.0 sec (B), a reflection peak was suddenly appeared at around 615.5 nm. This peak corresponding to the red structural color. The peak position shifted to 615.5 nm at 15.0 s (B). Since then, at 27 sec (C), 31 sec (D), and 50 sec (E), the reflection peak showed a blue shift continuously over time.
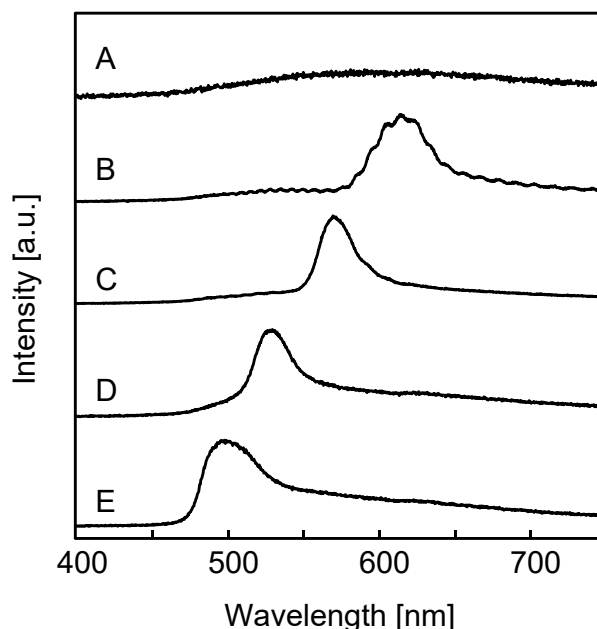

Figure 3.4 A change of reflection spectra in drying process by the evaporation. The elapsed time of A) 11 sec, B) 15 sec, C) 27 sec, D) 31 sec, and E) 50 sec, after the pulling out the substrate from the suspension.

The detail of the change between spectrum A and B in Fig.3.4 are shown in Fig.3.5. At 11.5 sec, a small and broad peak was formed around 645.6 nm. The reflection peak at 12.0 sec, which first appeared from the periodically-ordered structure in the drying process, was located around 629.6 nm. The detailed changes of the spectra from B to D and around E are shown in Fig.3.6 and Fig.3.7, respectively.

Figure 3.8 shows the change of the reflection peak wavelength depending on the

Figure 3.5 A change of reflection spectra in drying process by the evaporation. The elapsed time of A) 11 sec, B) 11.5 sec, C) 12 sec, D) 12.5 sec, E) 13 sec, F) 14 sec, and G) 15 sec, after the pulling out the substrate from the suspension.

Figure 3.6 A change of reflection spectra in drying process by the evaporation. The elapsed time of A) 27 sec, B) 28 sec, C) 29 sec, D) 30 sec, E) 31 sec, F) 32 sec, G) 33 sec, and H) 34 sec, after the pulling out the substrate from the suspension.
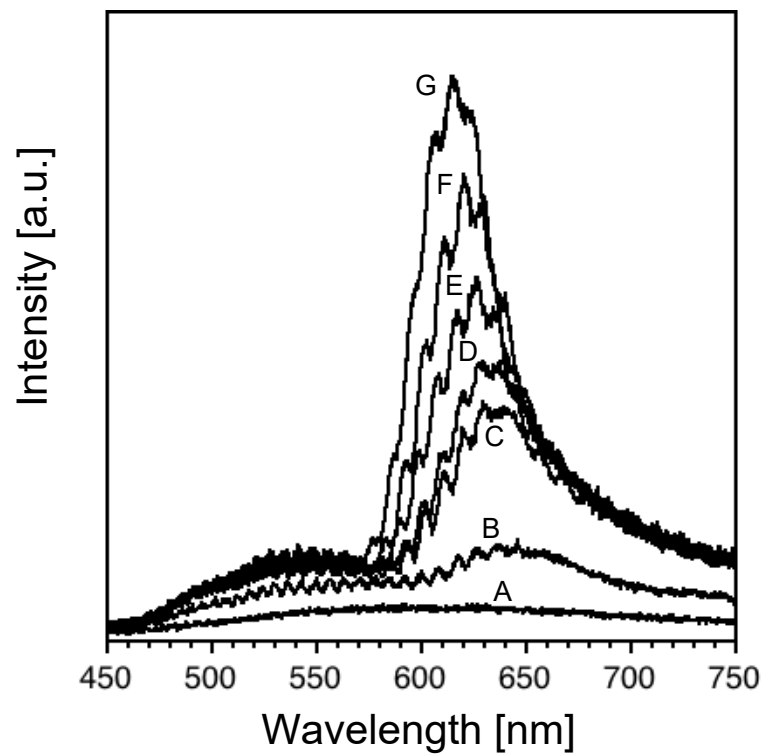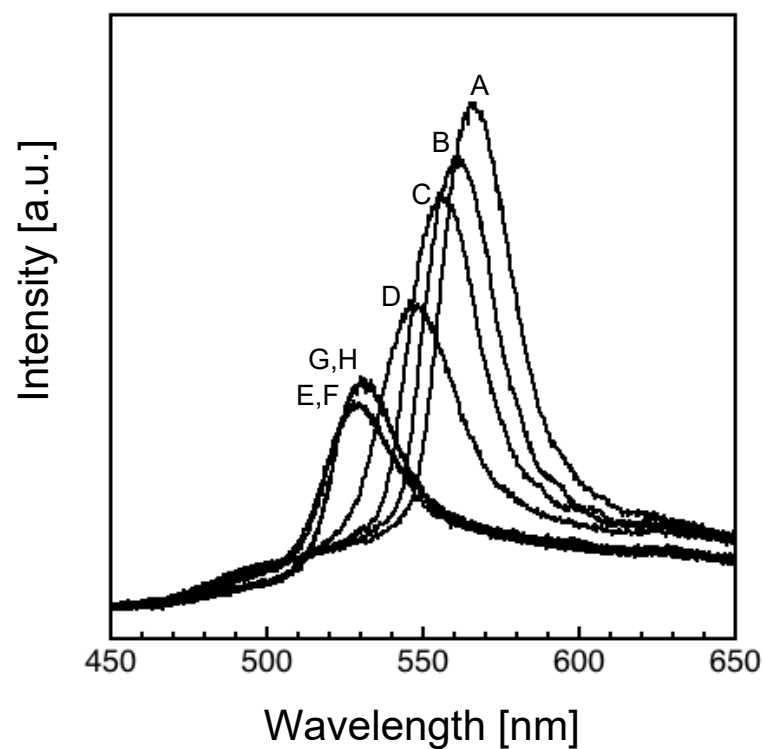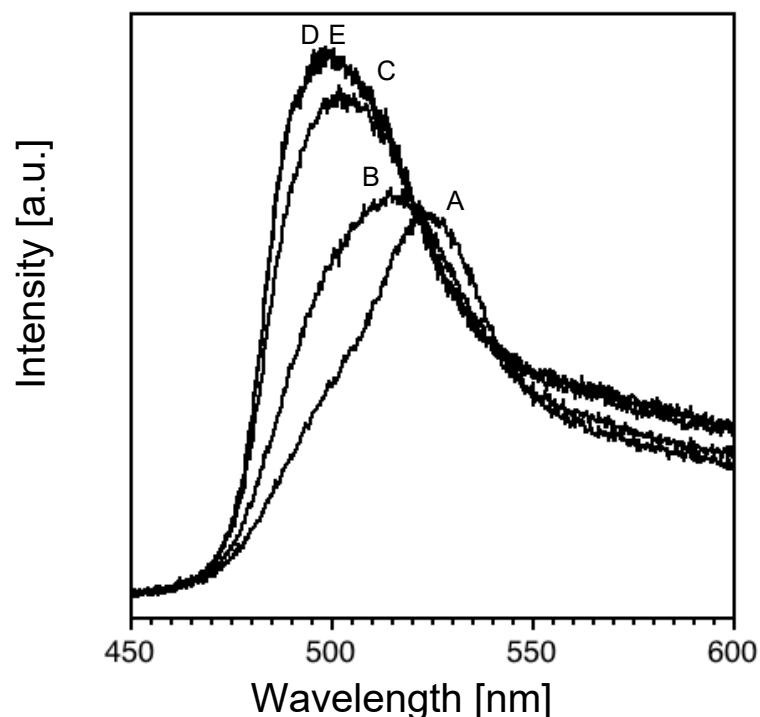
Figure 3.7 A change of reflection spectra in drying process by the evaporation. The elapsed time of A) 45 sec, B) 47 sec, C) 49 sec, D) 51 sec, and E) 53 sec, after the pulling out the substrate from the suspension.

elapsed time after pulling out the substrate from the suspension. From 0 sec to just before 11.5 sec (defined as range 1), colloidal particles in the aqueous EtOH suspension have the non-ordered structure, *i.e.*, random disorder state. And then, at 11.5 sec, the reflection peak corresponding to the structural color appeared, *i.e.*, colloidal particles in the concentrated suspension suddenly began to form the ordered structure caused by Alder's phase transition. A similar phenomenon was reported on the oil covering method to form the high-quality colloidal crystal film [6]. From 11.5 sec to 31 sec (defined as range 2), the blue shift of the reflection peak wavelength continued from 645.6 nm to 528 nm. The intensity of the diffraction peak increased from 11.5 sec to 15 sec, in the first part of range 2 as shown in Fig3.5, while it decreased from 27 sec to 31 sec in the second part of range 2 as shown in Fig.3.6. From 31 sec to 43 sec (defined as range 3), the wavelength of reflection peak kept almost plateau. From 31 s to 34 s shown in Fig.3.6, diffraction peaks showed stable features, *i.e.*, similar peak position and intensity. Thereafter, from 43 sec to 60 sec (defined as range 4), the blue shift of the reflection peak wavelength took place once again, and finally, it kept the constant wavelength of around 500 nm after around 51 sec. Figure 3.7 shows the spectrum change of range 4, the final stage of the

drying process. From 45 sec to 49 sec, the diffraction peak wavelength showed a little blue-shift from 522 nm to 502 nm. This 2nd-time reflection peak wavelength change was not observed in the oil covering method [6].
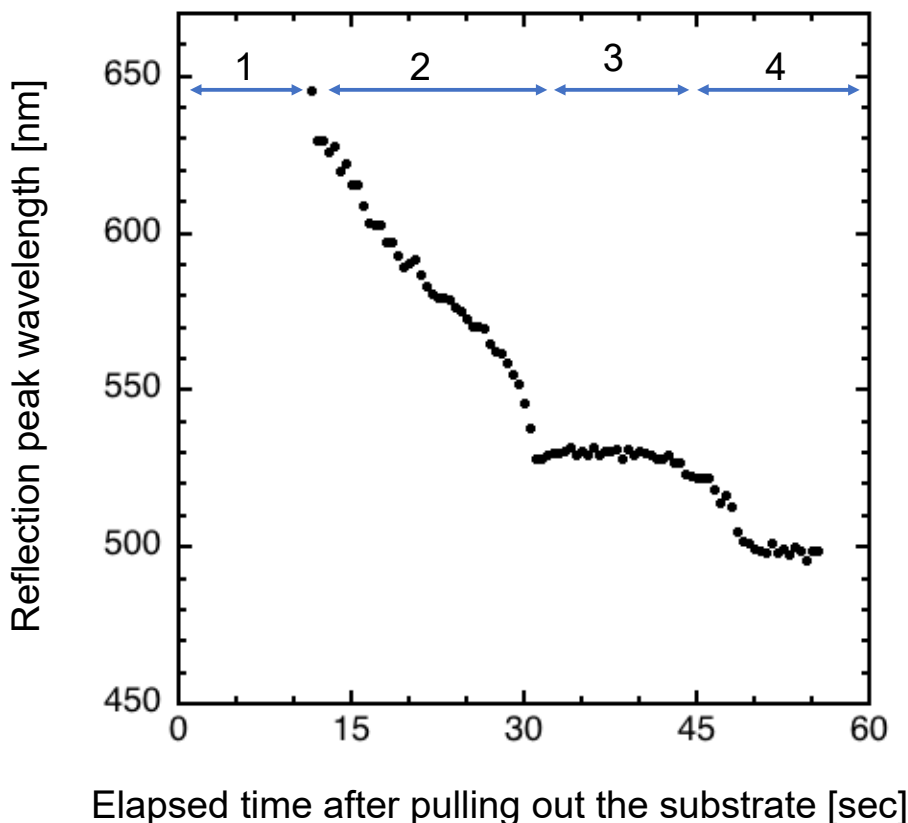

Figure 3.8 Bragg's diffraction peak position change depending on the elapsed time after the pulling out the substrate from the suspension.

Furthermore, a morphology change during the drying process of the film with an optical microscope was investigated. Figure 3.9 shows optical microscope photos during the drying process, from the wet suspension liquid film to the dried colloidal crystal film. The photo Fig.3.9-i shows the colloidal suspension on the substrate at the end of Alder's phase transition. After Alder's phase transition, the structural color was observed as shown in the photo Fig.3.9-i and ii. The color changed from red to orange then yellow as shown in the photo Fig.3.9-iii. From the photo Fig.3.9-i to the photo Fig.3.9-iii, the morphology was almost uniform. After that, between the photo Fig.3.9-iii (elapsed time: 15 sec) and the photo Fig.3.9-iv (elapsed time: 19 sec), many cracks occurred in the colloidal crystal film. Between 31 sec and 34 sec elapsed time (the photo Fig.3.9-v), there was almost no color change (range 3 of the Fig.3.8). After 42 sec elapsed time, structural color changed from green to blue, and after 52 sec elapsed time (the photo Fig.3.9-vi),

the blue color was kept constantly. This color change from green to blue, was caused by drying the wet colloidal crystal film, corresponding to the range 4 of Fig.3.8. One of the things to be noticed in the optical microscope imaging is the fact that the multi-grain (observed in SEM images as shown in Fig.3.2) was formed during the early stage of the drying process, but not in the last stage. As shown in Fig.3.9, no crack was formed until 15 sec elapsed time (the photo Fig.3.9-iii). After 15.5 sec elapsed time, crack was formed until 19 sec elapsed time (the photo Fig.3.9-iv). After that, no more crack formation was observed. This shows that cracks were formed in a very short period for about 4 sec, and thereafter crack development stops, *i.e.*, crack formation and development take place in the middle of the range 2 of Fig.3.8. Thus, the crack formation is originated from the non-homogeneous lattice space reduction of the arrayed colloid film during the range 2 of Fig.3.8.
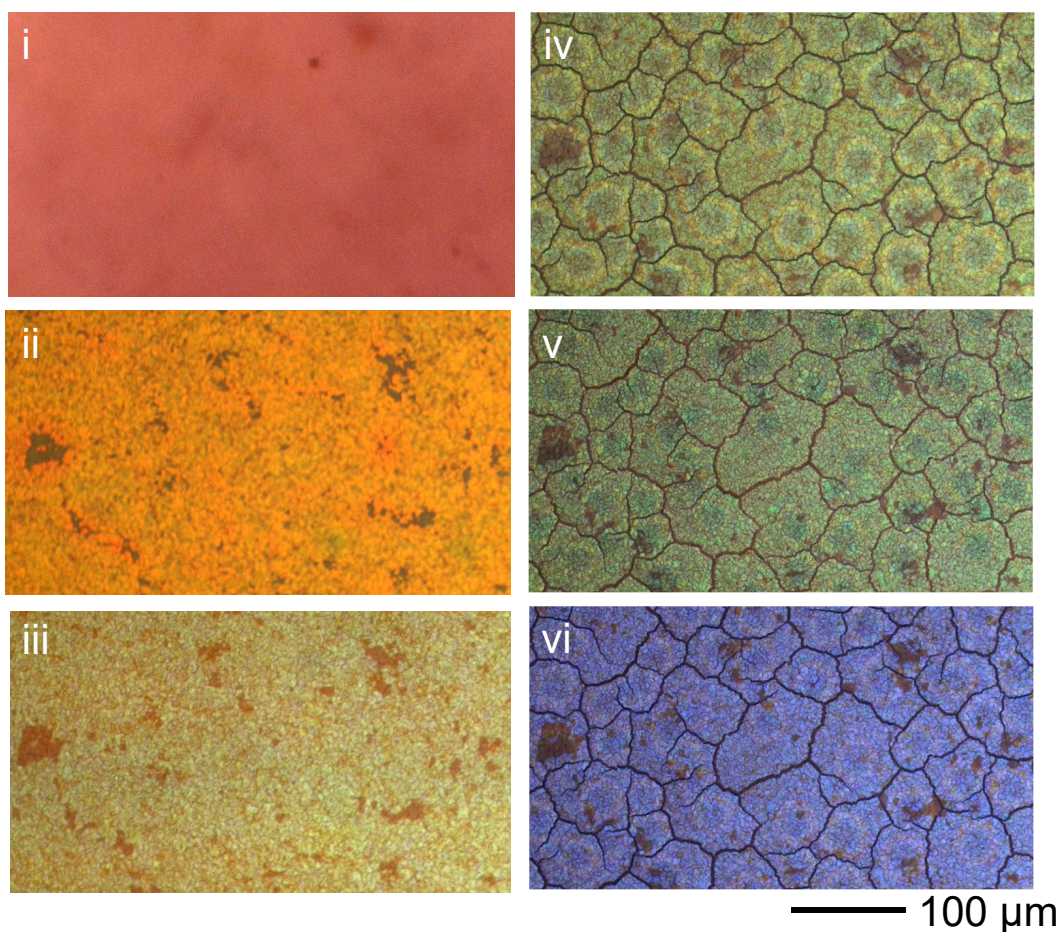

Figure 3.9 Optical microscope images during the drying process by the evaporation. i) structural color (red), ii) structural color (orange), iii) structural color (yellow), iv) Cracks formation, v) wet film (green), and vi) dry film (blue).

3.5 Model of colloidal crystal film formation

Based on these results, we proposed a model of the colloidal crystal formation accompanied by an evaporating solvent. Figure 3.10 shows the schematic model of the colloidal crystal film formation categorized into four stages.

Stage 1 (Disorder-to-order transition):

After the electrophoresis, the surface of the ITO/Glass is covered with a colloidal suspension containing PS particles as a liquid film composed of a mixture of EtOH and water. In this period, PS particles are dispersed in the liquid with Brownian random motion. No specific reflection peak is observed so that the color of the film looks milky white. By the progress of suspension drying, a self-assembled non-closely packed PS colloidal crystal film is formed, due to the phase transition from disorder to order state, *i.e.*, disorder-to-order Alder's phase transition (between Fig.3.5-A and Fig.3.5-B). This makes the color change of the film from milky white to red (corresponding to the range 1 of Fig.3.8). Around 10s to 11s, the phase transition of colloidal crystallization suddenly occurred, and the color quickly changed.

Stage 2 (Tuning the lattice distance and changing the colloidal crystal from non-contact to contact):

The evaporation of aqueous EtOH solvent from the wet film of the colloidal suspension continues. At the same time, the lattice spacing and the interparticle distance, d, shrinks continuously. In finally, colloidal crystal reaches a dense, closely packed structure. At this stage, a lattice spacing, d, plays an important role in the peak shifting. This process causes the shift of the reflection peak wavelength from red to green color (the range 2 of Fig.3.8). In addition, crack formation is involved in this stage due to the volume shrinking of the colloidal crystal film from the observation of the optical microscope.
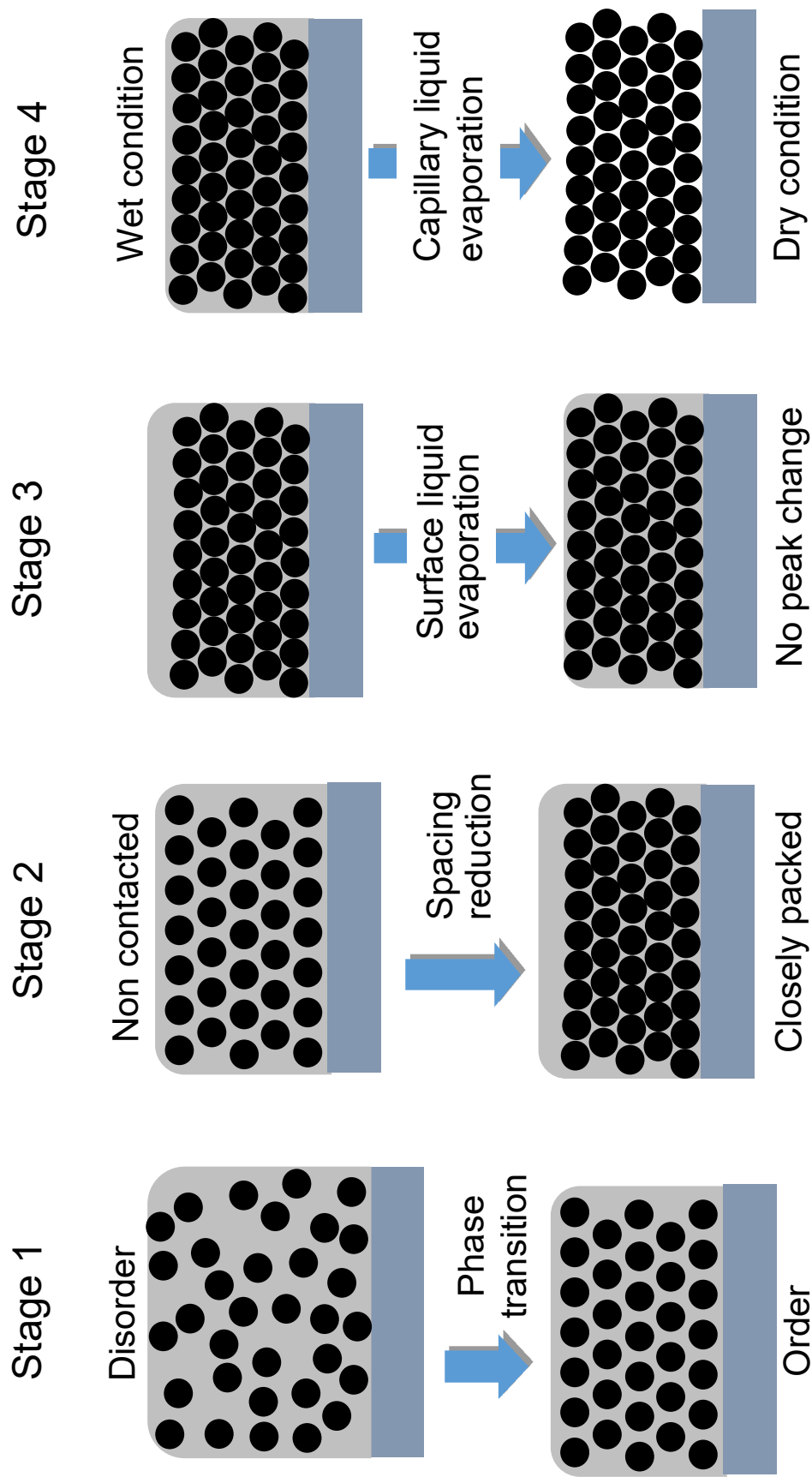
Figure 3.10 Schematic of the colloidal crystal film formation mechanism during drying process after EPD process.

Stage 3 (Evaporating surface liquid on the colloidal crystal film):

After forming a closely packed structure, PS particle layer was covered with a liquid film of aqueous EtOH. The reflection peak shows the constant wavelength at green color because the d value almost does not decrease (the range 3 of Fig.3.8), *i.e.*, shrinking of lattice spacing, d, almost stops. Bragg's diffraction is caused only by the particle layers. During the evaporation, we observed tentatively the iridescence color shown in the photo iv in Fig.3.9. The iridescence due to the thin-film interference of the surface liquid over the colloidal crystal.

Stage 4 (Liquid evaporation from the interparticle spacing of the colloidal crystal film):

Evaporation of interparticle liquid, *i.e.*, capillary liquid, takes place. This leads to the change of n_{eff}, due to the exchange of interparticle medium from the liquid to air. Consequently, the reflection peak wavelength shifts from green to blue color and realizes the dry closely-packed colloidal crystal structure (the range 4 of Fig.3.8). In this stage, the change of the refractive index becomes an important parameter to determine the Bragg's diffraction peak. During stage 4, the peak shift was 20 nm (from 522 nm to 502 nm, from Fig.3.8). The effective refractive index can be calculated as follows. From eq.3.1 and eq.3.2, $n_{eff} = \sqrt{0.74n_p^2 + 0.26n_m^2}$. By the use of n_p=1.59 (PS), n_m=1.0 (dry, air) or 1.36 (82 Vol% aqueous EtOH), the n_{eff} can be obtained as 1.46 and 1.53, respectively. This is corresponding to the diffraction peak position reduction of 95.4%. And, this reduction rate is reasonable corresponding to the peak shift from 522 nm to 502 nm (96.2%). However, the change of d_{111} planes during Stage 4 is not clear.

The above crystallization mechanism is basically a similar process based on Alder's phase transition in the colloidal process due to concentrating colloidal suspension [6–11]. In the case of the oil covering method [6], the colloidal crystal film is formed under silicone oil layer by Stage 1 (Phase transition) and Stage 2 (Spacing reduction). The crystal growth rate is very slow. A few days are required to form a colloidal crystal film on a 4-inch silicon substrate. In contrast, the crystal growth rate in this work is 0.5 mm/s. These results suggest that the growth rate is about 1000 times faster if we do not consider the quality of colloidal crystal films. In the case of the evaporative self-assembly process, Koh *et al.*, have reported a similar model using a vertical and horizontal colloidal deposition process [7, 8]. In the model and reflectance spectra, they proposed a crystallization process as the

following three steps, *i.e.*, phase transition, decreasing lattice space and dry up. In this work, there are corresponding to similar model stage 1, stage 2 and stage 4. However, stage 3 in our model is a little different from the previous similar drying processes [7, 8].

At this time, the phenomena (the reflection peak of the plateau in region 3 in Fig.3.8) is tentatively explained for our Stage 3 model. We have been interested in similar phenomena reported by following previous works. Marlow *et al.*, investigated in detail mechanism by capillary deposition [9, 10]. They have reported in-situ observation of wet opal formation from a dilute colloidal suspension by spectroscopy. They conclude that three specific internal changes in wet opal films: Crystallization, compression and defect formation [10]. They also previously reported the drying of the colloidal crystals process and strange redshift due to the transformation of water from shells to a neck-type distribution (v-event) [9]. In their process (Capillary deposition), Bragg's diffraction peak shift is a slow process for dozens of hours. Meng *et al.*, have reported on colloidal crystal formation by evaporation induced self-assembly using CCD camera and spectroscopy [11]. From their paper, the entire drying process contains three stages: crack-initiation stage, crack-propagation stage, and crack-remained stage. They found a redshift of Bragg's diffraction when the crack begins to propagate in the crack-propagation stage. At this time, the phenomena have not been completely explained for our Stage 3 model, and further detailed analysis is needed in the future. However, the peak shift time is completed within 1 minute. This colloidal crystallization is an extremely rapid process compared with previous reports [6–11].

3.6   Summary

A growth mechanism of the colloidal crystal films from the concentrated aqueous EtOH suspension has been investigated. Closely packed colloidal crystal film was formed within 55 seconds. By the analysis of the reflection spectra and the optical microscope images, the growth mechanism from the colloidal suspension to the colloidal crystal film was found to consist of 4 stages. The 1st stage is the formation of a liquid film of the concentrated colloidal suspension on a substrate. By the progress of evaporation, the phase transition from disorder to order to form the non-closely packed colloidal crystal by self-assembly takes place. At the moment of the phase transition, the Bragg's diffraction peak is detected and the structural color appears. In the 2nd stage, the diffraction peak

68

shifts toward the shorter wavelength direction (blue shift), due to the reduction of the interparticle distance of the non-close packed colloidal crystal. In the end, the closely packed colloidal crystal film is formed. In the 3rd stage, the liquid film covering on the colloidal crystal film evaporated and iridescence color due to thin-film interference is tentatively observed. In the 4th stage, the colloidal crystal film changes from wet to dry, by the evaporation of the interparticle aqueous EtOH solvent. The structural color changes from green to blue and the diffraction peak wavelength goes down with one more stage. This color change is dominated by the change of the refractive index of the interparticle medium from the liquid to air. One of the key findings in our process is rapid crystal growth using the EPD process from the concentrated aqueous EtOH suspension. The growth speed of the colloidal crystal is extremely rapid (within one minute for 900 mm^2 area) compared with those of previous papers, such as oil covering and capillary deposition methods (several to hundreds of hours). This process has the potential for high-speed deposition of the colloidal crystalline thin films.

References

[1] A. L. Rogach, N. A. Kotov, D. S. Koktysh, J. W. Ostrander, and G. A. Rgaisha. Electrophoretic deposition of latex-based 3D colloidal photonic crystals: A technique for rapid production of high-quality opals. *Chem. Mater.*, 12:2721–2726, 2000.

[2] Y. J. Huang, C. H. Lai, and P. W. Wu. Fabrication of large-area colloidal crystals by electrophoretic deposition in vertical arrangement. *Electrochem. Solid State Lett.*, 11:P20–P22, 2008.

[3] K. Katagiri, Y. Tanaka, K. Uemura, K. Inumaru, T. Seki, and Y. Takeoka. Structural color coating films composed of an amorphous array of colloidal particles via electrophoretic deposition. *NPG Asia Mater.*, 9:e355, 2017.

[4] C. H. Lai, Y. J. Huang, P. W. Wu, and L. Y. Chen. Rapid fabrication of cylindrical colloidal crystals and their inverse opals. *J. Electrochem. Soc.*, 157:23–27, 2010.

[5] H. Fudouzi. Fabricating high-quality opal films with uniform structure over a large area. *J. Coll. Interf. Sci.*, 275:277–283, 2004.

[6] H. Fudouzi. Novel coating method for artificial opal films and its process analysis. *Coll. Surf. A: Phys. Eng. Aspects*, 311:11–15, 2007.

[7] Y. K. Koh and C. C. Wong. In situ monitoring of structural changes during colloidal self-assembly. *Langmuir*, 22:897–900, 2006.

[8] Y. K. Koh, C. H. Yip, Y. M. Chiang, and C. C. Wong. Kinetic stages of single-component colloidal crystallization. *Langmuir*, 24:5245–5248, 2008.

[9] M. Muldarisnur and F. Marlow. Spectroscopic investigation of opal formation from suspensions. *J. Phys. Chem. C*, 121:18274–18279, 2017.

[10] M. Muldarisnur and F. Marlow. Observation of nano-dewetting in colloidal crystal drying. *Angew. Chem., Int. Ed.*, 53:8761–8764, 2014.

[11] D. Lin, L. Wang, L. Yang, Y. Luo, D. Li, and Q. Meng. Real-time synchronous CCD camera observation and reflectance measurement of evaporation-induced polystyrene colloidal self-assembly. *Langmuir*, 30:3949–3956, 2014.

[12] M. Koike, G. T. H. Tran, S. Azuma, H. Kiyono, T. Uchikoshi, and H. Fudouzi. Rapid fabrication of colloidal crystal films by electrophoretic deposition and its application for a volatile liquid and strain detection sensor. *J. Soc. Powder Techn., Japan*, 56:339–346, 2019.

[13] G. T. H. Tran, M. Koike, T. Uchikoshi, and H. Fudouzi. Fabrication of polystyrene colloidal crystal film by electrophoretic deposition. *Adv. Powder Tech.*, 31:3085–3092, 2020. DOI://doi.org/10.1016/j.apt.2020.05.029.

Chapter 4

PDMS elastomer filling at the interparticle space of the colloidal crystal films

4.1 Introduction

The soft colloidal crystal film is composed of submicron polystyrene (PS) particles with cubic closely packed (ccp) structure. The interparticle space is filled with polydimethylsiloxane (PDMS) elastomer. PDMS elastomer filling in the interparticle space of the colloidal crystal film gives the elasticity and mechanical strength [1].

By filling the colloidal crystal film with PDMS elastomer, the structural color based on the Bragg's diffraction changes. This phenomenon is originated from the change of the interparticle medium from dried air to PDMS elastomer and the consequent increase of the refractive index.

In this work, the effect of PDMS elastomer filling the interparticle space of the colloidal crystal film has been investigated by means of the reflection peak wavelength shift, corresponding to the structural color change. In the previous reports, the soft colloidal crystal film fabricated by the vertical technique and/or oil covering method was investigated by the same technique [1–3]. In the present work, the electrophoretic deposition (EPD) technique was employed to fabricate the colloidal crystal film. This technique realizes the fast and large size fabrication of the colloidal crystal film as discussed in Chapter 2 and 3. The applicability as a strain detection sensor has also been demonstrated.

4.2 Experimental procedure

PS colloids were synthesized by the standard emulsion polymerization method [4]. Subsequently PS colloids were monodispersed in water. The average diameter of PS colloids was ϕ204.2 nm. This aqueous PS colloidal suspension (7.54 wt%) was mixed with EtOH at the weight ratio of EtOH : aqueous suspension = 4 : 1.

To fabricate the PS colloidal crystal films by the EPD process, an indium tin oxide (ITO) coated PET (polyethylene terephthalate) sheet (ITO/PET) was used as a substrate/anode. A stainless-steel plate was used as a counter electrode/cathode. An ITO/PET sheet was cut in the dimension of 10 × 15 cm^2. The same size of a stainless-steel plate (SUS304) was used for a counter electrode. The distance between the ITO/PET and the stainless-steel plate was 2.5 cm. After immersing the electrodes in the colloidal suspension, DC constant voltage of 10 V/cm was applied for 5 minutes.

PS colloid particles migrate to anodic substrate since PS colloid is negatively charged in the suspension. After the EPD, the substrate was removed from the suspension at the withdrawing rate of 3 mm/sec. Then the substrate was dried horizontally at room temperature.

The mixture of PDMS elastomer (poly(dimethylsiloxane):PDMS, Shin-Etsu Chemical Co., Ltd., KE-106), curing accelerator (Shin-Etsu Chemical Co., Ltd., CAR-RG) and Silicone oil (volatile, kinematic viscosity 0.65 cSt, Shin-Etsu Chemical Co., Ltd., KF-96L-0.65cs) in the weight ratio of 10 : 1 : 10 was prepared to fill the interparticle space of the colloidal crystal film. Hereafter, this mixture is called as PDMS elastomer. The colloidal crystal film filled with this PDMS elastomer was heated at 50 °C for 3 hours for the polymerization. The procedure is schematically shown in Fig.4.1.
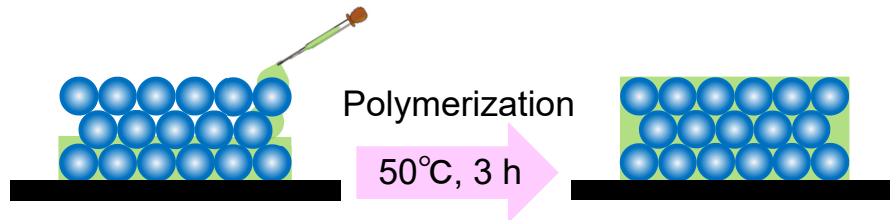

Figure 4.1 Schematic of the PDMS elastomer filling, dripping and polymerization.

The microstructure of the colloidal crystal films was observed using a Scanning Electron Microscope, SEM (JSM-6500F, JEOL). Local transmission and reflection spectra were measured by a miniature fiber-optic spectrometer (USB2000+, Ocean Optics).

4.3   Colloidal crystal films with and without PDMS elastomer filling

Figure 4.2-A shows the colloidal crystal film fabricated by the EPD technique. This film showed a pale blue color. After filling the interparticle space with PDMS elastomer, the color changed to green as shown in Fig.4.2-B. This color change from pale blue to green is also observed as a red shift of the peak wavelength in the reflection spectra of the colloidal crystal films shown in Fig.4.3. Figure 4.4 shows the surface SEM images of the colloidal crystal film fabricated by the EPD technique followed by filling the interparticle space with PDMS elastomer. Almost whole interparticle space is filled with the PDMS elastomer without hollows, and the closely packed structure is maintained (Fig.4.4-A).

To the contrary, the lower magnification image (Fig.4.4-B) indicates that cracking area is not filled with the PDMS elastomer.
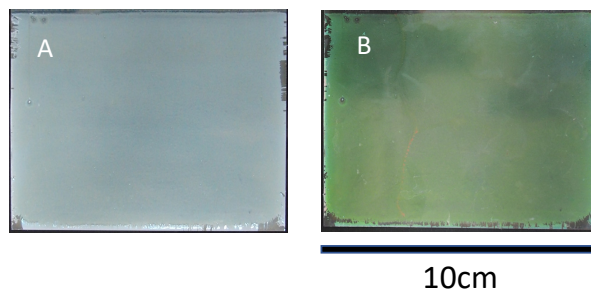

Figure 4.2 Optical photographs of the colloidal crystal film fabricated by the EPD technique showing the chromogenic variation: before (A) and after (B) filling the interparticle space with PDMS elastomer.
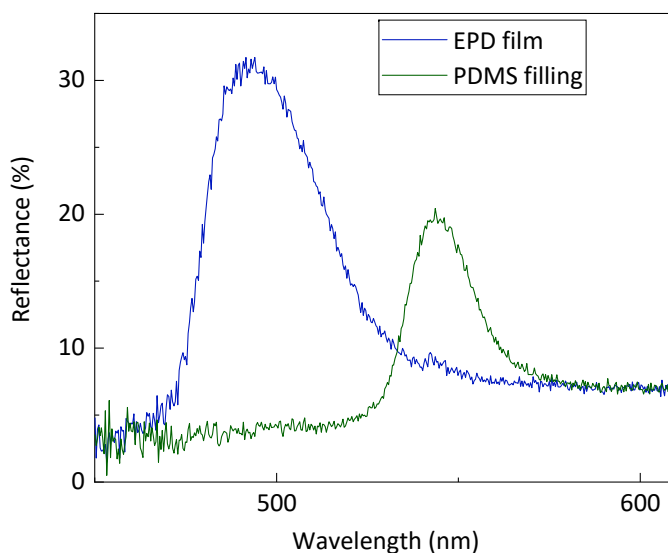

Figure 4.3 Comparison of reflection spectrum peaks of 2 kinds of colloidal crystal films shown in Fig.4.2-A and B.
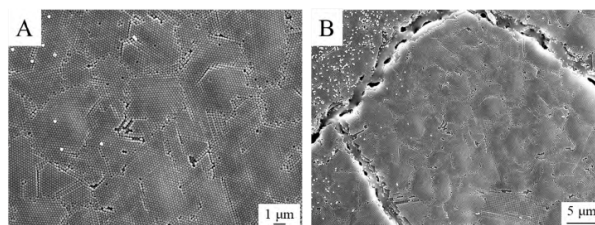

Figure 4.4 Surface SEM images of the EPD colloidal crystal film after filling the interparticle space with PDMS elastomer (Fig.4.2-B), (A) higher and (B) lower magnification.

4.4 Transmission peak wavelength shift by the PDMS elastomer filling

Figure 4.5-A shows the transmission and reflection spectra of the colloidal crystal film fabricated by the EPD technique after filling the interparticle space with PDMS elastomer (Fig.4.2-B) under the incident light irradiated from a direction normal to the substrate. Both peaks were observed around 540 nm. This first-order Bragg diffraction of the cubic closely packed (ccp) planes determines the structural color of the opal film. Figure 4.5-B shows the transmission spectra measured by tilting the colloidal crystal film at each angle, Θ, from $0°$ to $40°$ against the incident light.

These peak wavelengths of the diffracted light in Fig.4.5-B, λ, from the 3 dimensional colloidal crystal, in general, can be expressed by the Bragg's equation taking into account the Snell's law as follows [5];

$$\lambda = 2d_{111}\sqrt{n_{eff}^2 - sin^2\Theta} \tag{4.1}$$

where d_{111}, n_{eff}, and Θ are, the interplanar spacing of the ccp (111) planes, the effective refractive index, and the angle from the normal to the substrate, respectively. Eq.4.1 can be rewritten as a linear function between $sin^2\Theta$ and λ^2 as follows;

$$sin^2\Theta = -\frac{1}{2d_{111}}\lambda^2 + n_{eff}^2 \tag{4.2}$$

By the linear fitting of the plot between $sin^2\Theta$ and λ^2, d_{111} and n_{eff} can be calculated, since $-\frac{1}{2d_{111}}$ and n_{eff}^2 are corresponding to the slope and the intercept, respectively. Figure 4.5-C shows the plot between $sin^2\Theta$ and λ^2. By the linear fitting the Fig.4.5-C with the eq.4.2, d_{111} and n_{eff} of the colloidal crystal film with the PDMS elastomer filling (Fig.4.2-B), were obtained as 174.02 nm and 1.553, respectively.

The red shift from pale blue to green could be mostly attributed to the refractive index n change of the interparticle space from the air ($n = 1.0$) to the PDMS elastomer ($n = 1.4$), since the theoretical n_{eff} is expressed as follows;

$$n_{eff}^2 = V_p n_p^2 + V_m n_m^2 \tag{4.3}$$

where n_p, n_m, V_p and V_m are refractive indices of PS particles ($n = 1.59$) and surrounding

medium, volume fractions of the PS particles and surrounding medium, respectively. In the case of the colloidal crystal film without PDMS elastomer filling, n_m is 1.0 since the surrounding medium is air. In the case of the colloidal crystal film with PDMS elastomer filling, n_m is 1.4 since the surrounding medium is PDMS elastomer.

Taking into account the eq.3.2, the theoretical n_{eff} of the colloidal crystal film with PDMS elastomer filling is calculated to be 1.543 by the eq.4.3. This value is slightly smaller than that of 1.553 experimentally obtained from eq.4.2. This indicates that the PS particles are also swollen by the PDMS elastomer. If V_p in the eq.4.3 becomes smaller, the n_{eff} becomes smaller. It means that the V_p became larger by the PDMS elastomer filling since the experimentally obtained n_{eff} from eq.4.2 became larger. The theoretical d_{111} ($d_{111} = \sqrt{\frac{2}{3}}D =$) is 166.7 nm ($D$ is the diameter of the PS particle) without PDMS elastomer filling. However, the experimentally obtained d_{111} also increased to 174.02 nm by the PDMS elastomer filling. If the interparticle distance increased without the swelling of PS particles, V_p decreases because V_m increases. It means that PS particles were also swollen by the PDMS elastomer filling, and consequently, V_p also increased. In this way, the reason why the experimental n_{eff} value from eq.4.2 was larger than the theoretical n_{eff} value from eq.4.3, could be explained.
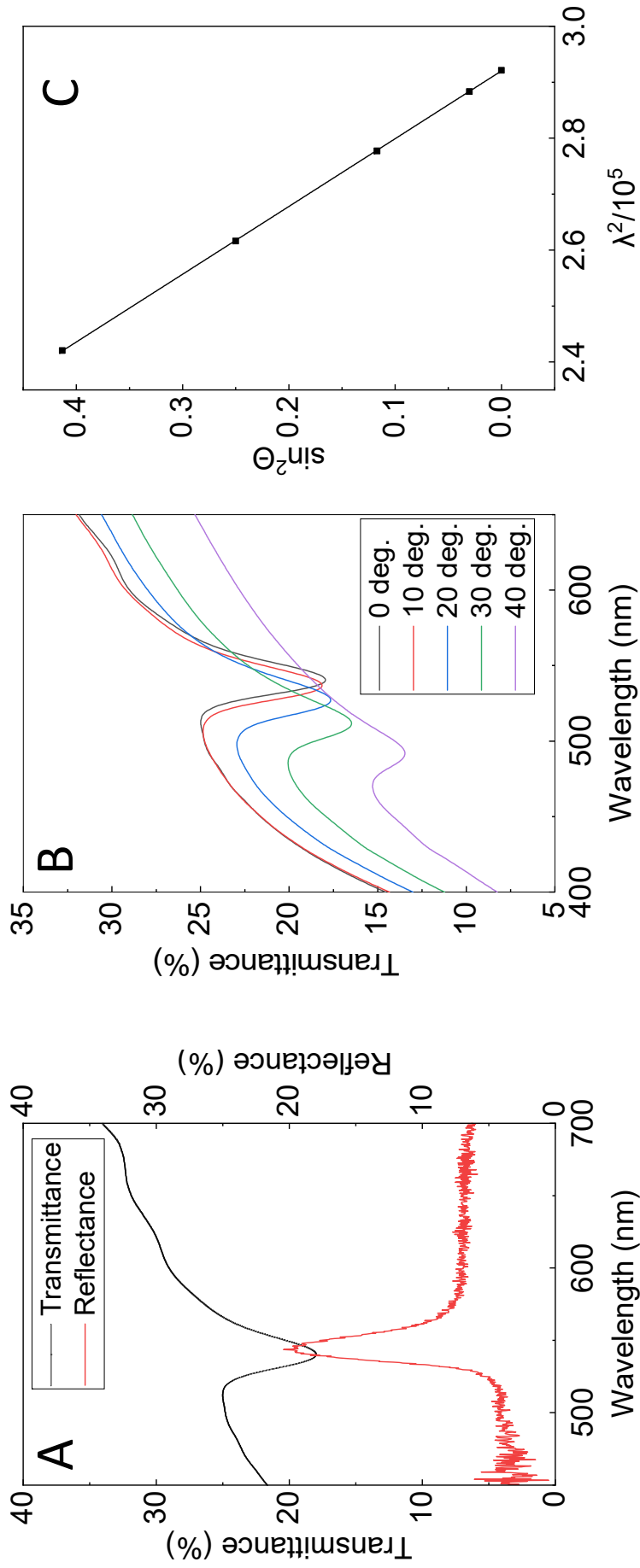
Figure 4.5 Transmission and reflection spectra of the colloidal crystal film fabricated by the EPD technique after filling the interparticle space with PDMS elastomer (Fig.4.2-B) under the incident light normal to the substrate (A), transmission spectra measured by tilting the colloidal crystal film at each Θ from $0°$ to $40°$ against the incident light (B), and $sin^2\Theta$ versus $\lambda^2/10^5$ based on the Bragg's equation (eq.4.2) (C).

4.5 Strain detection sensor

Applicability of the colloidal crystal film with PDMS elastomer filling to the strain detection sensor was examined. Prior to the tensile test, the PDMS elastomer filling into the interparticle space was repeated for 4 times in order to expand the interplanar space enough. Figure 4.6 shows the reflection peak wavelength shift by the PDMS elastomer filling. By repeating the PDMS elastomer filling, the reflection peak wavelength shifted continuously. This shows that the interplanar space increased continuously by repeating the PDMS elastomer filling. By the 4 times PDMS elastomer filling, the structural color changed from green to red. Hereafter, the red colored colloidal crystal film after 4 times PDMS elastomer filling is called the strain visualization sheet.
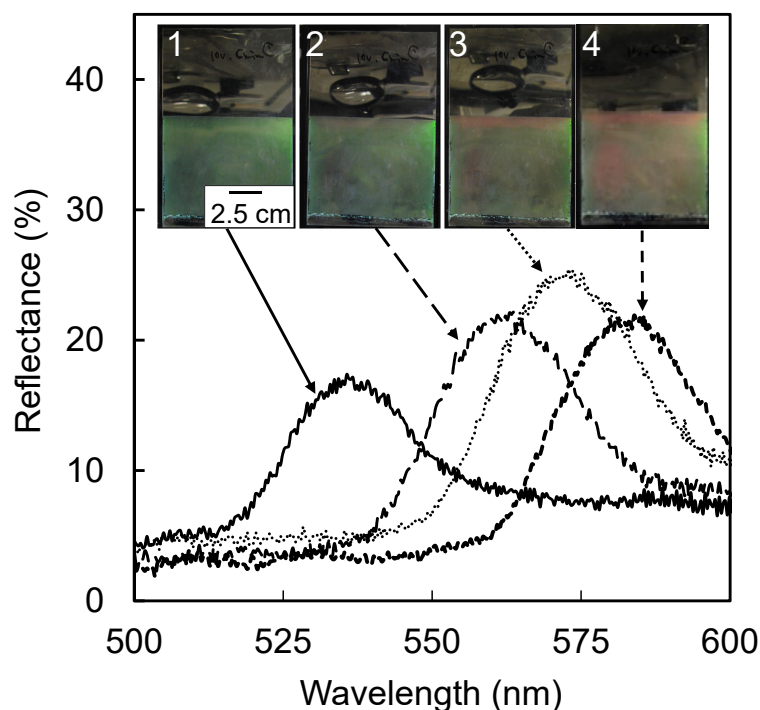

Figure 4.6 Optical photographs of the colloidal crystal film after each PDMS elastomer filling, and the corresponding reflection spectra. Continuous shift of the reflection peak wavelength was observed by repeating the PDMS elastomer filling into the interparticle space of the colloidal crystal film.

Upon the tensile test, the strain visualization sheet was cut and pasted on the black anodized aluminum test piece. Figure 4.7 shows the strain visualization sheet after the tensile test. The test piece was extended 1.0 mm. The undeformed area showed the original red structural color, while the deformed area showed the green structural color. Figure 4.8 shows the reflection spectra at the undeformed and deformed places of the strain

visualization sheet after the tensile test. Blue shift of the reflection peak wavelength from 600 nm at the undeformed area to 570 nm at the deformed area was clearly observed.
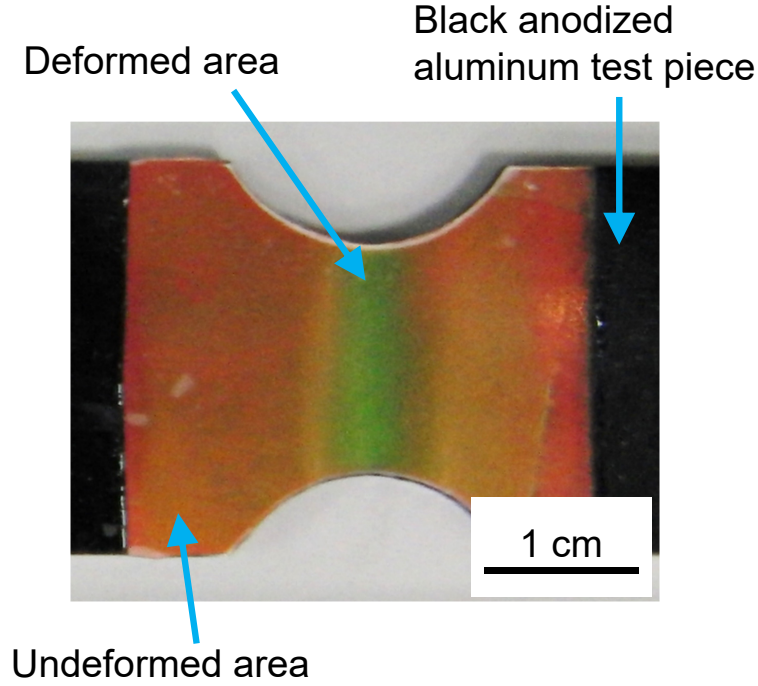

Figure 4.7 Photograph of the strain visualization sheet after the tensile test; the sheet was adhered on the black anodized aluminum test piece.

The relation between the strain of the vertical direction, ϵ_{zz}, and that of the horizontal direction, ϵ_{xx} and ϵ_{yy}, is expressed using Poisson's ratio, ν, as follows [6];

$$\epsilon_{zz} = -\frac{\nu}{1-\nu}(\epsilon_{xx} + \epsilon_{yy}) \tag{4.4}$$

The interplanar space, d_1 and d_0, corresponding to after and before the tensile test shown in Fig.4.9, respectively, is expressed as follows;

$$\epsilon_{zz} = \frac{d_1 - d_0}{d_0} \tag{4.5}$$

By combining the Eq.4.4 and Eq.4.5, d_1 can be expressed as follows;

$$d_1 = (\epsilon_{zz} + 1)d_0 = \left(1 - \frac{\nu}{1-\nu}(\epsilon_{xx} + \epsilon_{yy})\right)d_0 \tag{4.6}$$

The Bragg's diffraction with Snell's law is expressed as follows [5];

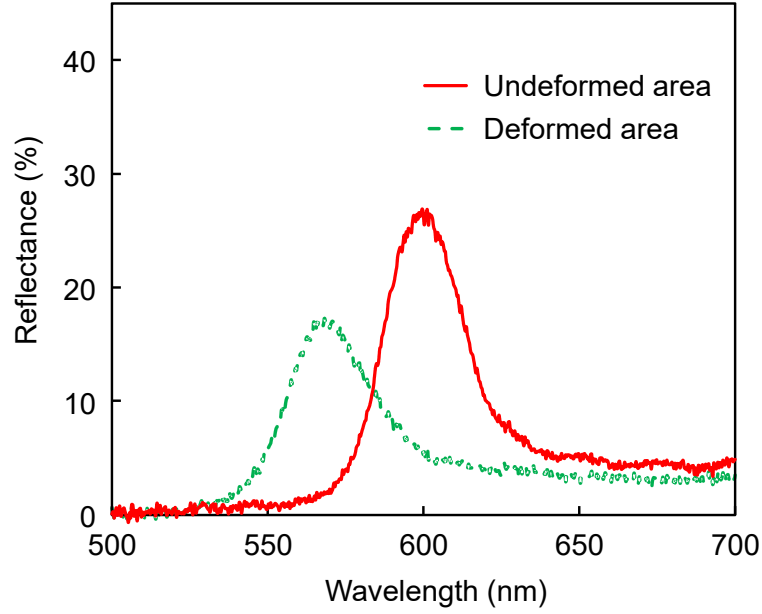$$\lambda = 2d_{111}n_{eff} \tag{4.7}$$

Figure 4.8 Reflection spectrum of the undeformed and deformed area of the strain visualization sheet after the tensile test.

where d_{111} and n_{eff} are the interplanar space of ccp (111) and the effective refractive index, respectively. Here, n_{eff} can be considered as constant for the case of the elastic rubber deformation. From Eq.4.6 and Eq.4.7, the relation between λ and ϵ can be obtained as follows;

$$\lambda = 2\left(1 - \frac{\nu}{1-\nu}(\epsilon_{xx} + \epsilon_{yy})\right) d_0 n_{eff} \tag{4.8}$$

This equation indicates that the Bragg's diffraction peak wavelength depends on the sum of the horizontal strain ($\epsilon_{xx} + \epsilon_{yy}$). Figure 4.9 shows the schematic of the structure change of the colloidal crystal with PDMS elastomer filling by the tensile test. By the tensile test, the strain visualization sheet is extended in the horizontal direction. Consequently, the horizontal interparticle distance is extended, which is corresponding to the increase of the $\epsilon_{xx} + \epsilon_{yy}$ in Eq.4.8. Because of this, the interplanar distance d_0 is shrunk to d_1 in Eq.4.6, and the structural color shows blue shift in Eq.4.8.

Actually, if x is the same as the uniaxial pulling direction, y could be shrunk. However, since the structural color showed the blue shift, $\epsilon_{xx} + \epsilon_{yy} > 0$ and λ becomes smaller in Eq.4.8, i.e. $\epsilon_{xx} > \epsilon_{yy}$.
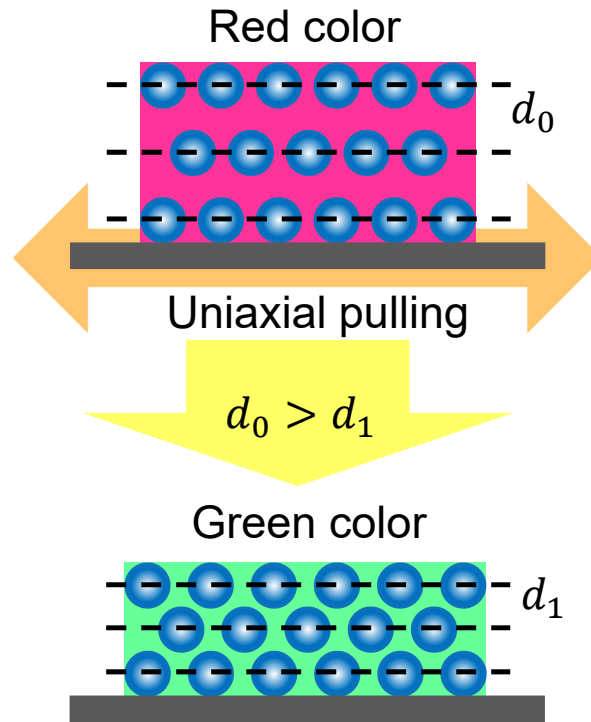
Figure 4.9 Cross sectional schematic of the strain visualization sheet, before and after the tensile test.

4.6　Summary

Colloidal crystal films with large size have been fabricated by the EPD technique. The interparticle space of these films was filled with the PDMS elastomer to realize the soft photonic crystals. Structural color change was observed as a red shift of the peak wavelength by the PDMS elastomer filling. The potential of the colloidal crystal film with PDMS elastomer filling as a strain detection sensor was shown experimentally. By the uniaxial pulling of the strain visualization sheet, the undeformed area showed the original red structural color while the deformed area showed the blued shifted green structural color.

References

[1] H. Fudouzi and T. Sawada. Photonic rubber sheets with tunable color by elastic deformation. *Langmuir*, 22:1365–1368, 2006.

[2] H. Fudouzi and Y. N. Xia. Photonic papers and inks: Color writing with colorless materials. *Adv. Mater.*, 15:892–896, 2003.

[3] H. Fudouzi and Y. Xia. Colloidal crystals with tunable colors and their use as photonic papers. *Langmuir*, 19:9653–9660, 2003.

[4] S. Furumi, H. Fudouzi, and T. Sawada. Dynamic photoswitching of micropatterned lasing in colloidal crystals by the photochromic reaction. *J. Mater. Chem.*, 22:21519–21528, 2012.

[5] H. Fudouzi. Fabricating high-quality opal films with uniform structure over a large area. *J. Coll. Interf. Sci.*, 275:277–283, 2004.

[6] H. Fudouzi, T. Sawada, Y. Tanaka, I. Ario, T. Hyakutake, and I. Nishizaki. Smart photonic coating as a new visualization technique of strain deformation of metal plates. *Prod. of SPIE*, 8345:83451S, 2012.

Chapter 5

Effect of volatile solvents on the swelling ratio of the colloidal crystal films

5.1 Introduction

Structural color based on the Bragg's diffraction changes by swelling the colloidal crystal film filled with PDMS elastomer. This phenomena is characterized with the expansion of the interparticle PDMS elastomer and the consequent increase of the interparticle distance and the interplanar spacing of the ccp (111) planes, d_{111}, by the additive solvents such as silicone oil (SO) and other organic compounds. As soon as these volatile compounds are dried up, the structural color comes back to the original green color in a reversible and repeatable ways. A cross-linked polymer network of PDMS can absorb a large amount of the solvent without dissolving [1]. The degree of swelling is mostly dependent on the affinity of the solvent for the PDMS. The affinity is mostly correlated with the solubility parameter, δ. That is why, the degree of swelling depends on the kind of the solvent. Swelling effect on the colloidal crystal film by means of the reflection peak wavelength shift corresponding to the structural color change [2–4], and on the PDMS itself [1] have been investigated in detail. However, the detailed swelling ratio of the colloidal crystal film filled with PDMS elastomer and its dependent on the different solvents have not been investigated yet.

In this work, the effect of swelling phenomena on the colloidal crystal film filled with PDMS elastomer, the determination of the swelling ratio, and their dependence on the different solvents have been investigated. In the previous reports, the soft colloidal crystal film was fabricated by the vertical technique and/or oil covering method [2, 3, 5]. In the present work, the electrophoretic deposition (EPD) technique was employed to fabricate the colloidal crystal film, as discussed in Chapters 2, 3 and 4, which realizes the fast and large size fabrication of the colloidal crystal film [6, 7]. The possibility as a volatile liquid sensor has also been demonstrated.

5.2 Experimental procedure

The detailed process to fabricate the colloidal crystal film filled with PDMS elastomer was explained in Chapter 4. In this work, these films were used to investigate the swelling phenomena.

As additive solvents, methanol (MeOH) (Kanto Chemical Co., Inc.), EtOH (Kanto Chemical Co., Inc.), 1-propanol (1-PrOH) (Kanto Chemical Co., Inc.), 2-propanol

(2-PrOH, IPA) (Nacalai Tesque, Inc.), 2-butanol (2-BuOH) (Kanto Chemical Co., Inc.), and Heptane (Kanto Chemical Co., Inc.) were used. Silicone oils (Gelest, Inc.) with different viscosity from 0.65 to 20 cSt (DMS-T00 ∼ DMS-T12) were also used as additive solvents.

Local transmission and reflection spectra were measured by a miniature fiber-optic spectrometer (USB2000+, Ocean Optics).

5.3   Liquid sensor

By dropping the 2-PrOH (IPA) and silicone oil (DMS-T00) onto the colloidal crystal film with PDMS elastomer filling, the green color changed to yellow and red, respectively. Figure 5.1-C and D show the color change just after dropping. These yellow and red colors recovered to green color by the evaporation of the volatile liquids (2-PrOH (IPA) and silicone oil) and simultaneous drying the film. Also, this phenomenon, i.e. red shift by dropping and recovering blue shift by the evaporation, could be operated repeatably. This shows that the colloidal crystal film with PDMS elastomer filling has a possibility as a volatile liquid sensor.

These color changes from green to yellow and red are also observed as a red shift of the peak wavelength in the reflection spectra of the colloidal crystal films shown in Fig.5.2. The red shift from pale blue to green could be explained by the change of the refractive index of the interparticle space n_m from the air ($n = 1.0$) to the PDMS elastomer ($n = 1.4$) as shown in the Chapter 4.4 using Eq.5.1.

$$n_{eff}^2 = V_p n_p^2 + V_m n_m^2 \tag{5.1}$$

where n_{eff}, n_p, n_m, V_p and V_m are the effective refractive index, refractive indices of PS particles ($n = 1.59$) and surrounding medium, volume fractions of the PS particles and surrounding medium, respectively. However, the additional red shift from green to yellow and red cannot be explained in the same way, because the refractive indices of 2-PrOH/IPA (n=1.377) and DMS-T00 (n=1.375) are smaller than that of PDMS elastomer (n=1.4). This means that the effect of the change of d_{111} on the red shift from green to yellow and red is dominant in the Eq.5.2.
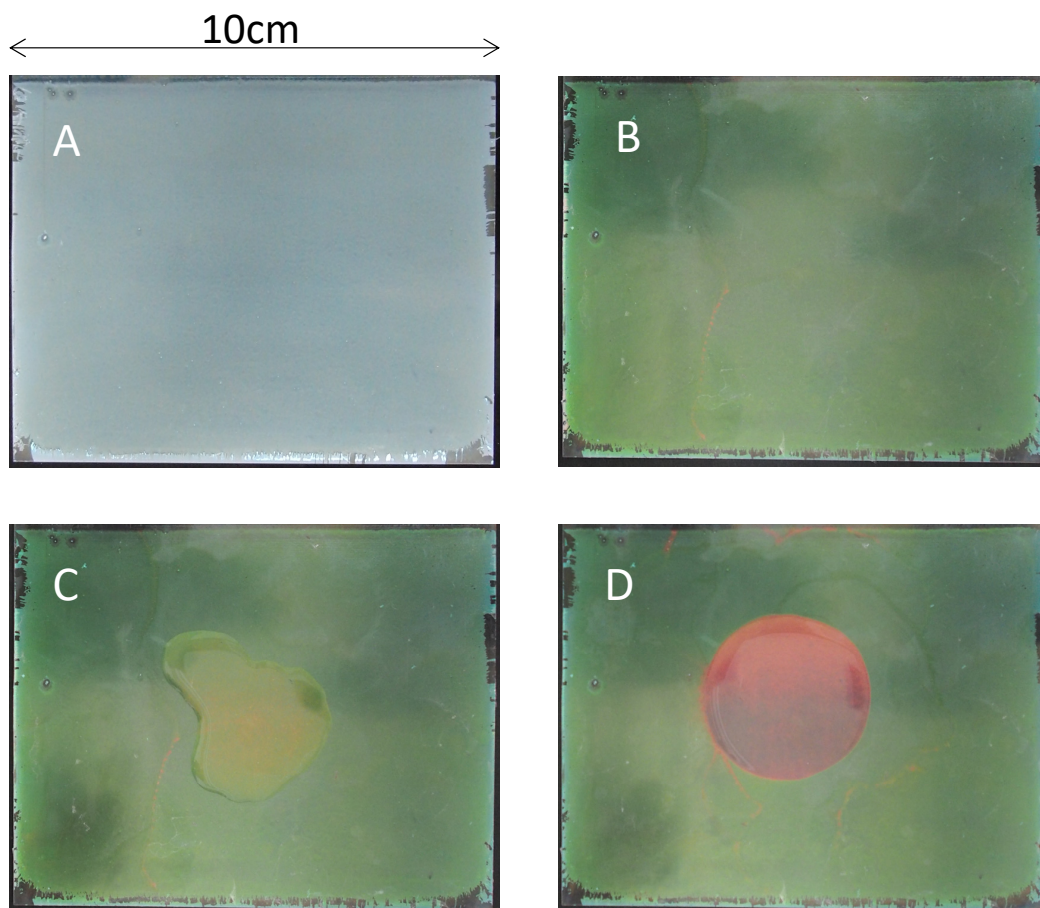
Figure 5.1 Optical photographs of the colloidal crystal film showing the chromogenic variation as a volatile liquid sensor. A colloidal crystal film fabricated by the EPD technique, before (A) and after (B) filling the interparticle space with PDMS elastomer (obtained in Chapter 4). Structural color change by dripping volatile liquid, 2-PrOH (IPA) (C) and silicone oil (DMS-T00) (D).
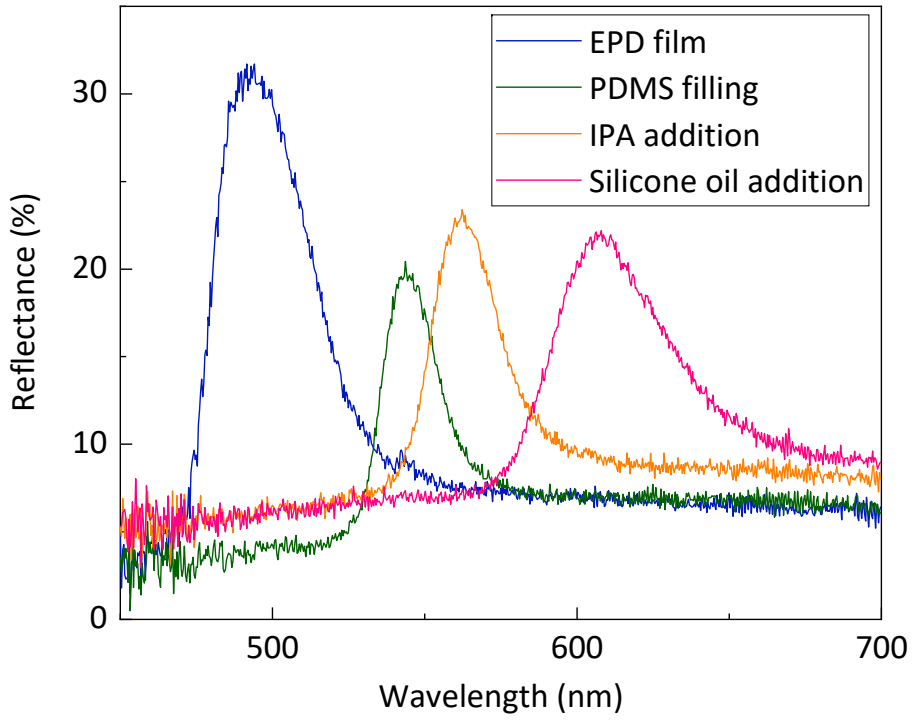
Figure 5.2 Comparison of reflection spectrum peaks of 4 kinds of colloidal crystal films shown in Fig.5.1-A to D. A and B are obtained in Chapter 4, and C and D are obtained in this chapter.

$$\lambda = 2d_{111}\sqrt{n_{eff}^2 - sin^2\Theta} \tag{5.2}$$

where d_{111} and Θ are, the interplanar spacing of the ccp (111) planes and the angle from the normal to the substrate, respectively.

In the following, the effect of the addition of different silicon oil and another organic compounds on the change of the d_{111} is investigated in detail.

5.4   Effect of silicone oil addition

Figure 5.3 shows the dependence of the peak wavelength in the transmission spectrum on the molar mass of the silicone oil as additives. Peak wavelength decreased almost linearly depending on the increase of molar mass, i.e. DMS-T00 which has the smallest molar mass within the investigated material has shown the highest peak shift from the dry film.

Figure 5.4-A shows the angle dependence of the transmission spectra measured just after dropping the DMS-T00 onto the colloidal crystal film fabricated by the EPD technique after filling the interparticle space with PDMS elastomer (Fig.5.1-D). From
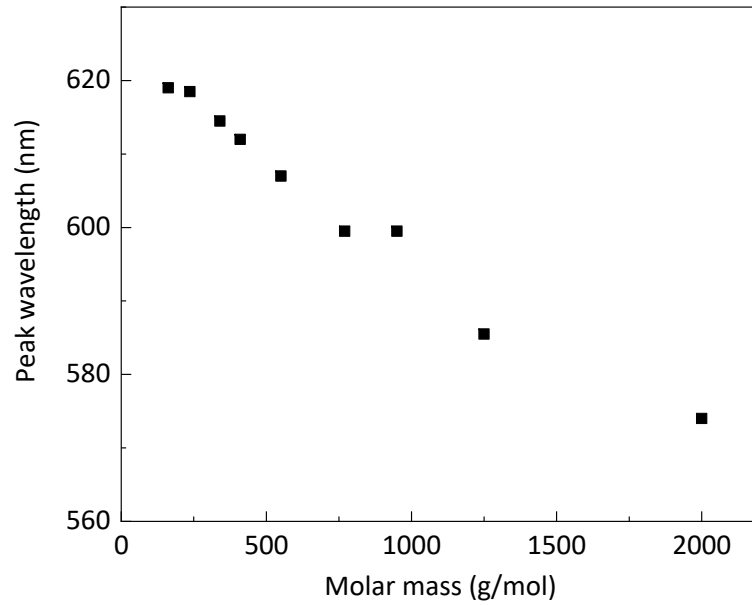
Figure 5.3 Dependence of the transmission peak wavelength on the molar mass of the silicone oil as the additive on the colloidal crystal film with PDMS elastomer filling.

Fig.5.4-A, $sin^2\Theta$-λ^2 plot was obtained as shown in Fig.5.4-B. This plot was linear fitted by the eq.5.3, and then d_{111} was estimated.

$$sin^2\Theta = -\frac{1}{2d_{111}}\lambda^2 + n_{eff}^2 \qquad (5.3)$$

Swelling ratio, s, was also calculated by

$$s = \frac{d_{111}}{d_{111}^{PDMS}} \qquad (5.4)$$

where d_{111}^{PDMS} is the d_{111} of the colloidal crystal film with PDMS elastomer filling for the interparticle space (Fig.5.1-B). Table 5.1 shows the summary of the properties of DMS-T00 as additive on the colloidal crystal film with filling the PDMS elastomer for the interparticle space, together with other different types of silicone oils. The swelling ratio increased regularly by the decrease of the solubility parameter, δ. The highest swelling ratio, 1.2008, was obtained by the DMS-T00 among the investigated silicone oils.

5.5   Effect of another organic compounds addition

Figure 5.5 shows the variation of the peak wavelength in the transmission spectrum by adding different alcohols as additives. Opposite to the case of silicone oil, the peak
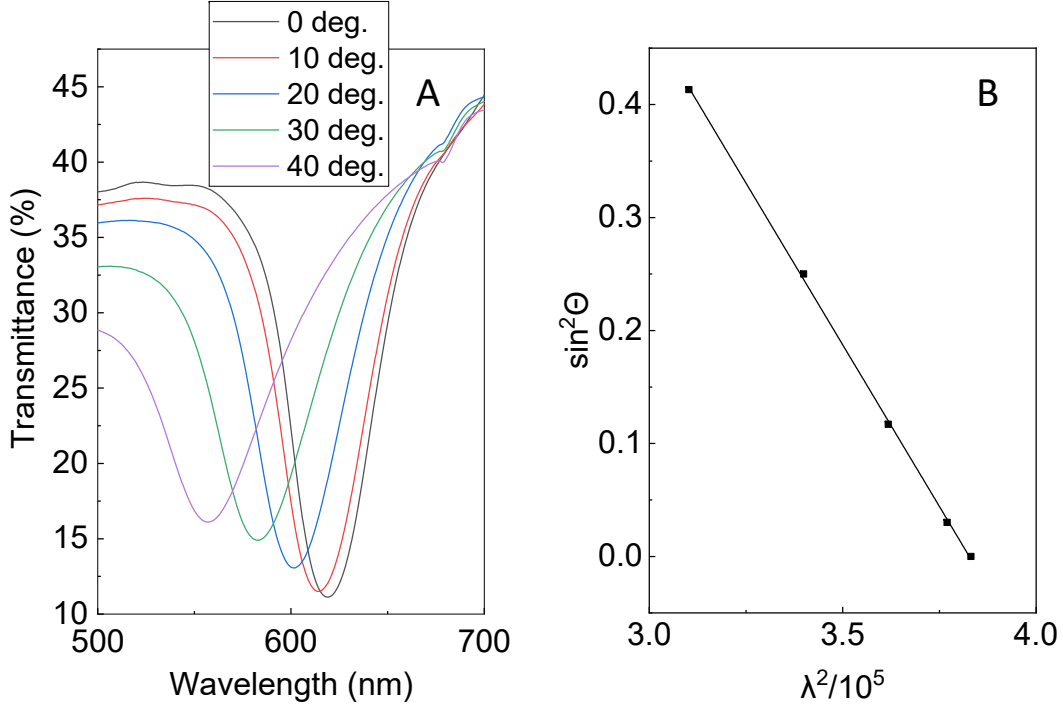
88

Figure 5.4 (A) Angle dependence of the transmission spectra measured by tilting the colloidal crystal film at each Θ from 0° to 40° just after dropping the DMS-T00 onto the colloidal crystal film fabricated by the EPD technique after filling the interparticle space with PDMS elastomer (Fig.5.1-D),. (B) $sin^2\Theta$ versus $\lambda^2/10^5$ based on the Bragg's equation (Eq.5.3).

Table 5.1: Comparison of the different types of silicone oils as additive on the colloidal crystal film with filling the PDMS elastomer for the interparticle space. M: Molar mass (g/mol), δ: Solubility parameter ($cal^{\frac{1}{2}}cm^{-\frac{3}{2}}$), λ: Peak wavelength of transmission spectrum (nm), d_{111}: Interplanar spacing (nm), s: Swelling Ratio (-). δ of PDMS are from Ref.[1], δ of silicone oils are from Ref.[8] (left side, catalogue's values for Dow Corning products, PMX-200 Silicone Fluid series) and Ref.[9] (right side, estimated for Shin-Etsu Chemical products, KF-96 Silicone Fluid series).

	M	δ		λ	d_{111}	n_{eff}	s
PDMS		7.3		540.5	174.02	1.553	-
DMS-T00 / 0.65 cSt	162	6.8	7.95	619.0	208.97	1.480	1.2008
DMS-T01 / 1.0 cSt	225	7.0	8.12	618.5	200.61	1.543	1.1528
DMS-T02 / 2.0 cSt	375	7.1	8.44	612.0	198.91	1.537	1.1430
DMS-T05 / 5.0 cSt	740	7.25	8.91	599.5	192.51	1.558	1.1062
DMS-T11 / 10 cSt	1200	7.3	9.43	585.5	191.80	1.525	1.1021

wavelength increased by the increase of the molar mass, i.e. 2-BuOH which has the highest molar mass within the investigated material has shown the highest peak shift from the dry film.
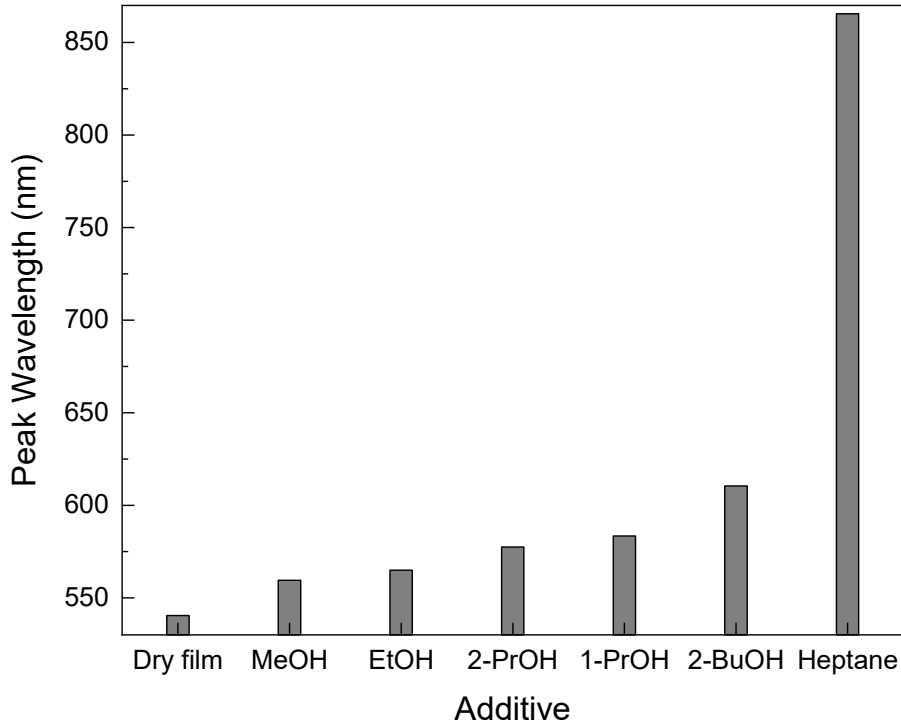

Figure 5.5 Variation of the transmission peak wavelength by the different alcohols and heptane as the additive on the colloidal crystal film with PDMS elastomer filling.

Figure 5.6-A shows the angle dependence of the transmission spectra measured just after dropping the 2-BuOH onto the colloidal crystal film fabricated by the EPD technique after filling the interparticle space with PDMS elastomer. From Fig.5.6-A, $sin^2\Theta$-λ^2 plot was obtained as shown in Fig.5.6-B. This plot was linear fitted by the Eq.5.3, and then d_{111} was estimated. Swelling ratio, s, was also calculated by the Eq.5.4. Table 5.2 shows the summary of the properties of 2-BuOH as additive on the colloidal crystal film with filling the PDMS elastomer for the interparticle space, together with other different types of organic compounds. The values of δ cited from Ref.[10] are called 'Hildebrand Solubility Parameters' based on the following relation.

$$cal^{\frac{1}{2}}cm^{-\frac{3}{2}} = 0.48888 \times MPa^{\frac{1}{2}} \tag{5.5}$$

The swelling ratio increased almost regularly by the decrease of δ, except 2-PrOH. The highest swelling ratio, 1.6114, was obtained by the Heptane among the investigated
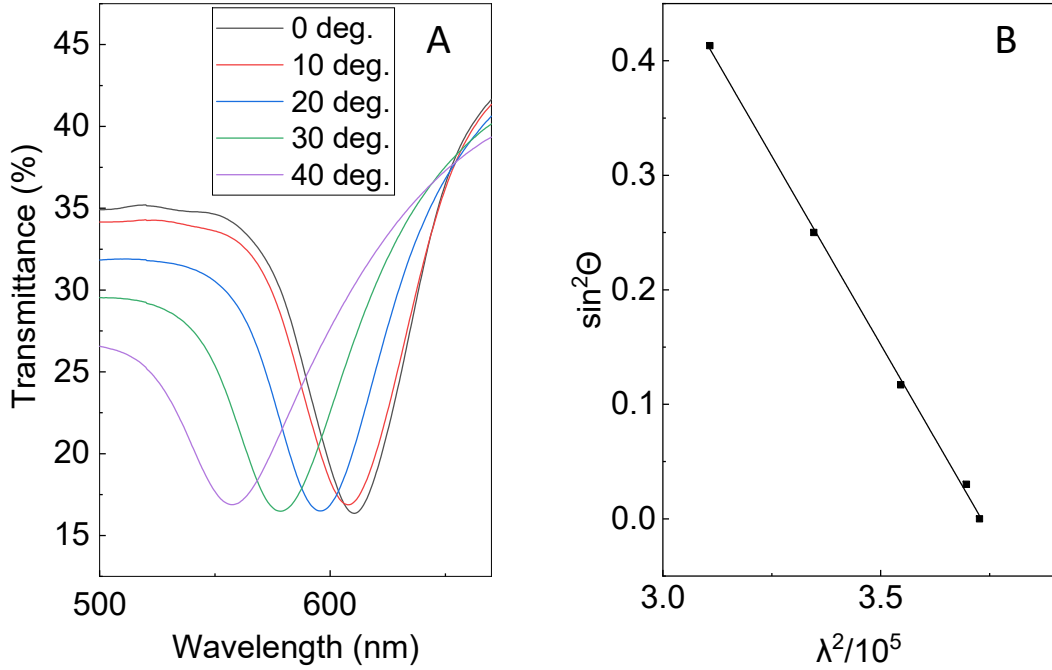
another organic compounds.

Figure 5.6 (A) Transmission spectra measured by tilting the colloidal crystal film at each Θ from 0° to 40° just after dropping the 2-BuOH onto the colloidal crystal film fabricated by the EPD technique after filling the interparticle space with PDMS elastomer,. (B) $sin^2\Theta$ dependence on $\lambda^2/10^5$ based on the Bragg's equation (Eq.5.3).

The increase of d_{111} corresponding to that of s agrees well with the red shift of the λ. The decrease of n_{eff} after dropping silicone oil is also understandable because the refractive index of DMS-T00 (n=1.375) is smaller than that of the PDMS elastomer ($n = 1.4$). However, even though the refractive index of IPA (n=1.377) is about the same as that of DMS-T00 and smaller than that of PDMS elastomer, the n_{eff} increased after dropping IPA. This might indicate that the dropping IPA swelled not only PDMS elastomer but also PS particles, i.e. the effect of n_p in the eq.5.1 ($n = 1.59$, PS particles) became larger by dripping the IPA.

Figure 5.7 shows the change of the colloidal crystal schematically, based on the above results. By filling the interparticle space of the colloidal crystal film with the PDMS elastomer, the refractive index of the interparticle space increases, although the interparticle distance almost does not change. By dropping the volatile additives, interparticle distance and d_{111} increase. These promote the change of the structural color, i.e. the peak wavelength shift to the longer direction (red shift).

To occur swelling in a polymer (PDMS) - solvent system, the free energy of mixing

Table 5.2: Comparison of the different types of other organic compounds as additive on the colloidal crystal film with filling the PDMS elastomer for the interparticle space. M: Molar mass (g/mol), δ: Solubility parameter ($cal^{\frac{1}{2}}cm^{-\frac{3}{2}}$), λ: Peak wavelength of transmission spectrum (nm), d_{111}: Interplanar spacing (nm), s: Swelling Ratio (-). δ of PDMS and organic compounds are from Ref.[1] and Ref.[10], respectively.

	M	δ	λ	d_{111}	n_{eff}	s
PDMS		7.3	540.5	174.02	1.553	-
H_2O	18.02	23.4	536.5	170.06	1.578	0.9772
MeOH	32.04	14.5	559.5	176.00	1.589	1.0113
EtOH	46.07	12.9	565.0	182.83	1.544	1.0506
1-PrOH	60.1	12	583.5	187.29	1.559	1.0762
2-PrOH	60.1	11.5	577.5	184.65	1.562	1.0611
2-BuOH	74.12	10.9	610.5	194.85	1.567	1.1196
Heptane	100.21	7.4	865.5	280.43	1.542	1.6114

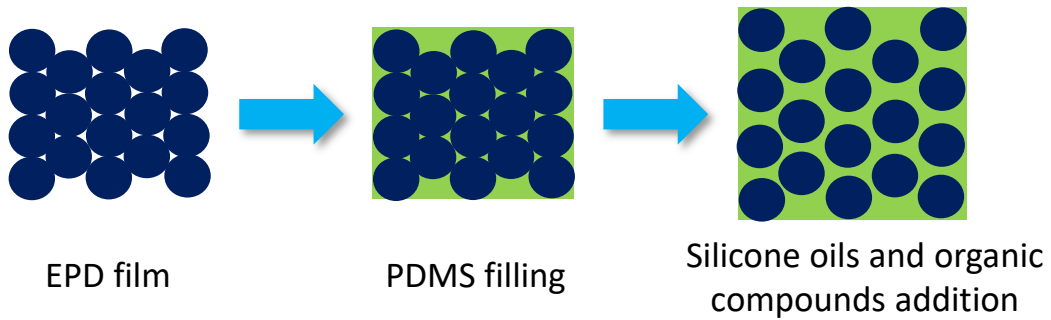EPD film   PDMS filling   Silicone oils and organic compounds addition

Figure 5.7 Schematic of the structure change of the colloidal crystal film.

$\Delta G = \Delta H - T\Delta S$ should be favorable, i.e. $\Delta G < 0$. The occurrence of swelling becomes maximum when $(\delta_p - \delta_s)^2$ goes to 0 ($\delta_p = \delta_s$), where δ_p and δ_s are the solubility parameter of the polymer (PDMS) and solvent, respectively, since ΔH is proportional to $(\delta_p - \delta_s)^2$ [1]. Figure 5.8 shows the plot of the swelling ratio versus the solubility parameter. The solubility parameter of PDMS was cited as 7.3 $cal^{\frac{1}{2}}cm^{-\frac{3}{2}}$ [1]. Since the smallest solubility parameter of the solvent investigated in this work is 7.4 $cal^{\frac{1}{2}}cm^{-\frac{3}{2}}$ of Heptane, the general tendency observed in Fig.5.8 was that the smaller the solubility parameter is, the higher the swelling ratio is. Actually, the value of $(\delta_p - \delta_s)^2$ between PDMS and Heptane is quit small. Some of irregularity such as 2-PrOH and the gap between silicone oil and alcohols were seen in Fig.5.8. However, this type of irregularity was already pointed out in Ref.[1].
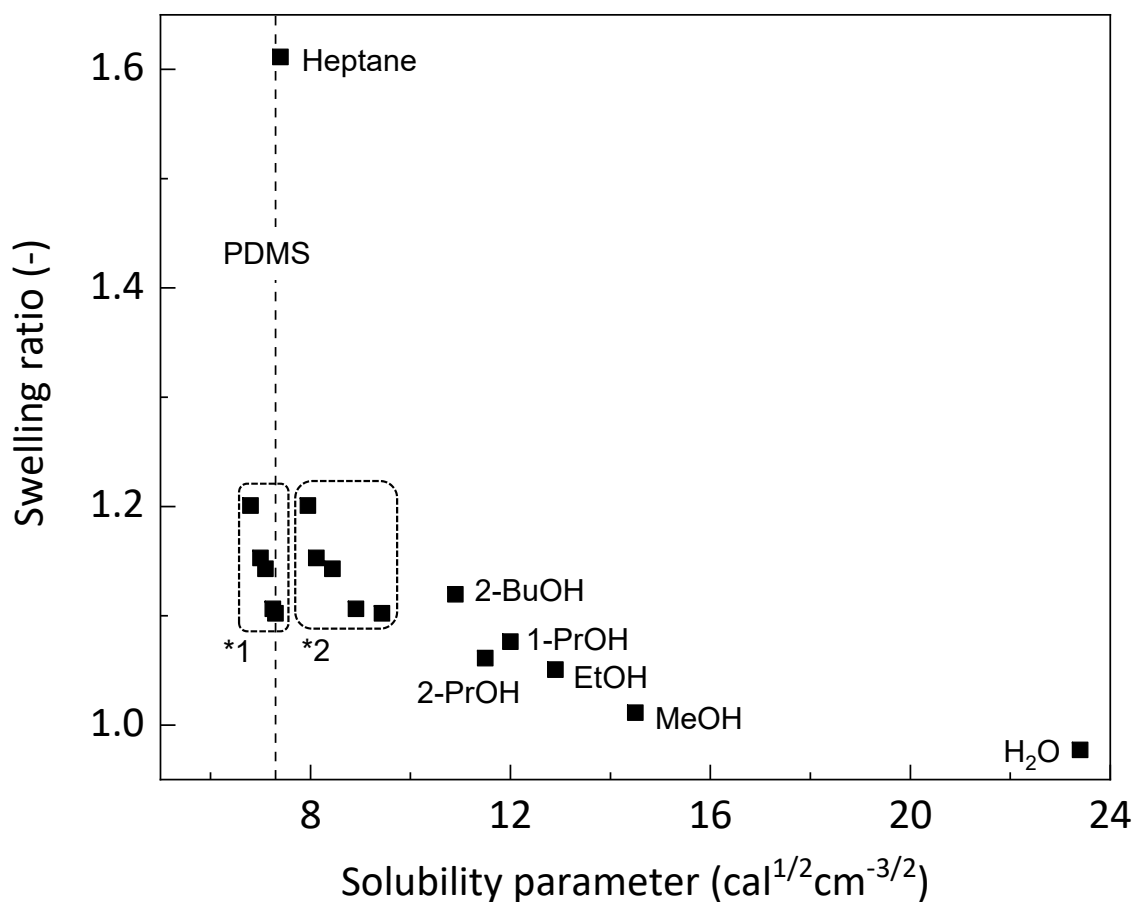

Figure 5.8 The swelling ratio dependence on the solubility parameter. *1: Silicone oils with δ shown by XIAMETER® [8]. *2: Silicone oils with δ reported by Watanabe et al. [9]

5.6 Summary

Swelling phenomena were investigated in detail by the different kinds silicone oils and other organic compounds as solvents. By dropping these solvents onto the colloidal crystal film with PDMS elastomer filling, structural color change was observed as a red shift of the peak wavelength. These red shifted peak wavelength again blue shifted to the original green color by drying up the volatile solvent. Since this phenomenon was reversible and repeatable, the possibility of the obtained colloidal crystal film with PDMS elastomer filling as volatile liquid sensor was shown.

In the case of silicone oil, the degree of the red shift of the peak wavelength decreased depending on the increase of the molar mass of the silicone oil. To the contrary, in the case of alcohols, the degree of the red shift of the peak wavelength increased depending on the increase of the molar mass of the alcohol.

Swelling ratio, s, for all solvents investigated was determined using the estimated d_{111}. Generally, s of the solvents was inversely dependent on the δ. The highest s, 1.6114, was obtained by heptane, of which δ, 7.4 $cal^{\frac{1}{2}}cm^{-\frac{3}{2}}$ was very close to that of PDMS, 7.3 $cal^{\frac{1}{2}}cm^{-\frac{3}{2}}$.

References

[1] J. N. Lee, C. Park, and G. M. Whitesides. Solvent compatibility of poly(dimethylsiloxane)-based microfluidic devices. *Anal. Chem.*, 75:6544–6554, 2003.

[2] H. Fudouzi and Y. N. Xia. Photonic papers and inks: Color writing with colorless materials. *Adv. Mater.*, 15:892–896, 2003.

[3] H. Fudouzi and Y. Xia. Colloidal crystals with tunable colors and their use as photonic papers. *Langmuir*, 19:9653–9660, 2003.

[4] H. Fudouzi and T. Sawada. Photonic crystal sensing of components of a liquid mixture using an optical fiber spectrometer. *Prod. of SPIE*, 6767:676704, 2007.

[5] H. Fudouzi and T. Sawada. Photonic rubber sheets with tunable color by elastic deformation. *Langmuir*, 22:1365–1368, 2006.

[6] M. Koike, G. T. H. Tran, S. Azuma, H. Kiyono, T. Uchikoshi, and H. Fudouzi. Rapid fabrication of colloidal crystal films by electrophoretic deposition and its application

for a volatile liquid and strain detection sensor. *J. Soc. Powder Techn. Japan,* 56:339–346, 2019.

[7] G. T. H. Tran, M. Koike, T. Uchikoshi, and H. Fudouzi. Fabrication of polystyrene colloidal crystal film by electrophoretic deposition. *Adv. Powder Tech.*, 31:3085–3092, 2020. DOI://doi.org/10.1016/j.apt.2020.05.029.

[8] XIAMETER® brand silicone fluids for the personal care industry. No.95-1166-01:AGP12812, 2013.

[9] H. Watanabe and T. Miyauchi. Determination of solubility parameter for siloxane segment. *J. Chem. Eng. Jpn.*, 6:109–114, 1973.

[10] A. F. M. Barton. Handbook of solubility parameters. *CRC Press*, 153-157, 1983.

Chapter 6

General Conclusions

In this thesis, optimal conditions to fabricate the colloidal crystal films by the EPD technique were explored for the sake of fast and large size fabrication. For this purpose, growth mechanism of the colloidal crystal film was investigated in detail. The sensing applications of the colloidal crystal films were also examined.

Chapter 1   The background and review, the overview of this thesis were described.

Chapter 2   The optimal condition for the EPD colloidal crystal film formation was investigated in detail. The aqueous PS colloidal suspension was not appropriate due to the generation of gas bubbles during the electrolysis and formed only amorphous films. Dialysis and the application of a pulse voltage could avoid the gas bubble generation, however, particle self-assembly was still amorphous. As a suspension for the EPD process, the effectiveness of mixing ethanol (EtOH) and water was confirmed by testing several alcohols as solvents, and explained from the different viewpoints including hydrogen bond, van der Waals force, and mobility/freedom of PS particles. The higher the EtOH concentration, the better the colloidal crystal film formation. In the investigated range, the most preferable condition for the EPD colloidal crystal film formation was from the 92.5 vol% EtOH suspension. The substrate withdrawing rate from the suspension also significantly affected the EPD colloidal crystal film fabrication. Too slow and too fast withdrawing rates were not good. The most preferable rate was 3.0 mm/sec. The large area colloidal crystal film formation by the EPD technique was also demonstrated. Comparable quality of EPD colloidal crystal films fabricated on small area indium tin oxide (ITO) coated glass (ITO/glass) and large area (over 50 cm^2) ITO coated PET (polyethylene terephthalate) sheet (ITO/PET) substrates was confirmed by the SEM observations and the reflectance spectra measurements. These results demonstrate the advantage of the EPD technique for large scale production of colloidal crystal, considering the fast fabrication rate compared to the other conventional techniques. The growth rate of the colloidal crystal is extremely rapid (within one minute for 900 mm^2 area) compared with those of previously reported methods, such as oil covering and capillary deposition methods (several to hundreds of hours). This process has the potential for high-speed fabrication of the colloidal crystalline thin films.

Chapter 3 A growth mechanism of the colloidal crystal films from the concentrated EtOH aqueous suspension was investigated. Closely packed colloidal crystal film was formed within 55 seconds. By the analysis of the reflection spectra and the optical microscope images, the growth mechanism from the colloidal suspension to the colloidal crystal film was found to consist of 4 stages. The 1st stage is the formation of a liquid film of the concentrated colloidal suspension on a substrate. By the progress of evaporation, the phase transition from disorder to order to form the non-closely packed colloidal crystal by self-assembly takes place. At the moment of the phase transition, the Bragg's diffraction peak is detected and the structural color appears. In the 2nd stage, the diffraction peak shifts toward the shorter wavelength direction (blue shift), due to the reduction of the interparticle distance of the non-closely packed colloidal crystal. In the end, the closely packed colloidal crystal film is formed. In the 3rd stage, the liquid film covering on the colloidal crystal film evaporated and iridescence color due to thin-film interference is tentatively observed. In the 4th stage, the colloidal crystal film changes from wet to dry, by the evaporation of the interparticle aqueous EtOH solvent. The structural color changes from green to pale blue and the diffraction peak wavelength goes down with one more stage. This color change is dominated by the change of the refractive index of the interparticle medium from the liquid to air.

Chapter 4 The interparticle space of the colloidal crystal film was filled with the PDMS (poly-dimethylsiloxane) elastomer to realize the soft photonic crystals. After filling the interparticle space with PDMS elastomer, the color changed from pale blue to green due to the increase of the interparticle distance and the refractive index increase of the interparticle space. By the 4 times PDMS elastomer filling, the color changed to red with the further increase of the interparticle distance. By the tensile test of this film, the deformed area exhibited green color with the shrinking of the interplanar distance although non-deformed area did not show any color change. This result demonstrated the potential use of the colloidal crystal films with PDMS filling for the strain detection sensors.

Chapter 5 Swelling phenomena was investigated in detail by the different kind of silicone oil and other organic compounds as solvents. By dropping these solvents onto the colloidal crystal film with PDMS filling, structural color change was observed as a

red shift of the transmission peak wavelength (the diffraction peak shifts toward the longer wavelength direction). These red shifted peak wavelength again blue shifted to the original green color by drying up the volatile solvent. Since this phenomenon was reversible and repeatable, the possibility of the obtained colloidal crystal film with PDMS elastomer filling as volatile liquid sensor was shown. The swelling ratio for all investigated solvents was determined using the estimated interplanar distance. Generally, the swelling ratio of the solvents was inversely dependent on the solubility parameter. The highest swelling ratio, 1.6114, was obtained by the heptane, of which solubility parameter, 7.4 $cal^{1/2}cm^{-3/2}$, was very close to that of PDMS, 7.3 $cal^{1/2}cm^{-3/2}$.

In this study, high speed colloidal crystal film fabrication was demonstrated. As a next step, quit a large size fabrication from cm order to m order would be required for the future mass production. For this purpose, rolled long PET sheets would be one of the candidates as a substrate.

Strain detection sheet was demonstrated in this work. For further development, the long-term reliability at outdoor condition would be required.

Volatile liquid sensor was demonstrated in this work. For further development, the creation of big data to be used as a sensor would be necessary, in order to define and detect the liquid from the randomly selected test liquid.

List of research achievements

I. Publications

1. Rapid fabrication of colloidal crystal films by electrophoretic deposition and its application for a volatile liquid and strain detection sensor
   Journal of the Society of Powder Technology, Japan, **2019**, 56, 339-346.
   DOI://doi.org/10.4164/sptj.56.339
   M. Koike, **G. T. H. Tran**, S. Azuma, H. Kiyono, T. Uchikoshi, H. Fudouzi

2. Fabrication of polystyrene colloidal crystal film by electrophoretic deposition
   Advanced Powder Technology, **2020**, 31, 3085-3092.
   DOI://doi.org/10.1016/j.apt.2020.05.029
   G. T. H. Tran, M. Koike, T. Uchikoshi, H. Fudouzi

3. Rapid Growth of the colloidal crystal films from the concentrated aqueous ethanol suspension
   Langmuir, **2020**, In press
   DOI://doi.org/10.1021/acs.langmuir.0c01048
   G. T. H. Tran, M. Koike, T. Uchikoshi, H. Fudouzi

II. Presentations

1. Rapid formation and structural color tuning of colloidal crystal films by electrophoretic deposition method
   The 69th Divisional Meeting of Division of Colloid and Surface Chemistry, Tsukuba, Japan (September 18-20, 2018)
   G. T. H. Tran, M. Koike, H. Fudouzi, T. Uchikoshi

2. Rapid and large area fabrication of 3D EPD colloidal crystal
   The 11th International Conference on the Science and Technology for Advanced Ceramics (STAC-11), Tsukuba, Japan (July 9-11, 2019)
   G. T. H. Tran, M. Koike, H. Fudouzi, T. Uchikoshi

Acknowledgements

I would like to heartily thank all the persons who have advised and contributed to the completion of this thesis.

First and foremost, I would like to express my gratitude to my research supervisor, Prof. Tetsuo Uchikoshi (NIMS, Hokkaido University), who has given me the opportunity to work in the fascinating field of materials science and whose ideas and contribution to this work have played a major role.

I would like to thank Dr. Hiroshi Fudouzi (NIMS) for his inestimable help in all my works.

I am also deeply indebted to Prof. Kiyoharu Tadanaga (Hokkaido University), Prof. Toshihiro Shimada (Hokkaido University), and Prof. Naoto Shirahata (NIMS, Hokkaido University) for their valuable comments and suggestions on this dissertation. I deeply appreciate Prof. Kiyoshi Shimamura (NIMS) for his insightful comments and encouragement.

Special thanks to Mr. Masaki Koike (NIMS, Shibaura Institute of Technology) for his continuous support with the EPD experiments, SEM of this work. Also I want to thank all my friends and members of my laboratory for their cordial support during the most difficult period of my work.

I have been continuously receiving support from the secretary sections of Fine Particles Engineering Group and Hokkaido University, and I wish to thank Ms. Yoko Watanabe for her assistance during the whole Hokkaido University-NIMS Joint Graduate School Program.

I would like to express my thankfulness to my parents for every form of support, encouragement and love that they have given me over all of my studies and life.

Finally, I would like to thank my little son, who is always beside me and gives me strength to not give up my dream.

September 2020

Tran Thi Hoai Giang